11-19-2020

Applications of Nanoporous Gold to Drug Release and Glycoscience

Dharmendra Neupane
University of Missouri-St. Louis, dnfzf@umsystem.edu

Recommended Citation

Neupane, Dharmendra, "Applications of Nanoporous Gold to Drug Release and Glycoscience" (2020). *Dissertations*. 1011.
https://irl.umsl.edu/dissertation/1011

Applications of Nanoporous Gold to Drug Release and Glycoscience

By

Dharmendra Neupane

M.S. Chemistry-Graduate, University of Missouri-St Louis, 2018

M.Sc. Chemistry-Graduate, Tribhuvan University, Nepal, 2012

A Dissertation

Submitted to the Graduate School of the

University of Missouri-St. Louis

In partial fulfillment of the requirements for the degree

Doctor of Philosophy in chemistry, December 2020

Advisory Committee

Chair and Advisor Keith J. Stine, Ph.D.

Alexei V. Demchenko, Ph.D.

Chung F. Wong, Ph.D.

Michael R. Nichols, Ph.D.

ABSTRACT

Applications of Nanoporous Gold to Drug Release and Glycoscience

December 2020

Dharmendra Neupane, M.S. Chemistry-Graduate, University of Missouri-St Louis, MO, USA

Chair and Advisor: Professor Keith J. Stine

Nanoporous gold (NPG) is a versatile material because of its three-dimensional nanoscale network, facile surface functionalization, biocompatibility, and potential usage in biotechnology applications. The field of glycoscience is growing in significance as the importance of glycans in human health and disease becomes more fully understood at the molecular level. NPG can be applied to several needs in the field of glycoscience. Our lab has applied NPG to applications in glycoscience including the capture and release of glycoproteins, and the detection of glycoprotein interactions by using either electrochemical methods or localized surface plasmon spectroscopy (LSPR). The capture of glycoproteins onto high surface area NPG is demonstrated using both lectin-glycan interactions and interaction between glycoproteins and NPG modified with boronic acid functional groups. Thermogravimetric analysis and use of a UV-visible HPLC detector in a flow cell containing monoliths of NPG were applied to monitor capture of glycoprotein and its elution by flow of free ligand. The modification of NPG by self-assembled monolayers (SAMs) with terminal boronic acid groups has been used together with LSPR to monitor the capture of glycoprotein by the induced shift in the LSPR peak wavelength. Square-wave voltammetry methods can also be applied to monitor the binding of

glycoproteins to NPG modified either by SAMs with terminal boronic acid groups or by conjugated lectins.

Thiolated β-cyclodextrin modified NPG wire was used for the pH sensitive release of doxorubicin (DOX) in a controlled manner, with an ultra-high DOX payload. Thiolated β-cyclodextrins are attractive macrocycles as they can form supramolecular inclusion complexes with doxorubicin affording the possibility of altering the controlled release behavior. Doxorubicin is one of the most potent anti-tumor drugs used in the treatment of different cancers. The binding of thiolated β-cyclodextrin with the anti-cancer drug doxorubicin has been examined with the use of spectroscopy and electrochemistry. Moreover, the prepared structure exhibited excellent properties for controlled drug release outlining the potential of a pH sensitive drug implant or carrier for biomedical application. This delivery system could improve localized targeting of the drug as well as alter the rate of release of the doxorubicin near a tumor.

Dedication

TO MY FAMILY

ACKNOWLEDGEMENTS

I would to thank my research advisor prof. Keith J Stine for allowing me to work in his laboratory, providing all my needs in doing my research and with his all support. I appreciate the opportunities he provided that help me to improve my research skills. He was always approachable, and his deep understanding of chemistry was inspiring and, I shall remain grateful that he agreed to accept me as a part of his research group. I would like to thank Professor Dr. Alexei V. Demchenko for collaboration and valuable guidance in the current study and for the synthesis of carbohydrate molecule and polystyrene-based polymer. I would also like to express sincere gratitude towards my committee members, Dr. Chung F. Wong, and Dr. Michael R. Nichols who have both taught me during my masters and have provided valuable insights in my projects during my dissertation proposal.

I want to acknowledge my lab mates and postdoc Dr. Jay K. Bhattarai for mentoring me in my research projects and creating excellent working environment with collaboration in different projects. I want to thank my current lab member Mr. Bishal Nepal, Miss Palak Shondhi, and Dhanbir Lingden for helpful discussion on different projects as well as collaboration in different projects. I would like to thank all the masters, undergraduate, and high school students who have directly or indirectly worked with me to move the projects forward. I am thankful to Dr. Matteo Panza and Prof. Demchenko for the collaboration in the projects to synthesize the polystyrene based polymer known as Panzajel. I would like to wish them all better and successful future.

I am also thankful to all of my family members my father Hari Prasad Neupane, mother Shreedhara Neupane, brother Shiva Neupane, brother in-law Reema Neupane, wife Sarita Pandey and daughter Alison Neupane for their love, support, and encouragement.

Finally, I would like to thank the respected professors, staff, graduate students, and undergraduate students in the UMSL department of Chemistry and Biochemistry and Center for Nanoscience for creating friendly and productive environments.

TABLE of CONTENT

LIST OF ABBREVIATIONS

AFM	Atomic Force Microscopy
APBA	Aminophenylboronic acid
APMBA	Aminophenylmethylboronic acid
AUC	Area Under the Curve
AuNP	Gold nanoparticles
BET	Brunauer-Emmett-Teller
BJH	Barrett-Joyner-Halenda
BSA	Bovine serum albumin
CE	Capillary electrophoresis
Con A	Concanavalin A
Cyt C	Cytochrome C
DMTMM	4-(4,6-dimethoxy-1,3,5-triazin-2-yl)-4-methylmorphominium chloride
DOX	Doxorubicin
EDC	1-Ethyl-3-(3-dimethylaminopropyl) carbodiimide hydrochloride
EDX	Energy dispersive X-ray spectroscopy
EIS	Electrochemical impedance spectroscopy
ELISA	Enzyme linked immunosorbent assay
FITC	Fluorescein isothiocyanate
HPLC	High performance liquid chromatography

IUPAC	International Union of Pure and Applied Chemists
K_d	Dissociation Constant
LA	Lipoic acid
LAC	Lectin affinity chromatography
LC	Liquid Chromatography
LSPR	Localized surface plasmon resonance spectroscopy
MS	Mass spectroscopy
NHS	N-hydroxysuccinimide
NMR	Nuclear magnetic resonance
Ova	Ovalbumin
PEG	Polyethylene glycol
PNA	Peanut agglutinin
RT	Room Temperature
R_{ct}	Charge Transfer Resistance
SAM	Self-assembled monolayer
SBA	Soybean agglutinin
SDS-PAGE	Sodium dodecyl sulfate polyacrylamide gel electrophoresis
S_{BET}	BET specific surface area
SEM	Scanning electron microscopy

TEM	Transmission electron microscopy
TGA	Thermogravimetric analysis
TFA	Trifluoroacetate
Tris	Tris(hydroxymethyl)aminomethane
UV-Vis	Ultraviolet-visible
XRD	X-ray powder diffraction
XPS	X-ray photoelectron spectroscopy

LIST OF FIGURES

List of the Tables

Chapter I INTRODUCTION

1.1 Overview

The aim of these studies was to develop applications of NPG for use in electrochemical biosensors, drug release experiments, and the separation of glycoproteins. In contrast to flat gold surfaces, NPG as a substrate results in different properties with respect to surface to volume ratio and different behaviors with respect to molecular assembly. NPG has been utilized as a substrate material for the immobilization of biomolecules via conjugation or assembly onto functionalized monolayers, for the development of a drug carrier, for the study of carbohydrate-protein interactions, and for the separation of glycoproteins.

Chapter I presents an introduction to NPG and its application as a doxorubicin carrier for the in vitro release of this drug, methods of formation of the inclusion complexes, recent development in the drug delivery system, boronic acid modified material for the separation for the glycoprotein, and recent developments in the immunoassays. The material and methods applied in this research are detailed in Chapter II. Chapter III presents results and discussion of the inclusion complex formation on the surface of the nanoporous gold milli-rod for the controlled release of doxorubicin (DOX). Chapter IV concerns the results and discussion of the study of selective enrichment of the glycoprotein on boronic acid modified NPG and controlled release of the protein. Chapter V presents the result of the polymer synthesis and characterization and Chapter VI presents the result of the fabrication of the adhesion layer free LSPR sensitive transducer to study carbohydrate-protein interaction.

1.2 Nanoporous gold

Nanoporous gold (NPG) is a porous three-dimensional (3-D) nanostructure of gold, usually having pore sizes in the range of a few nanometers to a few hundreds of nanometers [1-2]. This range of pore size includes mesopores (2 to 50 nm) and lower range macropores (51 to around 200 nm) in the International Union of Pure and Applied Chemistry (IUPAC) classification of porous materials [2-3]. NPG does not display perfectly circular pores, but mostly consists of open gaps (pores) between the interconnected ligaments [4]. There are many important properties of NPG, such as high surface-area-to-volume ratio, excellent conductivity, chemical and physical stability, biocompatibility, and plasmonic effects [5-7], which intrigue scientists for use in different fields of nanotechnology. Furthermore, NPG is a suitable surface on which to prepare self-assembled monolayers (SAMs) of functional derivatives of thiolated alkanes, further broadening the interests and applications [8-9]. NPG has been explored for application in catalysis [10], optical and electrochemical bio-sensing/assays [11-12], chemical sensing [13], drug delivery [14], carbohydrate synthesis [15], biomolecule separation and purification [16-17], fuel-cell development [18], surface-chemistry-driven actuation [19], and supercapacitor development [20].

NPG can be prepared either as a self-supported structure or as a solid-supported structure. Self-supported NPG is fragile to handle when compared to solid-supported NPG structures, and it is most commonly used in applications where high total surface area is desired. On the other hand, the solid-supported NPG structures are physically robust and are mostly used for electrochemical or optical applications. The well-established method to prepare self-supported NPG is by immersing an alloy of gold and other less noble metals (e.g., Ag, Al, Cu, Zn, Sn, etc.) in concentrated acid or base for different periods of time [1].

Thickness and composition of the alloy, dealloying time and temperature, and concentration of acid or base are the important factors in determining the size of the pores and ligaments [5-6]. For example, submerging the alloy in the concentrated nitric acid for an extended period of time can increase the pore and ligament diameters, due to surface diffusion of atoms causing merging and separation of ligaments [21]. Furthermore, post-annealing using heat can be used for tuning the size of the pores and ligament [5]. The challenges in this field include creating small diameter pores, while completely removing the more reactive unwanted metals, controlled tuning of pores and ligament sizes, and avoiding crack formation. The high surface area of NPG is desired for electrochemically detecting small concentrations of analytes, however, self-supported NPG is inconvenient to use as an electrode because of its fragile nature, lack of proper means of handling, and difficulty in separating the area of NPG from the adjoining metal conductor for the transfer of electrons. Solid-supported NPG electrodes that are prepared and modified using electrochemical techniques can resolve these problems [4].

Besides NPG, different other types of nanostructures of gold have been extensively explored and used in various applications [22-24]. These gold nanostructures can be grouped based on their dimensionality into 0-D (e.g., nanoparticles), one-dimensional (1-D) (e.g., nanorods, nanowires), two-dimensional (2-D) (e.g., nanofilms), and 3-D (e.g., nanocomposite materials, monolithic NPG) [21-24]. The 0-D and 1-D gold nanostructures are prepared as a colloidal solution by reduction of gold ions, whereas 2-D nanostructures are surface confined on a solid support using different sputtering or deposition techniques. Zero-dimensional (0-D) and 1-D materials have shown huge potential in clinical settings, mainly for in vivo studies, such as for sensing, imaging, drug delivery, etc. [24]. However, reproducibility of data often becomes challenging in these materials because of the chance of agglomeration and necessity of using a stabilizing agent on the surface. On the other hand, 2-D and 3-D gold nanostructures have many applications in a broad range of in vitro studies, ranging from biosensing [22] to organic synthesis [25]. The advantage of NPG is that it can be prepared in any dimension and shape retaining the properties of nanopores, and hence have wider possibilities than any other form of gold nanostructure. Being such an important and well-explored nanomaterial, there are already many general reviews on NPG [26-27], but there clearly is a necessity of reviews that are more specific, such as the use of electrochemical methods to study different aspects of NPG.

The dealloying process is one of the effective routes to fabricate nanoporous gold. The morphology of the dealloyed material is affected by the choice of the less noble metal given that it will have a different rate of dissolution than gold. An interconnected network of pores and ligaments remains after the selective dissolution of the less noble metals. The gold form random clusters on the surface that grow in size and ultimately become the ligaments of the porous structure, and this continues as diffusion originates from deeper inside the material.

Multi-cyclic electrochemical co-alloying/dealloying of two sacrificial metals with gold can be used for the fabrication of hierarchical NPG. Zhang et al. fabricated a hierarchical NPG film electrode by this method with high roughness factor of 1250 and they demonstrated its uses as an excellent catalyst for methanol oxidation.[28] Hierarchical NPG with bimodal ligament size distribution can be fabricated by means of selective dealloying of Al followed by dealloying of Ag from Au-Ag-Al alloy combined by annealing operation with the pore size distribution ranging from 10 to 100 nm in all three dimensions. Zhou et. al successfully prepared this nanostructure by a two-step dealloying process combined with an annealing operation and found excellent electrocatalytic activities and excellent sensing performance.[29] The combination of nanocasting and chemical dealloying strategies can be applied to fabricate monolithic porous gold materials with hierarchical bicontinuous morphology with combined macro and mesoporosity using bijels as templates [30].

Monolithic nanoporous gold with hierarchical bicontinuity can be fabricated by using colloidal bijels, as done by Obery et. al using a synergistic combination of nano-casting and chemical dealloying. [30] Robinson et. al fabricated bimodal nanoporous material from electrochemically templated deposition routes using polystyrene opal templates which enabled enhancement of Raman scattering signal compared with the unimodal porous gold substrate.[31] The fabrication of porous gold structure can be done by using microstructural templates like colloidal crystals. Mann et. al fabricated gold sponges by the polysaccharides-mediated reduction of $AuCl_3$ on the dextran as templates followed by calcination at 800°C [32].

1.3 Self-assembled Monolayers

Organic molecules having functional head-groups (e.g., thiols, disulphides, and amines) and tail groups at the end of hydrophobic chains (e.g., alkanes and polyethylene glycols) can easily self-assemble on noble metal surfaces lowering the free energy of the interface to form densely packed monolayer films, called self-assembled monolayers (SAMs) [33]. Different types of functional groups can be attached to the terminal end of the hydrophobic part depending on the nature of the study, through which further chemistry can be performed linking fields of the material chemistry and organic/biochemistry. SAMs of organosulfur compounds are the most studied SAMs to date because of strong thiol-gold bond formation [34-35]. A schematic diagram of an ideal alkanethiol SAM immobilized on gold surfaces having terminal functional groups is shown in scheme 1**,** and the chemisorption reaction between thiol and gold is shown in equation 1 [36].

$$\mathrm{R-SH} + \mathrm{Au}_n^0 \rightarrow \mathrm{R}-S^- - \mathrm{Au}^+ \cdot \mathrm{Au}_n^0 + \tfrac{1}{2}\mathrm{H}_2 \qquad (1)$$

One of the common methods of preparing SAMs of organosulfur derivatives is by immersing a metal substrate into dilute (1–10 mM) ethanolic solution of the desired organosulfur compound for 12–24 h under ambient conditions [37]. When the sulphur atoms of alkanethiols come in contact with a clean metal surface, the molecules start forming monolayers instantly; however, the molecules reorganize themselves if the metal surface is left in the solution over a longer period, minimizing the density of defects [38]. Alkyl chains of SAMs arrange themselves in trans-conformations with nearly 20–30° tilt from normal to the metal surface [35]. However, studies have shown that overall arrangement and binding of SAMs on gold surfaces depends on a number of factors, including length of alkyl chains, the nature and distance between terminal functional groups, concentration and purity of adsorbate, immersion time, and substrate morphology [37].

Self-assembled monolayers (SAMs) of the alkanethiols have found many applications in nanoscience and nanotechnology. SAM are molecular assemblies formed spontaneously on the surface by adsorption and are organized into ordered domains. The formation of SAMs on Au surfaces has enabled the fabrication of many different types of devices used in biosensing, nanomedicine, biophotonics, molecular electronics and catalysis. Alkanethiol SAMs can protected gold surfaces and are used to passivate and stabilize gold nanoclusters and nanoparticles in many fields of nanoscience research [39]. Alkanethiol SAMs can be prepared by exposure of clean gold surfaces to solutions of thiols in solvents such as ethanol [40-41]. Formation of a SAM is an important step because it can then be used to attach a variety of organic and biological species to the gold surface either covalently or by electrostatic interactions. The homogeneity and the nature of the packing of the SAMs is an important factor in their applicability and incomplete coverage of the gold surface by the SAMs can be detrimental for their use in biosensing and other applications [42].

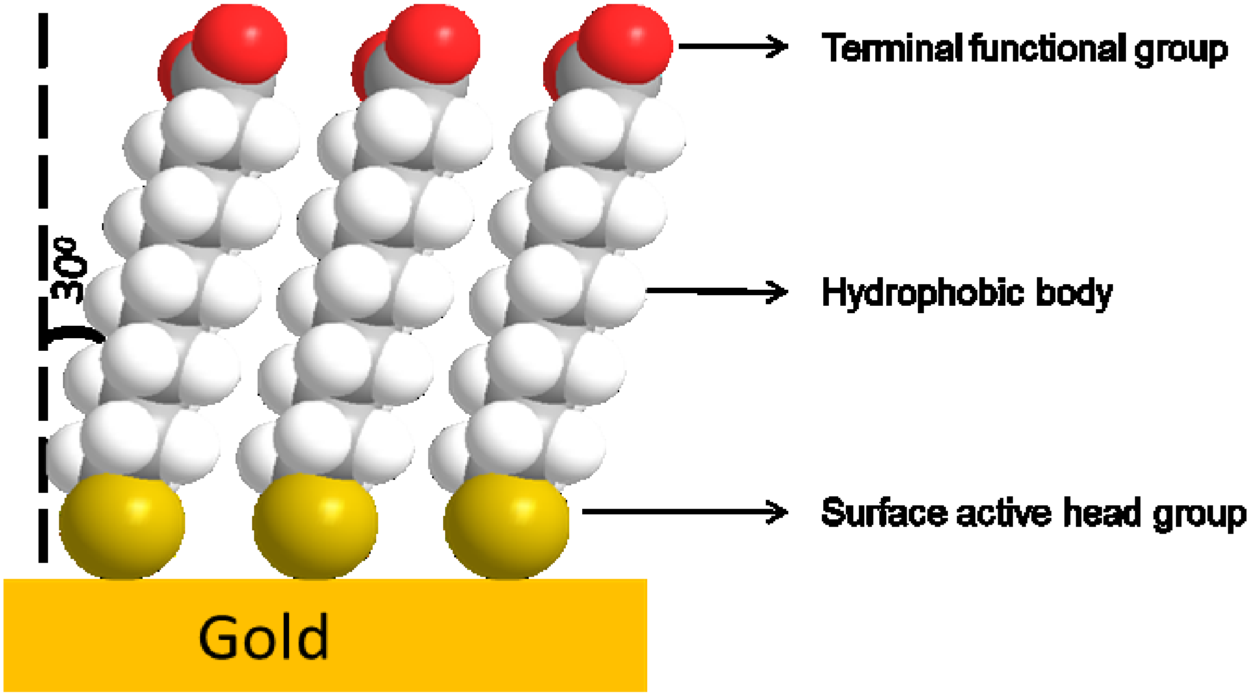

Scheme 1. Illustration of formation of a self-assembled monolayer on the surface of gold [43].

1.4 Boronic acid binding of cis-diols and carbohydrates

Glycoproteins are widely distributed and are one of the most important biomolecules which play vital roles in biological process such as molecular recognition, inter- and intracellular signaling, immune response and fertilization [1]. The state of glycosylation is related to the progress of cellular development and to disease states. Abnormal protein glycosylation is directly related to the occurrence of human diseases. However, the comprehensive analysis of glycoproteins is challenging due to the low abundance of many glycoproteins and heterogeneity of their glycans [44-45]. Molecular recognition of glycoproteins plays important roles in a range of biological processes. Boronate affinity is a powerful method for the selective capture and enrichment of cis-diol containing molecules such as many of the monosaccharides that are a part of the glycans on glycoproteins. Boronic acid forms five or six membered cyclic esters with a cis-diol molecule at high pH (basic conditions) and the cyclic esters will dissociate when the pH is lowered (acidic conditions) [46]. This pH dependent bonding to cis-diols makes boronic acids useful for the separation of carbohydrates and some other cis-diol molecules from complex media and mixtures. The advantages of the boronic acid materials are numerous including biocompatibility, rapid response rates, and long-term stability. *Cis*-Diol containing biomolecules are a large family of important compounds including glycoproteins, mono- and oligosaccharides, nucleosides, nucleotides, and many others. The ability of the boronic acid to bind cis-diol containing molecules reversibly at physiological pH enables binding in these biological applications [47]. The biological system and samples are very complex and targeting the specific moiety is difficult, when the concentration is very low. As boronic acids can reversibly bind with cis-diols, boronic acid as ligands are found in applications such as sensing, separation and self-assembly. Boronate affinity is not specific to glycans or the glycoprotein and will bind all cis-diol containing compounds available in the sample. However, boronic acid interaction are severely hampered by non-biocompatible binding pH, weak affinity, and non-specific selectivity.

Benzoxaborole-modified NPG monoliths offer a solution by avoiding tedious synthetic routes, binding at slightly basic and neutral pH and enhancement of the affinity by confinement within nanoscale spaces. Glycoproteins are one of the most important biomolecules and play vital roles in biological processes. The details of glycan structures are related to states of cellular development and to the progress of disease. Abnormal protein glycosylation occurs frequently in human diseases. However, the comprehensive analysis of glycoprotein is challenging due to the low abundance of many glycoproteins and heterogeneity of glycans. Derivatives of boronic acid were immobilized on the substrate and tested for the pH-dependent capture and release of cis-diol containing molecules and utilized to develop the affinity-based substrate using an NPG monolith. Among boronic acids that have been studied, benzoboroxoles have the novel property of preferential binding to the ring forms of saccharides, instead of to the linear isomers that are prefer by the other boronic acids [44, 48-50]. Benzoboroxoles derivatives undergo their covalent binding to the cis-diol containing molecules at physiological pH with higher binding affinity which makes this compound a potential substrate in the field of the glycomics [51], including the development of the receptors for glycans for use in biosensing and separations applications.

In this study, the interactions of glycan or glycoproteins with boronic acid are used to develop an NPG monolith substrate for isolation of glycoproteins. The NPG monolith can be used as the substrate for the chromatographic separation and extraction of the biomolecules after modification of the surface by a suitable self-assembled monolayer. The surface modified NPG monolith is free standing, has intact pore size within the range of tens of nanometers with the pore size able to be tuned according to the necessity of the experiment. NPG monolith is a nanostructured material produced by the removing less noble metal(s) from low carat gold alloy using selective dissolution by immersing in the concentrated nitric acid. The microstructure of NPG monolith has interconnected bicontinuous ligaments forming pores in the range of nanoscale.

1.5 Localized surface plasmon resonance-based biosensing

Localized surface plasmon resonance (LSPR) can be produced by nanostructures of different materials such as Au, Ag, Cu, C (e.g., graphene), Al, TiN, and alloys or composite of these materials. However, the most intriguing and investigated nanostructures for LSPR-based biosensing are those based on Au. Nanostructures of Au have many of the important properties required for designing an ideal LSPR-based biosensor. Their LSPR peak can be tuned from visible to NIR wavelength by simply controlling their shape and size. They can serve as supports for self-assembled monolayers (SAMs) of thiolated organic molecules, which can then be used for immobilizing biomolecules as receptors or directly capturing analytes. Additionally, they are biocompatible, chemically inert, and regenerable. Recently, the focus has been shifted from discrete nanostructures to nanostructured thin films of Au mainly because of three key reasons, (1) plasmonic-active nanostructured thin films (PANTFs) can generate both surface plasmon polaritons (SPP) and LSPR, which opens the possibility of using both types of sensors simultaneously, (2) PANTFs have better signal enhancement factor than discrete nanostructures in surface-enhanced Raman spectroscopy (SERS), and (3) PANTFs are conductive, unlike discrete ensemble nanostructures, therefore, electrochemistry can be introduced along with plasmonic for characterization and biosensing.

The PANTFs of Au on a suitable solid support can be prepared by applying different strategies before, during or after the deposition process[52]. The shape and size of nanostructures in the film can be controlled by predesigning the solid support using template-based techniques such as electron beam lithography (EBM), nanosphere lithography (NSL), nanoimprint lithography, and porous membrane-based lithography. A thin layer of Au can then be sputter or vapor deposited on as-prepared solid support to create PANTFs. Controlling the deposition parameters, such as deposition angle, temperature, etc., introduces more diversity to the nanostructures of the PANTFs. The nanostructures can also be constructed by post-deposition treatment of the Au film, such as by using thermal annealing, electrochemical deposition, and ion-beam lithography. However, the deposited Au films does not bind strongly to the silicon or glass support. For the PANTF to be used as a transducer of a biosensor, it should not only be sensitive but also be stable under the operating conditions. Therefore, different strategies have been explored to create stable PANTFs of Au on solid support. However, the trade-off between physical stability and sensitivity of PANTFs is an obvious hinderance for the development of LSPR-based biosensors.

The most common strategies for preparing PANTFs on silicon or glass substrates is to either use a metallic (e.g., Cr and Ti) or organic (e.g., silanes, polymers, etc.) adhesion layer between PANTF and substrate.[53-54] However, there are some problems associated with using these intermediate adhesion layers for PANTFs in LSPR-based biosensors or for modification to being used in other complementary technologies. Metals used as an adhesion layer have been known to dampen the LSPR signal and interfere in SERS enhancement.[55] Additionally, they lower the coverage of a functionalization agent due to interference with self-assembled monolayer formation. When used along with electrochemistry they create a galvanic cell, which may interfere with electrochemical response. On the other hand, silanes having terminal thiol or amine groups are the most commonly used intermediate organic molecules for attaching the gold nanostructures on silicon through the formation of oxides or hydroxides layer on the silicon surface.[53, 56] Although these molecular linkers act as an nondamping alternative to metal adhesive layers[57], they are not free from limitations. In our earlier work, we used epoxy as an adhesion layer for attaching a Au film on a Si-wafer.[17] The stability of the organic adhesion layer, however, is weaker compared to a metallic adhesion layer and also less compatible with many solvents and potentials, which are essential requirements for regeneration of PANTFs.

PANTFs on a silicon substrate have also been extensively used as a transducer for bioassay and biosensing applications, for example, patterning the surface with biomolecules[58], determining the binding constants of the interactions of different biomolecules, and label-free detection of bacteria, virus, and disease biomarkers (e.g., proteins and DNA)[59-60]. In addition to biosensing, stable Au films on silicon surfaces have widespread application in different technologies. For example, it is widely used in soft lithography for micro- and nano-scale patterning [61], and for attaching an integrated circuit on a circuit board. Despite the importance of intermediate adhesion layer free attachment of Au and silicon, a suitable strategy to prepare it at low temperature is lacking. Si-Au binding can be attained by heating 18.6% Si and 81.4% Au at the eutectic temperature of 363 °C. However, these conditions are not desired for making PANTFs as thin films convert to an island-type structure.

1.6 Electrochemical Impedance Spectroscopy

The current response of a circuit to an alternating voltage is known as the impedance and differs from resistance, which is the response to a direct voltage. In the technique of electrochemical impedance spectroscopy (EIS), the magnitude of the impedance can be plotted versus the frequency but due to a phase lag the impedance can have in-phase and out-of-phase components and is typically represented as a complex number [15]. The method of EIS has been around for more than 100 years [16]. The foundation for impedance spectroscopy was laid by Oliver Heaviside in the late 19th century [17]. In those early days of development, EIS was mostly employed to measure the capacitance of ideally polarizable electrodes which resulted in the development of various models for electrified interfaces [16-17]. Despite having such a long history, it took until the 1970s for EIS to be explored as a tool for electrochemical measurements, a step that is credited to development of instruments that combined a potentiostat with a frequency response analyzer [16]. Since then, EIS has been continuously developed and used to study various processes, such as metal corrosion [18], the transport of electrons in dye-sensitized solar cells [19], and for the development of biosensors [20]. The concept of the impedance is related to that of resistance (R), which is defined as the ratio of voltage (E) to current (I) in Ohm’s law. Ohm’s law only applies to the application of a direct voltage or current, does not describe the frequency and time-dependent phase shift that occurs between a sinusoidal current and voltage. When expressed as a function of time (t), the excitation sinusoidal potential is expressed as (E_t) = $E_0\mathrm{Sin}(\omega t)$ and the response current (I_t) = $I_0\mathrm{Sin}(\omega t + \phi)$, where E_0 and I_0 are the amplitudes of potential and current respectively, ω is radial frequency in radians/second (= $2\pi f$, where f is frequency in hertz), and ϕ is the phase angle difference between current and potential. Then impedance (Z) can be expressed as [21]

$$Z = \frac{E_t}{I_t} = \frac{E_0 \mathrm{Sin}(\omega t)}{I_0 \mathrm{Sin}(\omega t + \phi)} = Z_0 \frac{\mathrm{Sin}(\omega t)}{\mathrm{Sin}\,(\omega t + \phi)} \qquad (1)$$

Using Euler’s formula, the impedance can be expressed as a complex function [22],

$$Z(\omega) = |Z| e^{j\phi} = Z_0(\cos\phi + j\sin\phi) = Z' + jZ'' \qquad (2)$$

Where $j = (-1)^{1/2}$, and Z' and Z'' are the real and imaginary impedance, respectively.

Since EIS can probe the nature of the electrode by applying a small sinusoidal potential (2–10 mV) as a function of frequency, it became an ideal tool for studying biomolecular interactions. In the past decade, EIS has been heavily used for studying different types of biomolecular interactions, including carbohydrate–protein, protein–protein, and protein–DNA mainly because of the simplicity, cost-effectiveness and sensitivity of the technique [23-25]. This also led to its use in the detection of various disease biomarkers, bacteria and viruses as a biosensor technique [26]. EIS is also of particular interest because of its possibility to be used as a miniaturized point-of-care device. One of the critical issues for the biosensor detection is the background noise in the original sample, such as arising from untargeted proteins, lipids, electrolytes etc. in the serum sample. To overcome this challenge, the sample should either be purified or diluted. The dilution technique is a good way to reduce the background noise; unfortunately, the analyte of interest will also get diluted. With EIS, detection of a very small concentration of sample from nanomolar to attomolar range is possible [27].

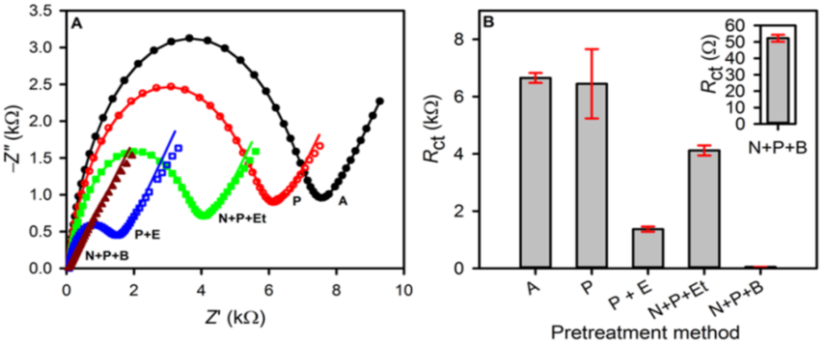

Figure 1.1 Comparison of bare GW before and after pretreatment A) Nyquist plots of the bare GW as-purchased (A) and after piranha cleaning (P), piranha + one-step chronoamperometric cleaning in 0.5 M H_2SO_4 providing potential of − 1.0 V for 1 min, 5 times (P + E), nitric acid + piranha + ethanol cleaning (N + P + Et), nitric acid + piranha + sodium borohydride + ethanol cleaning (N + P + B). B) Bar graph showing error bars in R_{ct} of different pretreatment methods, where error bars indicate the SD of four measurements [31].

EIS data are usually depicted as what is known as a Bode plot [28] or as a Nyquist plot [29]. In a Bode plot, impedance is plotted versus the frequency. In a Nyquist plot imaginary component of the impedance is plotted versus the real component of the impedance [30]. Each data point represents a different frequency and the frequency increases as the plot approaches the origin. Most systems will show a semi-circle at higher frequencies and a linear portion at lower frequencies. The semicircle region in Nyquist plot represents a charge or electron transfer limiting process occurring at the electrode surface. The diameter of the semicircle associated with this process is referred to as the charge transfer resistance. The diameter of the semicircle is equal to the charge transfer resistance (R_{ct}). The linear component of the Nyquist plot represents a diffusion-limited process. The Nyquist plot can be fitted with different types of equivalent circuits to obtain the required information. One of the most commonly utilized equivalent circuits for biosensing experiments is the Randles equivalent circuit, which consists of solution resistance (R_s), charge transfer resistance (R_{ct}), Warburg impedance (Z_w) and a constant-phase element or non-ideal capacitor (Q) [31]. The kinetics of the redox reaction of the probe at the electrode surface can be represented by R_{ct} and Q. However, Q is easily affected by the surface roughness of the electrode and chemical inhomogeneity [32-33], so R_{ct} is commonly used for Faradaic-based biosensing and Q is used for non-Faradaic-based biosensing [33]. On the other hand, Z_w, which represent the diffusion phenomenon, and R_s are the properties of the electrolyte solution and do not represent the dielectric properties of the electrode-electrolyte interface [34].

1.7 Electrochemical biosensor

Supported NPG is a suitable solid support for immobilization of different types of proteins (e.g. antibodies, enzymes, and lectins), carbohydrates, and RNA/DNA molecules because of its clean surface, robust structure, high surface area and biocompatible nature. These immobilized biomolecules on NPG, called receptors, can be used as biosensors for the detection of various analytes such as metal ions, small organic molecules, and other biomolecules. Because of the highly conductive nature of NPG electrode, it can be used as a transducer for the detection of analytes using different electrochemical techniques. The commonly used electrochemical techniques for NPG based biosensing are cyclic voltammetry (CV), chronoamperometry (CA), chronocoulometry (CC), electrochemical impedance spectroscopy (EIS), differential pulse voltammetry (DPV) and square wave voltammetry (SWV). Except EIS which is based on the impedance of the electrode, all the other techniques are based on the measurement of current or charge whose signal is directly proportional to the concentration of the analyte. DPV and SWV are pulsed based techniques, that are able to discriminate against the charging current by only sampling the Faradaic current at the end of the pulse. As a result, a very small concentration of a sample can be detected precisely. Electrochemical biosensors can be classified into types including DNA aptasensor, enzymatic biosensor, and immunosensor based on the type of receptor molecule used.

Recently, Zeng *et al.* prepared a regeneratable DPV based aptasensor on the NPG surface for the detection of Hg^{2+} with the limit of detection as low as 0.0036 nM [62]. A non-enzymatic amperometric glucose sensor is possible using a NPG electrode [63] or by modifying the NPG surface with other metals or metal oxides [64]. However, the NPG surface can be modified with glucose oxidase to use the synergistic catalytic properties of both NPG and glucose oxidase for the detection of glucose. In one such study, a high sensitivity of 12.1 μA mM^{-1} cm^{-2} with the linear response ranging from 50 μM to 10 mM was obtained with a low detection limit of 1.02 μM [62]. The prepared structure possessed strong anti-interference capability against many molecules present in human serum. NPG was used for detecting various cancer biomarkers based on sandwich-type immunosensing. NPG electrode immobilized on graphene surface was combined with horseradish peroxidase-encapsulated liposomes as labels and thionine as electron mediator for the detection of cancer antigen 15-3 using DPV [65]. The linear range of the immunoassay was found to be 2×10^{-5} to 40 U mL^{-1} with a limit of detection of 5×10^{-6} U mL^{-1}. Similarly, DPV was used to detect carcinoembryonic antigen (CEA) by immobilizing anti-CEA on NPG [66] and CV was used to detect prostate specific antigen (PSA) by immobilizing anti-PSA [67].

1.8 Bortezomib

Bortezomib (BTZ) is a proteasome inhibitor, used to treat hematologic tumors as well as other solid tumors. BTZ was approved by the US Food and Drug Administration (FDA) in 2003 as the first approved proteasome inhibitor.

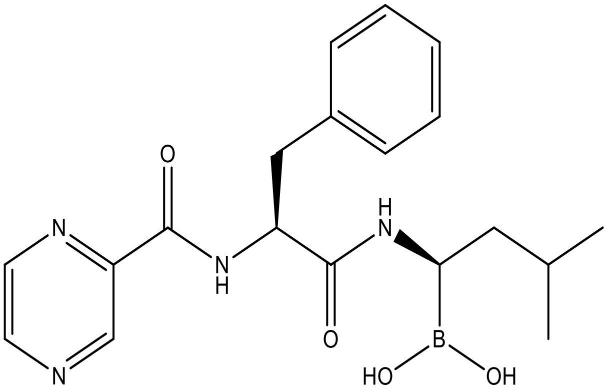

[(1R)-3-methyl-1-({(2S)-3-phenyl-2-[(pyrazin-2-ylcarbonyl)amino]propanoyl}amino)butyl]boronic acid

BTZ based therapies have become a milestone for the treatment of myeloma and some lymphomas. The use of BTZ for treating solid tumors therapy has been hampered by its poor stability and toxicity in vivo. Solid tumors, in particular, are often resistant to BTZ. BTZ is a dipeptide boronic acid derivative containing pyrazinoic acid, phenylalanine and leucine with boronic acid in its structure. BTZ is a boronic acid drug, which is easily chelated with reactive functional group present in the plasma protein. BTZ is a reversible inhibitor of the 26S proteasomes. The boronic acid group of the BTZ bind and form complex with the active site of threonine hydroxyl group in the β5-subunit, blocking the chymotrypsin like activity of the proteasome. It also binds the β1 subunit with lower affinity, inhibiting its (peptidyl-glutamyl peptide-hydrolyzing -like) PGPH-like activity, proteasome inhibition result in growth suppression and apoptosis induction in tumor cells [68-69]. Su et al. [47] conjugated BTZ onto the 1,2-diols on a catechol-PEG block copolymer. The catechol which contain cis-diols, can be used to bind and release the BTZ in a pH dependent manner. Under acidic conditions, BTZ can be released by hydrolyzing the cyclic boronate ester formed by the interaction between BTZ and the catechol unit. The interest in the drug delivery efficiency has risen to help improve efficacy of the available drugs and for the approving of new drugs. Boronic acid cis-diol interactions present opportunities for biological application and for drug delivery using the pH switchable interaction of boronic acid with cis-diol containing molecules. Boronic acid acts as a Lewis acid, and its affinity is strongly influenced by the electronegativity of neighboring groups. The physiological pH is constantly regulated throughout the body due to regular cellular metabolic activity. However, elevated metabolism in pathological environments such as tumors and inflammation lead to the dysregulation of the pH levels. It is widely accepted that extracellular pH (pH_e) of cancer cells is more acidic than normal cells. pH_e values of the normal tissue are in the range of 7.2-7.5. However, pH_e of tumor cells is mildly acidic in the range of 6.4-7.0. The endosomes have a pH of 5.0-6.8. The acidic pH can serve as a means to trigger intracellular drug delivery [70].

1.9 Monolithic Polymers

Polystyrene polymers have found applications in the separation and purification of pharmaceuticals, and in the solid-phase synthesis of polypeptides, oligosaccharides, glycans and oligonucleotides [71]. The development of new polymer supports and their use in organic synthesis has been growing in recent decades. Polymer supports in the form of beads have found wide use in supported organic synthesis. These beads may either be in the form of gels or can have a permanent pore structure [72]. Commercially available polymer supports are now widely available but have limitations; for example, in gel beads most of the reactive sites are located inside the bead and only become accessible after swelling in a solvent. The range of solvents that can be used with these beads is limited. Polystyrene-divinylbenzene (PS-DVB) with different degrees of crosslinking has found use in solid phase extraction chromatography, size-exclusion chromatography, high performance liquid chromatography, solid phase peptide and glycan synthesis, combinatorial chemistry, and enzyme immobilization due its good physical and chemical stability, high mechanical strength and high specific surface with regular morphology. The methods associated with the design of these porous materials depend upon the introduction of a porogenic agent (solvent, gas, small molecule or macromolecule) during the polymerization process, follow by its selective removal. Both the identity and amount of porogenic agent added can be varied to control the porous properties of the resulting polymerized material through the solvation of growing polymer chains during the polymerization process [73]. The choice of the porogen materials remains largely empirical rather than based on the empirical predicted considerations [74].

1.10 Cyclodextrin

Cyclodextrins are cyclic oligosaccharides containing six or more D-(+)-glucopyranose units. The structure of the cyclodextrin resembles a torus in which the interior part is hydrophobic due to the presence of glycosidic oxygens present in the cavity[75-76]. The α-, β-, and γ- cyclodextrin contain 6, 7, and 8 glucopyranose units and have internal diameters of 0.52, 0.66, and 0.84 nm, respectively[77]. The size of the cavity dictates the size of the molecules that can be encapsulated inside the cavity. Cyclodextrin can form inclusion complexes with hydrophobic molecules which are compatible with the size of the cavity, such as anthracycline drugs including doxorubicin (DOX) [78-79]. The driving forces for the formation of the CDs inclusion complex arises from apolar-apolar interactions between guest molecules and host cavities, the cyclodextrin ring strain release on complexation and van der Waals interactions[80].

The formation of self-assembled monolayers (SAMs) on gold surfaces is a common, inexpensive and versatile way to modify these surfaces to control their properties. Thiol modified CDs form SAMs on gold substrates [81-85]. The HS-β-CD appears to form a well-defined monolayer on gold [86]. Guest molecules of a size and shape compatible with the cavity of HS-β-CD should undergo inclusion on the SAM modified NPG wire.

Gao et al. reported that HS-β-CD forms an interfacial supramolecular SAMs on the gold surface and forms inclusion complexes with C_{60} [87].

1.11 Doxorubicin

Doxorubicin (DOX) is a chemotherapy drug in the anthracycline family of medications and was originally extracted from *Streptomyces peucetius.* DOX is one of the most effective anticancer drugs and has been successfully applied to treat hematological malignancies and a broad range of solid tumors. A major limitation of DOX is cardiotoxicity, with the total cumulative dose being the only criteria currently used to predict the toxicity. Severe side effects often restrict clinical application with an 11% incidence of acute cardiotoxicity within 2–3 days, possibly due to myocardial edema [88]. The stoichiometry for the β–CD/DOX complex has been determined as 1:1 [89]. The CDs are also able to prevent self-association of DOX in an aqueous medium that could diminish its anticancer activity [90-91]. The complexation of drugs with CDs is used to stabilize drug molecules and to enhance their bioavailability [92-93]. The formation of the thiolated β-cyclodextrin (HS-β-CD)/DOX inclusion complex arises from non-polar interactions and the ring strain released on complexation together with van der Waals interactions. Furthermore, the structural geometry and characteristics of CDs provide protection against oxygen, light, and other solvents as well as adjustable controlled release properties for drugs [93]. The formation of the inclusion complexes on the surfaces of NPG wire reduces the major barriers that limits the use of DOX such as the low water solubility, rapid phagocytic and renal clearance, and systematic toxicity [94]. Most of the available DOX delivery system, such as liposomes, polymeric micelles, or nanoparticles are usually administered intravenously. The major problem associated with the treatment of cancer by systematic chemotherapy is the difficulty of achieving therapeutic concentration of the drugs at the tumor sites without affecting the surrounding tissues. Due to the cardiotoxicity and narrow therapeutic index of the DOX, substantial increase in the systematic doses to achieve higher concentration of the drug at the targeted site is not possible and patients experience cardiotoxicity. Therefore, a localized and targeted drug delivery system is a logical choice and effective means of the minimizing the problems that may occur during the conventional methods.

1.12 Glycans and glycoprotein

Glycans, also called carbohydrates or as oligosaccharides, are the polymers of the O-glycosidic linkages of monosaccharides. Single sugar molecules such as glucose, fructose, mannose, and galactose are most widely known as the building blocks of the glycans. However, many other types of the monosaccharides exist in nature, and they assemble into polysaccharide chains to form complex branched shapes. Glycans are sources of the energy as well as having many other functions in the biological system. Glycans can be considered to have three main biological functions: (1) structural and modulatory properties, including nutrient storage and sequestration; (2) specific recognition by other molecules; and (3) molecular mimicry of host glycan [95]. Glycosylation is the most prevalent post-translational modification of proteins, and involves the complex and coordinated action of multiple enzymes. Glycans are found either glycosidically N-linked to asparagine or O-linked to serine and threonine. Glycans present on glycoproteins often have a pivotal role in protein folding, trafficking and protection against degradation, intracellular sorting, secretion, uptake, and cell and host microbial recognition [96]. However, glycoproteins also play crucial roles in tumor growth and metastasis. Glycan analysis of glycoproteins may be used as a diagnostic tool for the early detection of the diseases. Glycosylation of the protein is the most common post-translational modification that occurs by the help of glycosyltransferase enzymes. It has been estimated that 50% of human proteins are glycosylated through covalent bonds to asparagine to form N-linked glycan or serine and threonine residues to form an O-linked glycan. The detection, enrichment, separation, and identification of glycans, glycopeptides, and glycoproteins from biological samples are some of the major challenges in the world of glycoscience. The ionization efficiency of glycans is reduced by their hydrophilicity and this reduces their abundance in mass spectroscopic analysis [97]. To overcome this reduced ionization efficiency issue, an enrichment step is highly required. Glycoproteins may have multiples sites of glycosylation, a feature that complicates their characterization [98]. Also, the interpretation of the data obtained from mass spectroscopy (MS) can be time intensive and complicated [99]. The methods for glycan enrichment are boronate affinity, hydrazide chemistry, lectin affinity, hydrophilic interaction chromatography, and molecular imprinting. The major disadvantage of lectin separation is that for any single lectin, only a single glycopeptides presenting a specific saccharide unit can be purified. The hydrazide chemistry enrichment technique is expensive because it requires a large number of analytes and reagents. Hydrophilic interaction liquid chromatography (HILIC) is less specific. Boronic acid can form complexes with carbohydrates which involve covalent interactions that are reversible in aqueous solution depending on the pH of the solution. The use of boronic acid carbohydrate recognition molecules could provide an opportunity for the selective detection of specific sugars for future use in early diagnostics [100]. Boronic acid modified materials capture glycans via reversible covalent reaction between boronate and cis-diols under basic condition of pH around 8-9 and lowering the pH to acidic conditions allows the glycans to be released. The most general condition for the capture of the glycans is the pH should be greater than the pK_a of the boronic acid, however sialic acid binds to the boronate at lower pH. Porous materials can meet the research needs due to their high surface area, adjustable pore sizes, and tunable surface chemistry. Mesoporous silica and related materials, porous carbon, porous polymers, nanoporous gold, and porous alumina are widely use porous materials in carbohydrate chemistry and glycoscience. Materials with a hierarchical pore size distribution could become the materials of greatest interest in the field of glycomics because the proteins may pass through the large pores but be trapped inside the smaller ones, or may be unable to enter the smaller pores and have their diffusion restricted to the larger pores while smaller glycan molecules easily pass through the small pores. Matrix-assisted laser desorption/ionization time of flight (MALDI-TOF) mass spectrometry, and electrospray ionization (ESI) together with liquid chromatography are widely applied for the analysis in the improvement of the enrichment. Zhang et. al [101] synthesized 4-mercaptophenylboronic acid functionalized graphene oxide composites to selectively capture glycopeptides from the mixture with better selectivity and sensitivity for the N-linked glycopeptides. He et al. [102] reported the electrochemical detection of HRP by boronated affinity sandwich assay on gold nanoparticles combined with the graphene oxides with a linear range from 1 pg mL^{-1} to 100 ng mL^{-1} and low detection limit of 0.75 pg mL^{-1} from a real sample such as human serum. Liu et. al [103] reported the selective enrichment of trace glycoprotein on the branched boronic acid functionalized monolith. Nanoporous gold presents an opportunity for capture, enrichment, and release of glycans, for the development of the sensors, and for solid support synthesis of glycans after the modification of the surface with self-assembled monolayers. A stationary phase created by the modification of the Con A on the surface of NPG can be used in the chromatographic separation and extraction of intact glycoproteins. Stine et al captured target glycoproteins in the mobile phase by the reversible affinity of the immobilized lectins on NPG [104]. Molecular imprinting is the polymerization around the glycan templates using boronate affinity followed by the release of the glycan template and is a new and effective method for their enrichment[105]. Despite recent developments, a wide-ranging enrichment technique has not been developed yet.

An oligosaccharide which is covalently attached to the polypeptide chain exists in glycoproteins. Glycans are oligomeric/polymeric carbohydrate chains that are abundantly present naturally on the cell surface as a glycocalyx/glycoconjugate and inside the cell as different glycoconjugates [106]. Glycans can also be synthesized in the laboratory; however, synthesizing a complex glycan can be difficult and time-consuming. Naturally occurring glycans vary from very simple oligosaccharides to complex polysaccharides presenting different types of monosaccharides on the terminal end. These glycans are covalently attached to biological macromolecules, such as proteins and lipids by the process called glycosylation with the help of varieties of enzymes [107].

Besides being involved in designing the structure of living organisms and providing energy to them, glycan plays important roles in cell-cell adhesion, recognition, and transductions of signals through interactions with other glycans, glycan-binding proteins (GPBs) or lectins [108]. Although interactions of glycans with other macromolecules are continuously happening inside our body and are beneficial for human life, some interactions are fatal. Sialyl-Lewis^X, a glycan, is involved in the recognition and fertilization of egg cells by sperm at the beginning of life [109]. On the other hand, the same sialyl-Lewis^X along with other tumor-associated carbohydrate antigens (TACAs) aids in metastasis of cancer cells [110]. Similarly, HIV infects the host cell through high mannose-containing glycoprotein gp120 [111]. Additionally, glycans are also important for the stability and folding of different types diverse types of proteins. Alternation in number or type of monosaccharides, position, and stereochemistry of glycosidic linkages, and nature and location of non-glycan substituents could be useful as biomarkers for various diseases. It is particularly important to study and understand the binding affinities of glycans for the development of therapeutics and for using them as vaccines [112].

To this end, it would be convenient to present glycan units on solid supports mimicking cell surface or glycoconjugates so that we can perform in vitro experiments to understand glycans and their interactions with various analytes. Binding characteristics of different biomolecules such as antibodies, proteins DNA, and cells and pathogens such as bacteria, and viruses can be determined using glycan-immobilized surfaces [113]. Solid supports for glycan immobilization should be chemically inert and physically stable. Commonly utilized solid supports for glycan immobilization are glass, polymers, and gold. Glass and silicon can be modified by silanes, followed by binding with glycans whereas gold can form self-assembled monolayers of glycans directly or indirectly on its surface.

1.13 Lectins

Lectins are proteins that can recognize specific carbohydrate groups and play key roles in cell recognition and communication, host pathogen interactions, embryogenesis, and tissue development. Lectins can be found in animals, plants, fungi, and bacteria. The interaction of lectins with carbohydrates is of high interest due to their role in recognition in biological process as well as their use as tools for studying glycoforms, either in solution or on cell surfaces [114-115]. Many useful lectins can be easily obtained in large quantities via extraction from plants. Lectins have been widely used to isolate and separate glycans, glycopeptides and glycoproteins from biological samples by affinity chromatography and have been used as tools for investigating glycans in biological systems [116]. Lectins can bind specifically and reversibly, to multiple carbohydrate residues present on the surface of a cell membrane. Lectins have a broader specificity and hence ensure a wider coverage of the glycans. The individual lectin-glycan interactions are rather weak (dissociation constant, $K_d = 10^{-4} – 10^{-7}$ M) compared to typical antigen-antibody interactions (dissociation constant, $K_d = 10^{-8} – 10^{-12}$ M) [117]. Each lectin is a unique protein that has evolved to interact with distinct carbohydrate epitopes. Deriving from many different species, if grouped by the terminal sugar that the lectin binds, each will differ in the strength of binding due to affinity and avidity for the epitope. This may be due to the protein interacting with the rest of the underlying carbohydrate and/or carrier structure (N-glycan, O-glycan, glycolipid, etc.), or due to the presentation and density of the epitope [118]. Glycoproteins are frequently isolated and purified from protein mixtures using columns presenting lectins. After applying a protein mixture, unwanted proteins are washed off of the column and the glycoproteins bound to the lectins are then eluted with a sugar that competes for binding [119].

3. CHAPTER II: MATERIALS AND METHODS

2.1 *Reagents*: 10 carat yellow gold plates and 10 karat gold wires were purchased from Hoover and Strong, (Richmond, VA). Trace metal grade nitric acid was purchased from Fisher Scientific (Pittsburgh, PA, USA). Potassium dicyanoargentate (I), Potassium dicyanoaurate (I) (99.95%), Sodium dodecyl sulfate, N-tetradecyl-N,N-dimethyl-3-ammonio-1-propanesulphonate, ethylene glycol (98%), 2-hydroxyehtyl methacrylate (≤ 250 ppm monomethyl ether hydroquinone, 97%), 4-vinylphenylboronic acid (>=95%), L-ascorbic acid (Bioxtra), sodium borohydride (reagent grade, 99%), gold (III) chloride hydrate (99.995%, trace metal basis), Polyvinylpyrrolidone (Av. Mol. Wt. 40k), Ethyl alcohol (pure 200 proof, HPLC/Spectroscopic grade), D-sorbitol (99%), 4-aminophenyl phosphate monosodium salt, 8-mercaptooctanoic acid (95%), 4-vinylbenzoic acid (97%), 4-pentenoic acid (97%), Uridine (99%), 4-vinylaniline (97%), 4-vinylbenzylchloride (90%), Styrene (reagentplus contain 4-tert-butylcatechol as stabilizer, ≥ 99%), Divinylbenzene (tech., 80%), azobisisobutyronitrile (12 wt% in acetone), Fluorescein sodium salt, 4-aminomethylphenylboronic acid, Chlorosulphonic acid (99%), 2, 2'-azobisisobutyronitrile (98%), ethylenediamine, absolute, cysteamine hydrochloride, Span ™ 80, Concanavalin A type IV: FITC labeled, 3-aminophenylbornic acid, 4-aminophenylboronic acid (95%), poly(D, L-lactide-co-glycolide) lactide (glycolide 65:35, MW 40k-75k), lectin from peanut-arachis hypogaea, N-(3-dimethylaminopropyl)-N-ethylcarbodiimide hydrochloride, N-hydroxysuccimide (98%), Trizma base, 4-chlorostyrene (97%), 4-vinylaniline (97%) , 4-vinylbenzylchloride (90%), allylamine (99%), Tween ® 20, were purchase from Millipore Sigma (Milwaukee, WI, USA). HEPBS, Boric acid (99.97% trace metal basis), Phosphoric acid (≥ 99.99% trace metal basis), acetic acid (≥ 99.7%, ACS grade), Albumin from chicken egg white (ovalbumin) of ≥ 98% purity, bovine serum albumin (BSA) of ≥ 98% purity, holo-transferrin of ≥ 97% purity, immunoglobulin G (IgG) from rabbit serum, fetuin and asialofetuin from fetal calf serum and horseradish peroxidase (HRP) were purchase from Sigma Aldrich (St. Louis, MO) USA. Heptakis-(6-deoxy-6-mercapto)-β-cyclodextrin (molecular weight 1247.44 g mol^{-1}) was purchased from Cyclolab Cyclodextrin Research and Development Laboratory Ltd. (Budapest, Hungary). Doxorubicin hydrochloride (molecular weight 579.98 g mol^{-1}) was purchased from TCI (PA, USA). Gold wire was purchased from Ted Pella, Inc. (Redding, CA, USA) and EMS Microscopy Academy (PA, USA). Alkaline phosphate labeling kit-NH_2 was purchased from Dojindo Molecular Technologies, Inc. (Rockville, MD, USA). Fetuin A antibody (lyophilized) was purchased from Fitzgerald Industries International (MA, USA). Sambucus Nigra (Elderberry), Wheat germ agglutinin (WGA), Maackia amurensis Lectin II, Aleuria Aurantia Lectin, Lotus tetragonolobus lectin, were purchased from Vector Laboratories (CA, USA). 6’-sialyllactose sodium salt was purchased from Carbosynth (CA, USA). 8-arm PEG-SH (MW 40K), mPEG-SH (MW 10K) were purchased from creative PEGworks (NC, USA). Human α-1-acid glycoprotein was purchased from Novus (CO, USA). HS-PEG-COOH (MW 1k) was purchased from the Creative PEG Works (China). 5-amino-2-(hydroxymethyl)benzene boronic acid hemiester hydrochloride (95%) from Alfa Aesar (MA, USA).

2.2 *Instrumentation*: A Hummer VI sputter coater (Anatech Ltd) was used to sputter gold onto substrates. The AFM imaging was performed in tapping mode with a multimode AFM from Veeck (Santa Barbara, California, USA). Thermogravimetric analysis was done using a TA Instruments Q500 TGA (DE, USA). UV-visible absorbance spectroscopy was performed using a Cary 50 UV-vis spectrophotometer from Agilent (Santa Clara, CA). Scanning electron microscopy (SEM) was carried out using a JSM-6320F field emission SEM from JEOL (Peabody, MA, USA). Milli-Q water (18.2 MΩ.cm at 25 °C) was prepared using a simplicity UV system from Millipore Corporation (MA, USA). All the electrochemical experiments were 5carried out using either a Potentiostats/galvanostat model 273A or PARSTAT 2273 (EG and G Princeton applied Research, MA, USA) operated by PowerSuite software and a three-electrode cell having Ag/AgCl as reference electrode (CH Instruments Inc., Tx, USA) and platinum wire (99.997% purity, Alfa Aesar, MA, USA) as a counter electrode. The Nyquist plot of the EIS were analyzed using ZSimpWin software by fitting to Randles equivalent circuit, R(Q[RW]0. Bruker Advance 300MHz NMR Spectrometer (CA, USA), and FTIR spectroscopy (Thermo Fisher Scientific, MA, USA) were used to characterize the formation of the inclusion complex. The LSPR spectra were acquired using reflection geometry. It consists of a light source (HL-2000 -BAL, Deuterium-Halogen Light, Ocean Optics), spectrometer (Jaz, Ocean Optics), a reflection probe(Ocean optics, QR400-7-SR), and a home-built Teflon flow cell (volume 0.6 mL) with a quartz window. The data obtained were plotted using SigmaPlot 12.0 (Systat Soft-Ware Inc.). Sputtering coating of the gold on the silicon wafer were done using sputter coater (Hummer VI, Anatech Ltd, NJ, USA). The morphology of sputtered thin Au film was compared using x-ray diffractometer (XRD, Ultima IV, Rigaku, MA, USA). Surface area and pore size analysis were done using a Beckman Coulter SA-3100 Gas Adsorption surface area and pore size analyzer (Beckman Coulter, Inc. CA, USA) and a standard BET sample holder (3cc RapiTube, model number 7215 006B, Beckman Coulter, Inc. CA, USA) were used to hold the sample.

2.3 *Fabrication and characterization of NPG wire monolith*: Commercially available gold alloy wire was cut to the desired size (0.2 mm diameter and 5 mm length) and then dealloyed by placing it in a concentrated nitric acid bath for 48 h with replenishing of the acid solution after 24 h. The length of the wire was chosen for experimental convenience and in practice can be varied. The sample was thoroughly rinsed with Milli-Q water. Dealloyed monolithic wires were then rinsed thoroughly with Milli-Q water followed by rinsing with ethanol. The general structure and surface morphology of the NPG wire was studied by SEM and the interior surface was also imaged after cracking the sample into pieces using mechanical force.

2.4 *NPG-coated gold wire*: NPG-coated gold wire was fabricated by electrochemical deposition of an alloy of gold and silver from a solution of the precursors ($K[Au(CN)_2]$) and ($K[Ag(CN)_2]$) in the molar ratio of 3:7 on 5 mm long and 0.2 mm diameter gold wires. An electrochemical cell consisting of a three-electrode system with platinum (Pt) as an auxiliary electrode, silver/silver chloride (Ag/AgCl) as reference electrode and gold wire (with and without NPG) as working electrode was used. The electrolyte solution is the mixture of 15 mM $K[Au(CN)_2]$ and 35 mM $K[Ag(CN)_2]$ in 0.25 M sodium carbonate. The electrolyte solution was deaerated by bubbling argon gas for 10 min and the electrochemical deposition of the alloy thin coating was performed at room temperature. The variables of deposition time and potential were fixed according to experiment. The as prepared alloy coated electrode was then dealloyed by immersion in concentrated nitric acid or by electrochemical dissolution in 1 M nitric acid solution depend upon the experimental condition. After completion of the dealloying, the NPG was then rinsed with Milli-Q water and store in ethanol until further use.

2.5 *Fabrication of nanoporous gold monolith plates*: Commercially available 0.25 mm and 0.5 mm thick ten carat yellow gold plates (41.7% Au, 20.30% Ag, and 38.0% Cu) were cut into the desired dimension for thermogravimetric analysis, and for solution depletion with spectrophotometric detection. The cut pieces were than dealloyed by placing them in a concentrated nitric acid bath for 48 h and replenishing the acid solution after 24 h. (CAUTION !!! HNO_3 is a very strong acid, extra care is needed to handle). A homemade Teflon plate was used in dealloying to ensure that all the surfaces of the Au alloy plates were exposed to acid. Dealloyed monoliths were rinsed thoroughly with Milli-Q water to neutral pH followed by rinsing with ethanol. NPG monoliths were dried with N_2 gas. NPG monoliths were kept inside a vacuum desiccator until used.

2.6 *Fabrication of ultra-flat gold*: Ultra-flat gold on mica was fabricated by sputtering gold onto the mica surface followed by thermal annealing. Hummer VI sputter coater (Anatech Ltd) was used to sputter gold onto the mica for 20 min, adjusting the current to 10 mA to obtain a thickness of about 200 nm. Then gold-coated mica was annealed at 350 °C for 3 h in the furnace (GSL-1500X, MTI corporation (CA, USA) in the presence of Argon gas. After cooling, gold-coated mica surface was used to immobilized HS-β-CD and then DOX.

2.7 *Preparation of NPG on flat silicon plate*: Flat gold on a silicon surface was prepared by sputtering gold on the silicon surface. The surface of the silicon wafer was scratched with fine grade silicon carbide abrasive sheet (3M^{TM}) and etched by submerging in 10 M NaOH for 20 min. Then the surface was thoroughly cleaned with Milli-Q water, rinsed with chloroform first and then with methanol, dried at 110 °C for 10 min and quickly transferred to the sputter coater (Hummer VI, Anatech Ltd). The wafer was sputter coated with Au for 20 min, adjusting the current to 10 mA to obtain a thickness of about 200 nm. The as-prepared thin film was left for least 17 h on room temperature for improving stability before electrodeposition. Potentiostats 273A (EG&G Princeton Applied Research) was used for electrodeposition of nanostructured Au on thin Au film to create NPG on the gold surface. For all the electrochemical experiments, a standard three-electrode electrochemical setup was used with a sputtered thin Au film working electrode, Ag/AgCl (KCl Satd.) reference electrode, and platinum wire (99.997% purity, 0.5 mm diameter) counter-electrode. Nanostructures were created on the sputtered thin Au film by applying potential of −1.2 V for 60 s followed by −1.6 V for 30 s using 50 mM potassium dicyanoaurate(I) electrolyte in 0.25 M sodium carbonate at room temperature. Nanostructures were created on the sputtered thin Au film by applying potential of −1.0 V for 90 s using 50 mM potassium dicyanoaurate(I) and potassium dicyanoargentate (I) electrolyte in different ratios of gold and silver salt in 0.25 M sodium carbonate at room temperature.

2.8 *LSPR Analysis*: All the LSPR spectra were recorded using UV-Vis reflection geometry. The setup consists of a light source (DH-2000-BAL, Deuterium-Halogen Light, Ocean Optics), spectrophotometer (Jaz, Ocean Optics), a reflection probe (Ocean Optics, QR400-7-SR), and a home-built Teflon flow cell (volume 600 μL) with a quartz window. The distance between probe and the NPG on the silicon surface was kept constant to 4 mm. The reflection spectra obtained were reciprocated and plotted versus wavelength using SigmaPlot 12.0 (SysTest Software Inc.).

2.9 *Preparation of solution of thiolated compounds*: SAM preparation on the surface of the gold were done by following established standard protocol. These gold surfaces were immersed in 1 mM ethanolic solution if experiment condition were otherwise of alkanethiols for overnight at room temperature. The resulting SAMs on the gold surfaces were copiously rinsed with ethanol, water and relevant solvent before performing any experiments. All thiolated compound used to form SAMs in this study were dissolved in HPLC grade ethanol and DMSO depending upon the experiments.

2.10 *Preparation of protein solutions*: Lyophilized powder of proteins (lectins: Con A, PNA, SNA, SBA; glycoproteins: OVA, HRP, Fetuin, Asialofetuin, Holo-transferrin: non-glycoproteins: BSA) were dissolved in buffer solution of the different pH. Concentration of the protein solution were determined using Beer-Lambert equation A280 = $\varepsilon(280) \times C \times L$, where A280 is the absorbance 280 nm using UV-spectrophotometer, C is the concentration in μM, L is the 1 cm path length and ε_{280} is the extinction coefficient of the protein at 280 nm in units of μM^{-1} cm^{-1}. The protein solutions were immediately used after preparation[120]. ε_{280} values of proteins were calculated as the weighted sum of the ε_{280} value of Trp, Tyr, and Cys using the proposed equation: ε_{280} (M^{-1} cm^{-1}) = no. of Tryptophan × 5500 + no. of Tyrosine × 1490 + no. of Cysteines × 125 [120]. The values were as follows: ε_{280} (Ova) = 0.031525 μM^{-1} cm^{-1} [120], ε_{280} (BSA) = 0.042925 μM^{-1} cm^{-1} [120], ε_{280} (IgG) = 0.21 μM^{-1} cm^{-1} [120], ε_{280} (Fet) = 0.01984 μM^{-1} cm^{-1} [121], ε_{280} (Asf)

= 0.04525 μM^{-1} cm^{-1} [122], ε_{280} (HRP) = 0.02525 μM^{-1} cm^{-1} [123]. The protein solutions were immediately used after preparation.

2.11 *Preparation of boronic acid solutions*: 3-amino phenylboronic acid, 4-aminophenylboronic acid and 5-Amino-2-(hydroxymethyl)benzeneboronic acid hydrochloride solution were prepared in HPLC grade ethanol and DMSO depending upon the experiment.

2.12 *Formation and analysis of monolayers via self-assembly*: Monolayers were formed by placing the NPG wire into 1 mM solution of HS-β-CD compound in DMSO and water in a 9:1 ratio. Reductive desorption for estimation of surface coverage of the HS-β-CD SAM was carried out in 0.5 M NaOH solution that had been degassed with argon for 10 min. Cyclic voltammetry scans were performed for HS-β-CD immobilized on separately prepared gold wires of length 5.0 mm and diameter 0.2 mm. The experiments were done using a three-electrode arrangement in a glass cell containing 4 mL of solution, a platinum wire as counter-electrode and an Ag/AgCl (sat'd. KCl) as a reference electrode. The CV scan was performed between 0 and −1.3 V (vs. Ag/AgCl) at the scan rate of 20 mV s^{-1}. Furthermore, thermogravimetric analysis (TGA) was used to quantify the monolayer formation based on the mass loss of organic molecules from the NPG sample.

2.13 *Loading of DOX in HS-β-CD modified NPG wire*: 1 mM DOX solution was prepared in acetate buffer and 0.5 mL of solution was added to the HS-β-CD modified NPG wire for overnight to form the inclusion complexes. The amount of drug loaded on the wire was quantified by TGA and the solution depletion method using UV-Vis spectroscopy.

2.14 *Formation of inclusion complex of DOX and HS-β-CD*: Formation of inclusion complexes with DOX with HS-β-CD was confirmed by ^{1}H NMR spectra at 300 MHz The

^1H chemical shifts are referenced to the signal of the residual tetramethyl silane (TMS) for solutions in $CDCl_3$. Fourier transform infrared spectroscopy (FTIR) was used to confirm the formation of the inclusion complex. The FTIR spectra of DOX and HS-β-CD were taken in solid state. Inclusion complex formation was achieved by mixing equimolar amounts of DOX and HS-β-CD in water and DMSO (10:90) followed by the evaporation of the solvent.

2.15 *In vitro DOX release study*: DOX immobilized inside HS-β-CD -modified NPG wires were placed in 5 mL of PBS (pH = 7.4), acetate buffer (pH = 5.5), and 10% calf serum solution in PBS (pH = 7.4) at 37 °C. 0.5 mL of the buffer media were taken and the amount of DOX released from the NPG monolith was quantified from absorbance of the band at 480 nm of DOX at various time intervals and replaced with equal volume of fresh buffer. The average of three measurements of DOX released was taken.

2.16 Electrochemical Characterization: Electrochemical measurements were performed using potentiostats with the electrochemical cell containing three electrode system. The formation of the SAM, immobilization and interaction study in the gold electrode and flat gold on the silicon wafer were monitor by EIS, CV, DPV and SWV.

2.17 Atomic force microscopy imaging: AFM images were collected for characterization morphology ultra-flat gold, interaction of boronic acid modified gold with glycoprotein, formation of the inclusion complex and morphology of Si wafer. NanoScope III microscope and silicon cantilevers having force constant 40 N/m and resonance frequency of 300KHz were used for the imaging in tapping mode. The images were processed using Gwydion software.

4. CHAPTER III RESULTS AND DISCUSSION

A pH SENSITIVE HS-β-CD MODIFIED NPG FOR CONTROLLED RELEASE OF DOXORUBICIN

3.1 *Characterization of NPG wires*: NPG wires were stored in pure ethanol. Surface characterization of the NPG wire was performed by SEM. The NPG wire was also broken into smaller pieces and the cleaved fragment was also imaged using SEM to characterize the bulk of the NPG wire and to confirm interior porosity. Figure 3.1a shows the NPG gold wire after dealloying. Figure 3.1b shows the cross-section of NPG wires and Figure 3.1c and 3.1d shows the surface of the NPG wire. The average pore size on the surface of the NPG wire is determined as 32 ± 5 nm (n=36) and the average pore size seen in the cross-section of the NPG wire was found to be 55 ± 10 nm (n==38) . These pore dimensions make the NPG wire highly suitable materials for loading of DOX following modification with HS-β-CD.

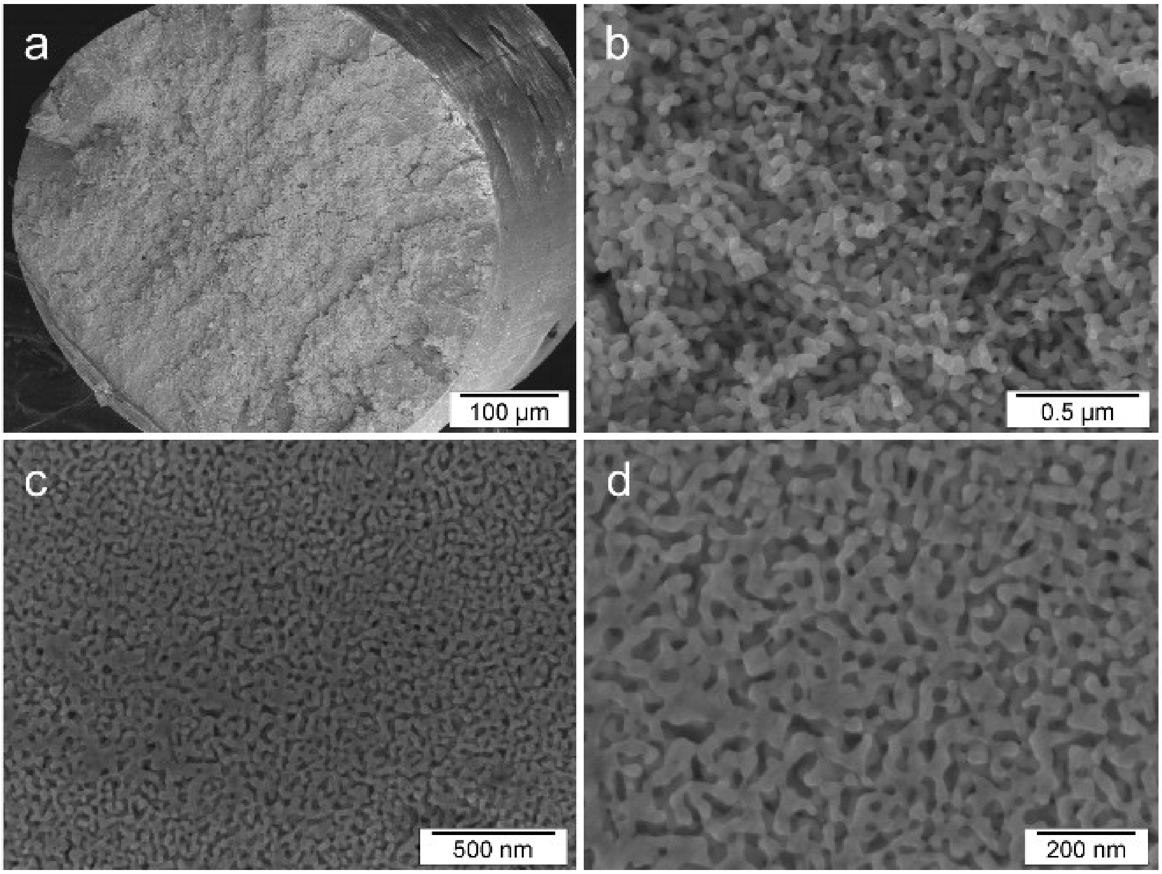

Figure 3.1. Scanning electron microscopy images of a representative NPG wire (a,b) cross-sectional view at low and high magnification, respectively and (c,d) top view at low and high magnification, respectively.

3.2 *Electrochemical determination of effective surface area and reductive desorption of HS-β-CD SAM*: Electrochemical characterization of NPG wire was done by cyclic voltammetry. Estimation of the effective surface area was done using the gold oxide stripping method in 0.5 M H_2SO_4 at a scan rate of 50 mVs^{-1} as shown in Figure 3.2. The charge passed during the gold oxide reduction was measured by integrating the charge under the oxide reduction peak and the charge in µC was then divided by the reported conversion factor of 450 µC cm^{-2} [12]. The surface area of NPG wire was found to be 6.4

± 0.54 m^2 g^{-1}. The amount of HS-β-CD adsorbed on the surface undergoes reductive desorption by breaking the Au-S bond in NaOH solutions [124]. The surface coverage of HS-β-CD was calculated as 4.32×10^{-11} mol cm^{-2}, which is lower than the value obtained on flat gold electrodes by Kaifer et al. of 7.5×10^{-11} mol cm^{-2} [82] The reductive desorption data are as shown in Figure 3.3 The complex inner structure of NPG presented regions of positive curvature around ligaments and of negative curvature near where ligaments join. There are reasons that one could justify lower coverage inside NPG such as impartial coverage due to hindered diffusion during SAM formation and some portions of the inner surfaces being inaccessible or unsuitable for binding of the molecules to the surfaces such as perhaps at the highly curved intersections of ligaments.

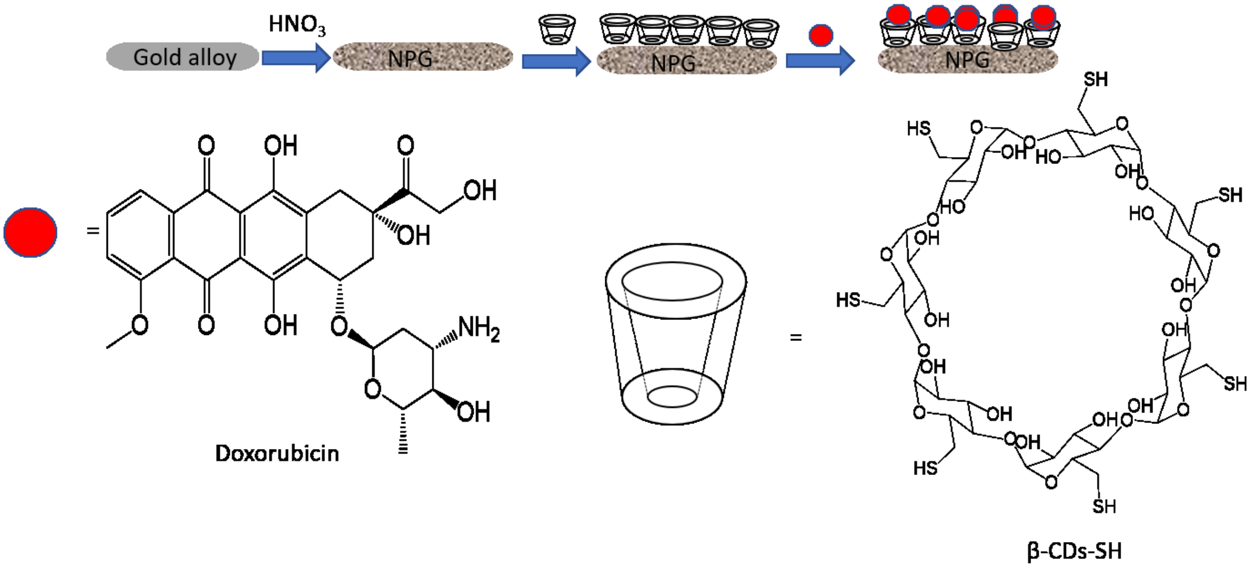

Scheme 2. Schematic diagram of formation of the inclusion complex of DOX and HS-β-CD on the surface of NPG milli rod.

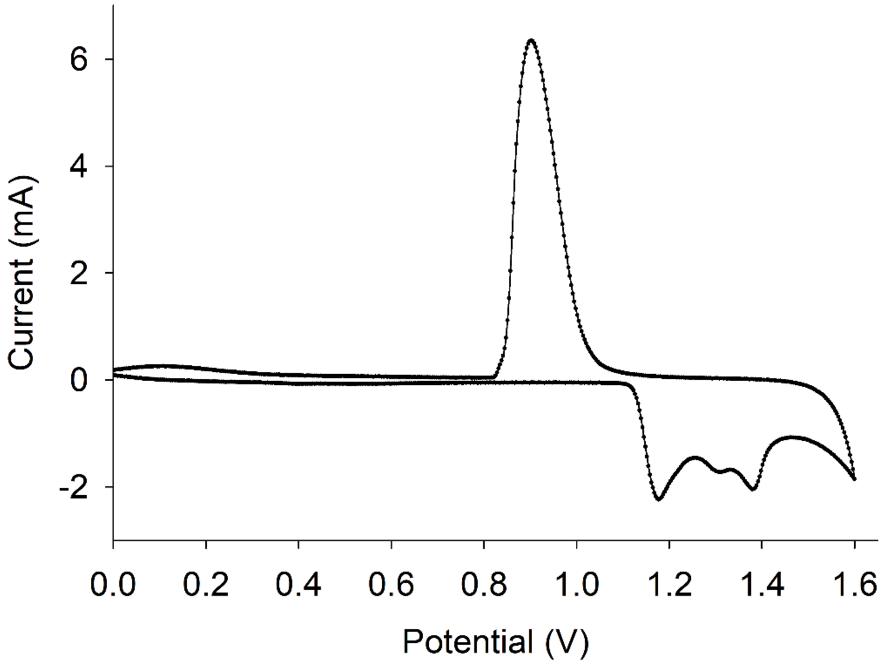

Figure 3.2. Cyclic voltammogram of NPG wire. Scans were performed in 0.5 M H_2SO_4 at 50 mV s^{-1} vs Ag/AgCl reference electrode.

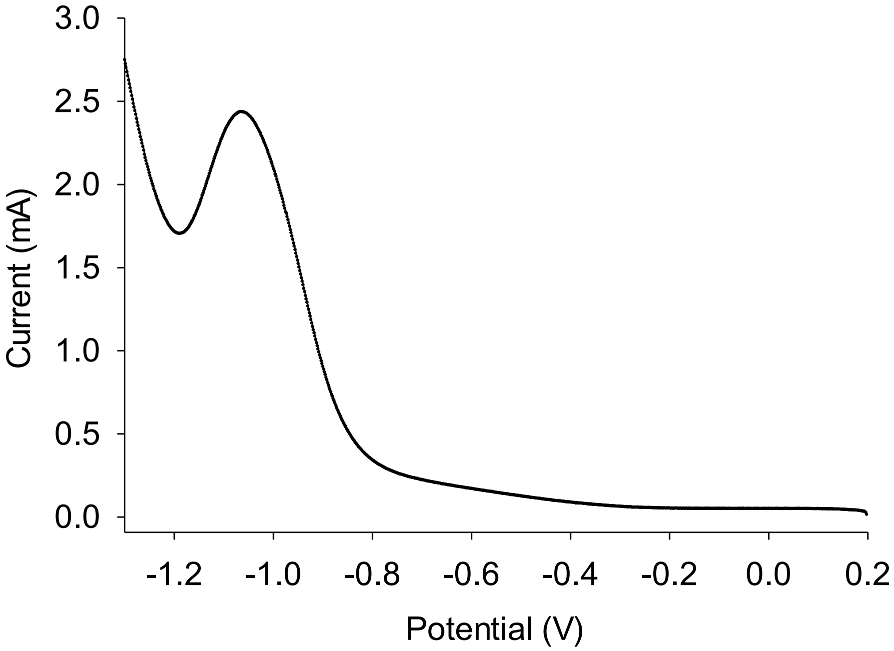

Figure 3.3. Reductive desorption of thiolated β-cyclodextrin in 0.5M KOH at 50 mV s^{-1} vs. Ag/AgCl reference electrode.

3.3 *Atomic force microscopy analysis of the HS-β-CD SAMs on ultra-flat gold surfaces*: Atomic force microscopy was used for the determination of thickness of HS-β-CD monolayers on the flat gold surface by scanning across the substrate (Figure 3.4). Ultra-flat gold surfaces were prepared by the sputtering of gold onto mica surfaces followed by annealing at 350 °C for 3 h. Tapping mode AFM was used to image the flat gold, and the SAMs of HS-β-CD before and after their exposure to DOX. The surface roughness of the flat gold surface increased after immobilization of HS-β-CD and the roughness slightly decreased after formation of inclusion complexes with DOX. The average roughness of flat gold surface was observed as 0.85 ± 0.17 nm. After formation of the SAMs of the SH-β-CDs, the roughness of the flat gold surface increased to 1.5 ± 0.07 nm and the roughness slightly decreased to 1.3 ± 0.06 nm after interaction with DOX due to formation of inclusion complexes on the surface.

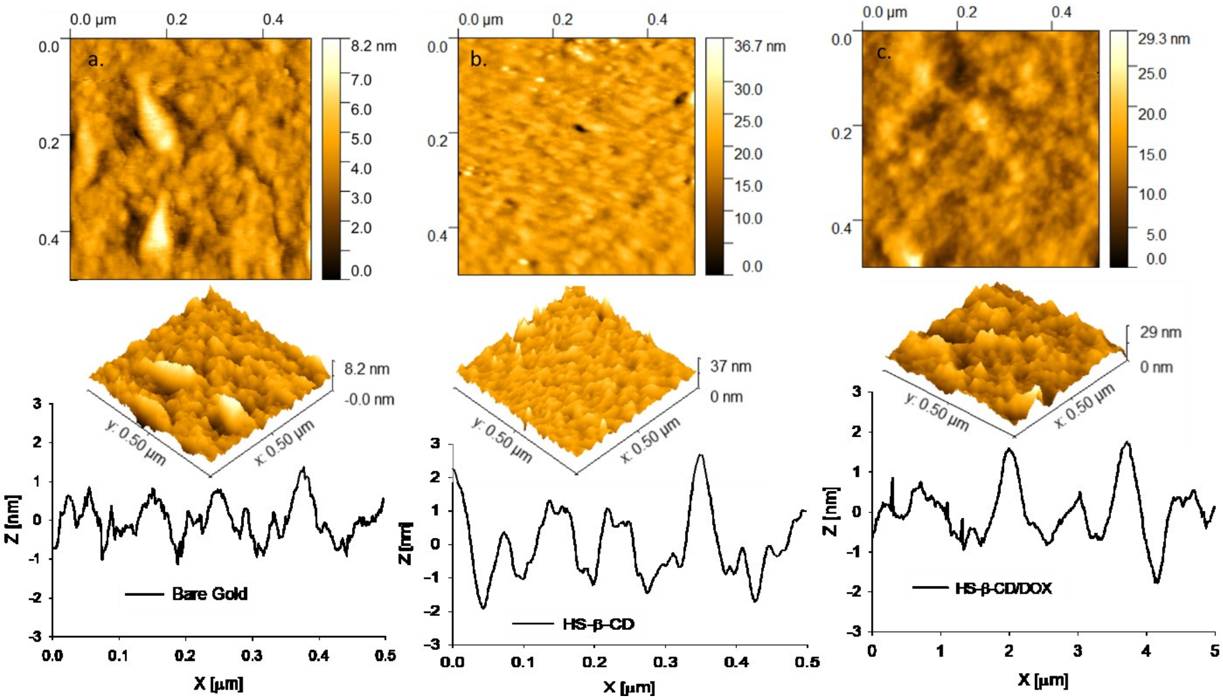

Figure 3.4 AFM topographs of bare gold (a) HS-β-CD modified gold (b) and DOX containing HS-β-CD modified gold (c). Image size is 0.5 µm × 0.5 µm. The 3D images and the roughness, as revealed from line scans is shown in the lower panels respectively.

3.4 *DOX loading into NPG*: The amount of DOX encapsulated into the HS-β-CD-modified NPG was studied by thermogravimetry and spectrophotometry. The specific surface area of the NPG wire was determined to be 6.4 ± 0.54 m^2 g^{-1} (64.66 cm^2 mg^{-1}). The total surface area of NPG wire used for the drug loading was calculated as 310 cm^2. NPG wire modified with HS-β-CD and complex of HS-β-CD and DOX were subjected to thermal decomposition up to 600 °C to determine the surface coverage. Figure 3.5 shows the weight loss verses temperature curve of HS-β-CD-modified NPG and DOX–HS-β-CD-modified NPG. The amount of weight loss after formation of SAMs of HS-β-CD on the NPG wire was found around 12 µg per 5 mg of the NPG wire and the weight loss after

DOX encapsulation was found to be 30 μg per 5 mg of NPG wire. The surface coverage calculation of HS-β-CD on the NPG wire calculated from the TGA analysis was found to be 3.18×10^{-11} mol cm^{-2} which is moderately lower than the surface coverage calculated from the reductive desorption methods. Thus, the total amount of DOX captured on the NPG wire was around 18 μg per 5 mg of NPG wire. These masses correspond to a ratio of ~3.2 DOX molecules per HS-β-CD molecule, indicating that many DOX molecules are physiosorbed inside the NPG in ways that cannot only involve direction binding by the HS-β-CD molecules. The mass of 12 μg of HS-β-CD was found to correspond to a surface coverage of 3.18×10^{-11} mol cm^{-2}. The coverage is less than determined by reductive desorption but is in a comparable range. It is possible that some residue remains inside the NPG after pyrolysis resulting in an incomplete loss of SAM mass to account for the discrepancy.

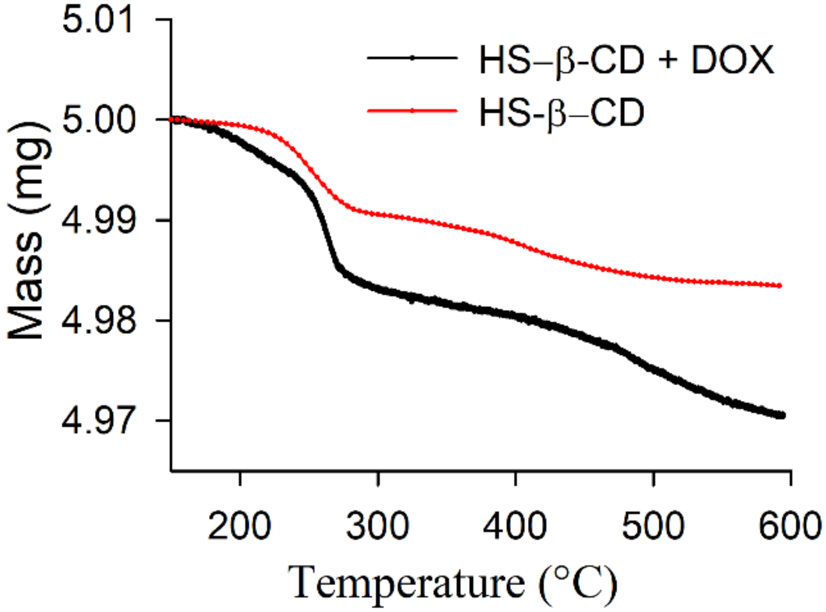

Figure 3.5 Thermogravimetric curves of thiolated β-cyclodextrin (black) and DOX–thiolated β-cyclodextrin (red) modified NPG wire.

3.5 *Formation of inclusion complexes between DOX and HS-β-CD*: UV-Vis absorbance experiments were used to demonstrate formation of inclusion complexes between guest (DOX) and host HS-β-CD molecules [92, 125]. Formation of CD-drug complexes has been investigated as a method to stabilize drug molecules and improve their general bioavailability [126]. HS-β-CD is not soluble in water but has solubility in DMSO. The solubility of DOX in water is reported as 10 mg mL^{-1} (17.2 mM) and as 100 mg mL^{-1} in DMSO (172 mM) and thus DOX is highly soluble in DMSO [92, 125, 127]. DOX molecules partially or fully encapsulated in the HS-β-CD cavity often exhibit changes in their absorbance [127-128]. The UV-Vis spectra of 25 μM DOX in DMSO in the absence and presence of various concentrations of HS-β-CD in DMSO were recorded. As displayed in Figure 3.6, with increasing concentration of HS-β-CD, the peak intensity of DOX increased while the absorption bands remained unchanged. This might arise from the individualization of DOX molecules due to breaking of hydrogen bonding, implying formation of host-guest inclusion complexes [128-131]. To prove the formation of inclusion complexes, six different concentration of HS-β-CD of 250 μM, 500 μM, 750 μM, 1.0 mM, 1.5 mM, and 2.0 mM were used and the absorbance of DOX was monitored at 480 nm. Enhancement in the intensity may be due to isolation of DOX from the solvent environment as shown in figure 3.7.

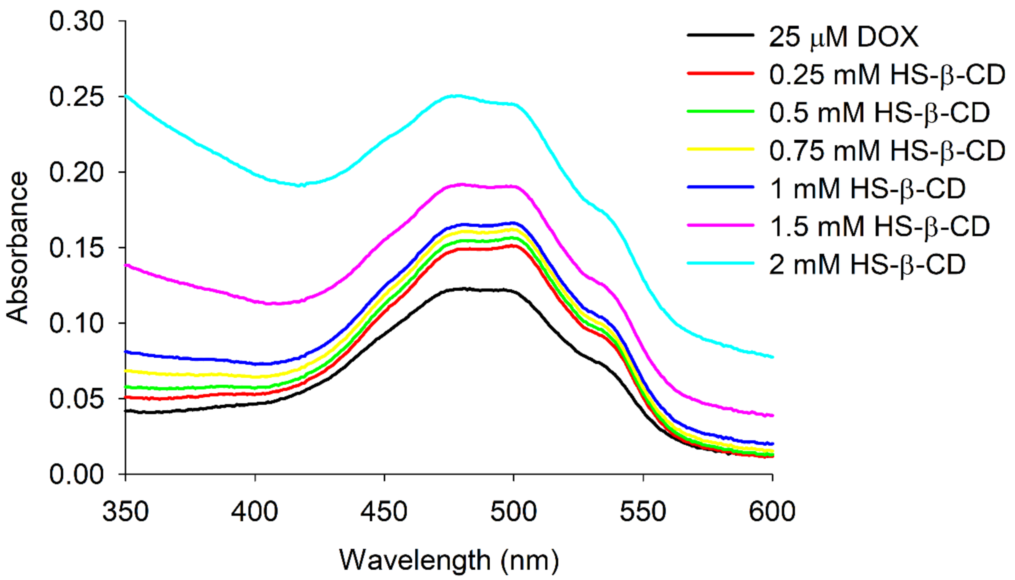

Figure 3.6. UV-Vis spectra of DOX (25 μM in DMSO) with added amounts of HS-β-CD.

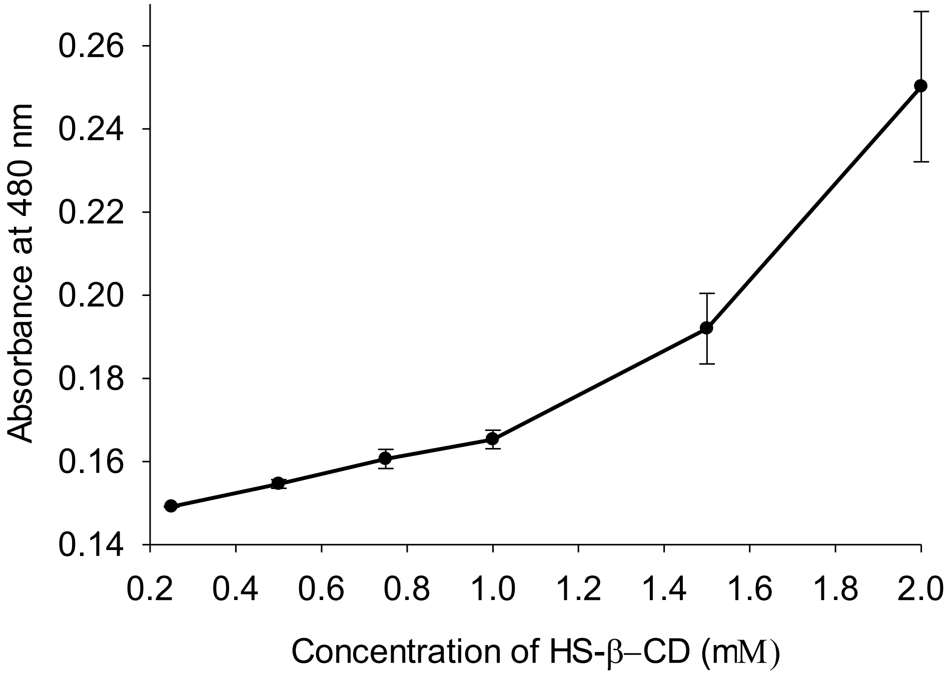

Figure 3.7 Absorbance at 480 nm versus added concentration of HS-β-CD in 25 μM DOX solution in DMSO. The error bars are the standard deviation for n=3 determinations.

3.6 *Characterization of the inclusion complex*: Formation of inclusion complex of DOX with HS-β-CD can be studied by the proton nuclear magnetic resonance spectroscopic method (^{1}H NMR) [127, 130], as shown in Figure 3.8. The influence of the host HS-β-CD on the ^{1}H-NMR spectra of the guest [130], and vice versa, were studied in deuterated DMSO on the basis of a 1:1 molar ratio. After mixing the solution of the guest molecules with HS-β-CD, neither the chemical shifts of the guest nor those of the host showed a significant change. The interaction of HS-β-CD with DOX was studied in DMSO-d_6 as a solvent. The ^{1}H NMR spectrum of pure DOX in DMSO-d_6 shows two peaks downfield with chemical shift of 13.28 ppm and 14.06 ppm indicating the formation of intramolecular hydrogen bonds between the hydroxyl groups and quinone groups [127, 131]. The addition of DOX removes the intramolecular hydrogen bonding with C2, C3 and C6 hydroxyl group of HS-β-CD. The absence of a downfield peak of DOX is due to the formation of inclusion complexes between them. The influence of the host HS-β-CD on the ^{1}H-NMR spectra of the guest[130], and vice versa, were studied in deuterated DMSO based on a 1:1 molar ratio. After mixing the solution of the guest molecules with HS-β-CD, neither the chemical shifts of the guest nor those of the host showed a significant change. The FTIR spectra of DOX, HS-β-CD and inclusion complex were characterized as shown in Figure 3.9. The characteristic absorption of free DOX appeared at 1,900-800 cm^{-1}; these peaks represent the characteristic absorption of the anthracene nucleus and molecular bond vibration of DOX, especially the peak of 1,795 cm^{-1}. The -OH stretching vibration was observed as ~3410 cm^{-1}. An additional S-H stretch around 2490 cm^{-1} to 2600 cm^{-1} was observed [132]. The FTIR spectra of DOX (black line), HS-β-CD (red line) and HS-β-CD-DOX (blue line) are presented in Figure 3.9. The FTIR spectrum of HS-β-

CD exhibited a characteristic peak due to the sulfhydryl group at 2600 cm^{-1}. The FTIR curves of inclusion complex and that of blank HS-β-CD are similar. This indicates that the frame of HS-β-CD in the complex is not change because the encapsulation of DOX does not cause significant change of spectra of HS-β-CD. However, the strong peak of the DOX around 1630 cm^{-1} and the fingerprint region disappear or shift to other wave length due to formation of inclusion complex [133-134].

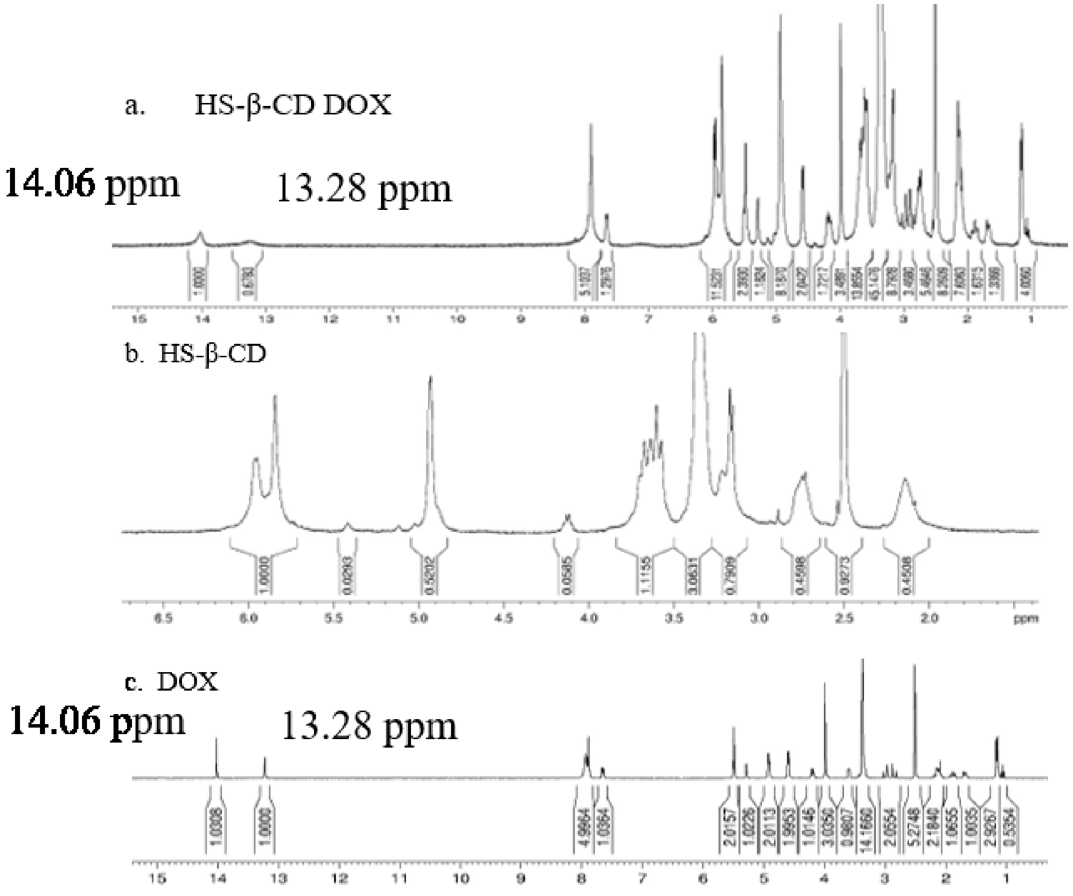

Figure 3.8. NMR spectra of doxorubicin, HS-β-CD, and of inclusion complex of DOX and HS-β-CD.

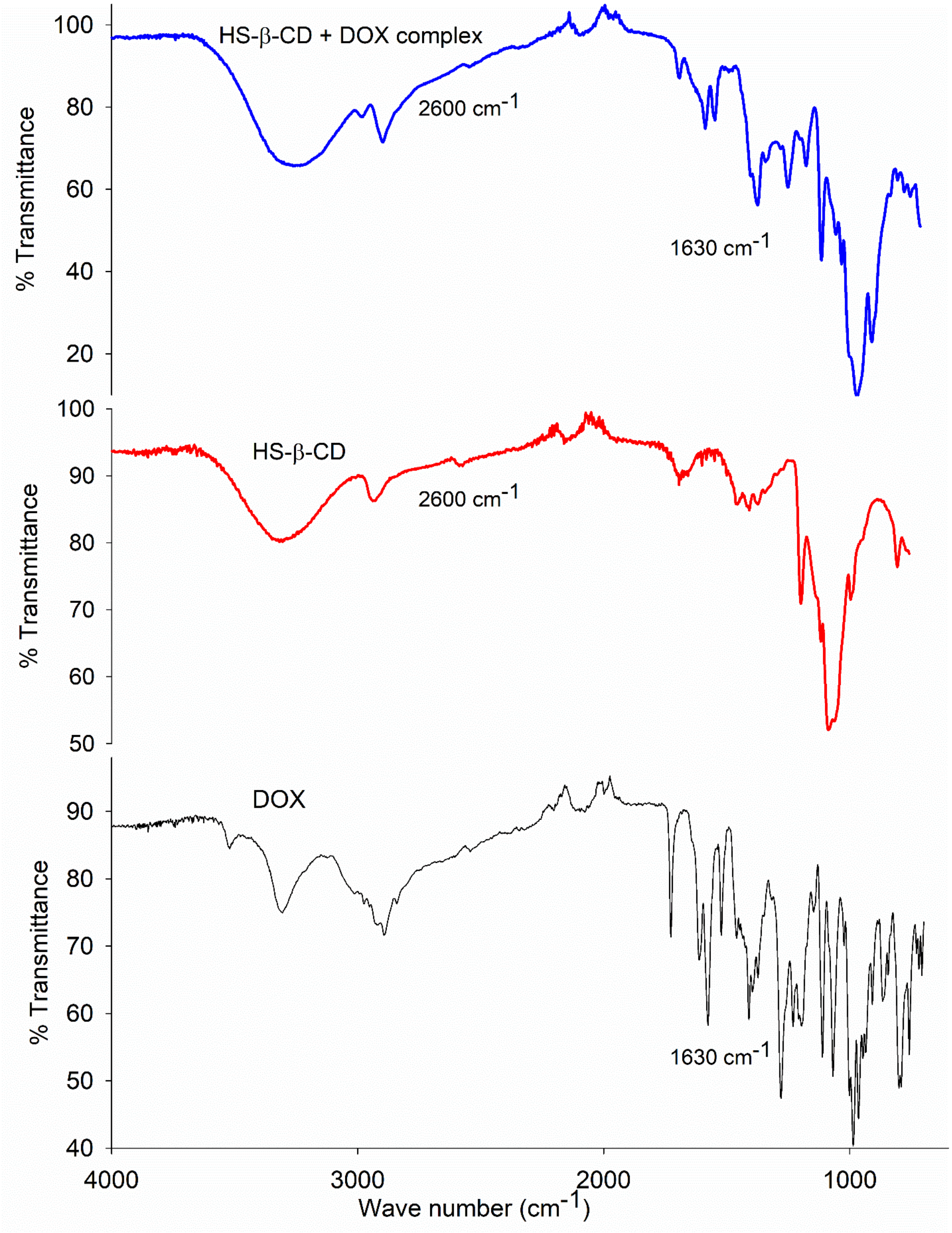

Figure 3.9 .The Fourier transform-infrared (FTIR) spectra of DOX, HS-β-CD, and inclusion complex of DOX and HS-β-CD

3.7 *In vitro pH-dependent drug release profile*: The release of the DOX from the modified NPG was determined at various pH values. The results revealed that the release of the DOX was heavily dependent on the pH of the medium. Considering the acidic microenvironment of tumor tissue (pH 6.0–6.5) and endosome/lysosome of tumor cells (pH 4.5–5.5) [135], the drug release rate increased as the pH of the medium decreased. The HS-β-CD modified NPG wire can spontaneously release the DOX under physiological (pH 7.4) and mildly acidic media (pH = 5.5). The drug release characteristics from NPG vary with pH conditions and the results are shown in Figure 3.10. Under physiological conditions (pH 7.4), only about 34 ±5 % of DOX release was observed over the period of 144 h, whereas approximately 74 ± 2 % cumulative release of DOX was observed over the same period of the time at acidic condition (pH 5.5). Similar experiments were performed in phosphate buffer (pH = 7.4) and the cumulative amount of drug release was about 39 ±3 % over the same period of the time. HS-β-CD modified NPG were found to exhibit very high binding potentials for these drugs making them good candidates for advanced drug delivery.

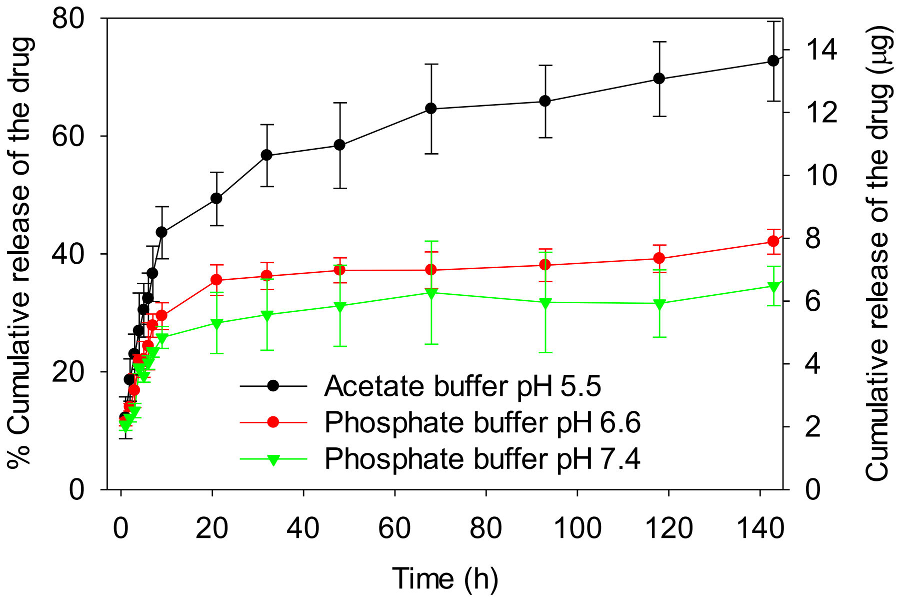

Figure 3.10. In vitro DOX release profiles at varying pH conditions (37 °C, 10 mM buffer solutions) from HS-β-CD modified nanoporous gold. The percent cumulative release and the amount released in micrograms is shown. The error bars represent the standard deviation for n=3 experiments

3.8 In vitro pH-dependent drug release: In order to evaluate the effect of pH on the overall release of DOX, the HS-β-CD modified NPG wires were incubated in three different media: phosphate buffer solution (PBS, pH 7.4), acetate buffer solution (pH 5.5), and bovine calf serum in PBS (pH 7.4). The release profile of the DOX showed a trend that was pH dependent as shown in Figure 3.10 and Figure 3.11. The HS-β-CD modified NPG wires loaded with DOX can spontaneously release DOX under physiological and mildly acidic media conditions (pH 5.5). The drug release characteristics from NPG at varying pH conditions and the results are shown in Figure 3.11 as followed for 48 h. Moving from physiological pH (7.4) more acidic (pH 5.5) caused a clear increase in the release rate (Figure 3.10). This was due to the release of the DOX from the inclusion complexes and the increase of the solubility due to protonation of amino group of DOX [136-137]. In other sets of the release experiment, phosphate buffer solution (PBS, pH 7.4), acetate buffer solution (pH 5.5), and bovine calf serum (pH 7.4) were taken as the release medium and encapsulated DOX with the HS-β-CD led to a linear initial release of DOX over 10 h (Figure 3.11b) and the release kinetics were monitored over 50 h. The rate of DOX release from bovine calf serum medium is slightly greater than the PBS buffer of identical pH (Figure 3.11a). This may be due to the replacement of DOX from NPG cavities by serum proteins. The amount of drug release was maximum in the pH 5.5 acetate buffer with eventual release of near 62 ±3 % NPG over the 4h h period of time, which is significantly higher in comparison of release of DOX at different condition as shown in Figure 3.10 and 3.11 (22 ±4 % of DOX from NPG at pH 7.4, 32 ± 5 % of DOX from NPG at serum at pH 7.4). The pK_a of the amine group in DOX is near 7.2–8.2 [17] and the protonation of the amine is seen to promote release of DOX from the complexes and otherwise promote dissociation and release of the molecules from NPG.

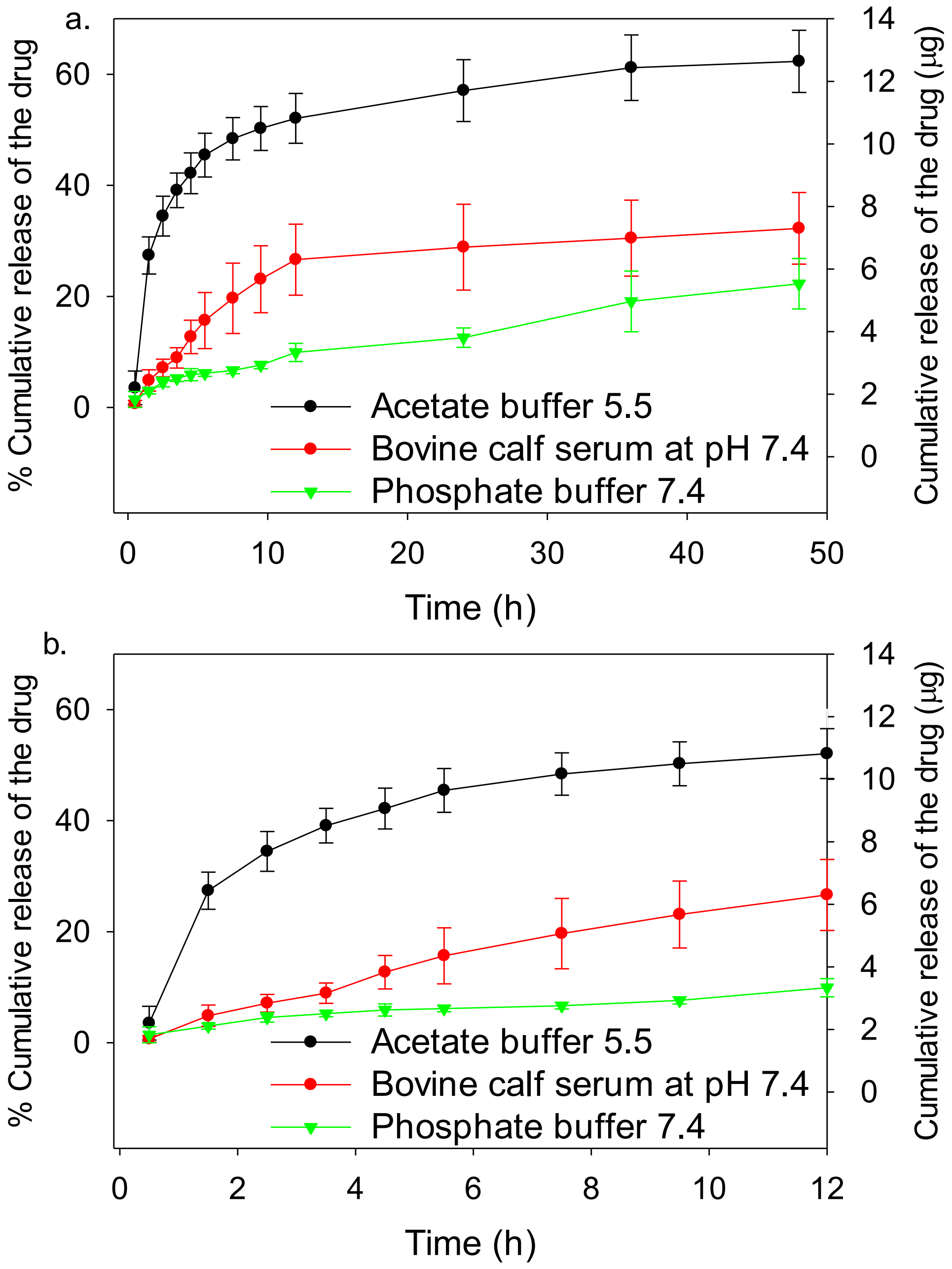

Figure 3.11 (a) In vitro DOX release profiles at varying pH conditions (37 °C, 10 mM buffer) and 10% fetal calf serum in PBS buffer (pH7.4) (b) The release pattern of the above-mentioned systems in a period of 0–12 h. The percent cumulative release and the amount released in micrograms is shown. The error bars represent the standard deviation

3.9 pH sensitive bortezomib release from dopamine modified nanoporous gold: BTZ has been tested in treating solid tumors, such as ovarian cancers and glioma. However, its therapeutic outcome is limited by its poor solubility, insufficient tumor specificity, drug resistance, and unsatisfactory efficacy toward solid tumors [138]. In this study, a dopamine modified pH-sensitive NPG conjugate for the sustained release of the BTZ. To improve the selective release of BTZ, we design a facile method using formation of boronate ester on the surface of the NPG milli rod, in which the ester bond serves as a pH-sensitive linker

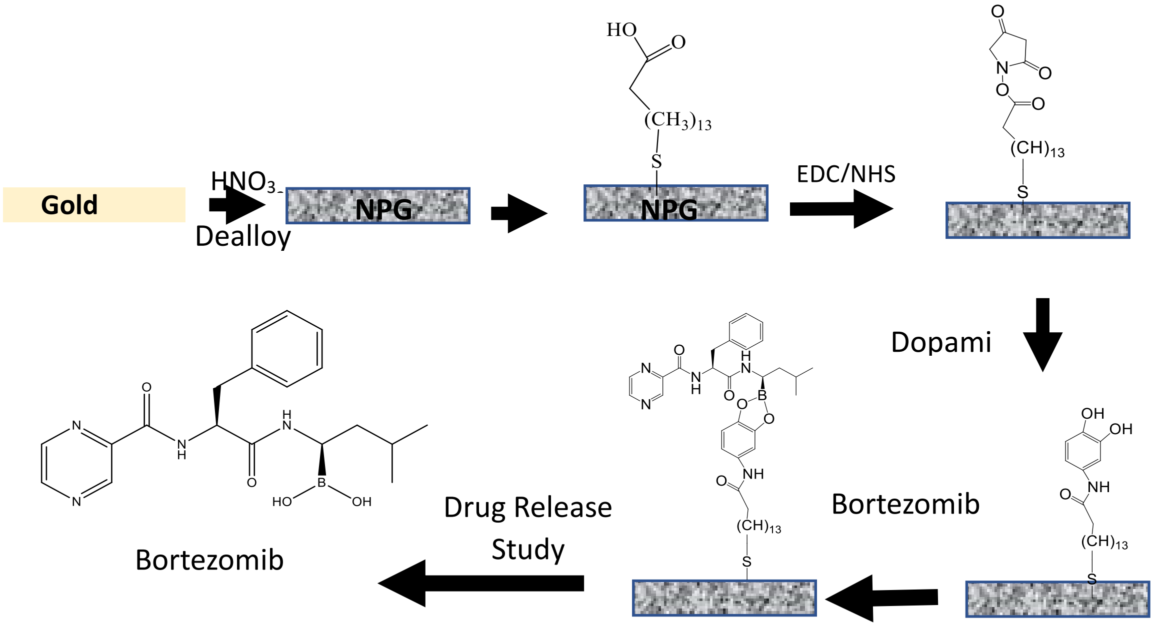

Scheme 3. Schematic diagram of capture and release of Bortezomib by Mercaptopentadecanoic acid modified NPG milli rod

NPG milli-rod was fabricated by leaching the reactive metals from gold alloys milli rods by submerging in concentrated HNO_3 for 24 h. After dealloying, the self-assembled monolayer of Mercaptopentadecanoic acid (MPDA) followed by the activation of the carboxyl group by EDC/NHS chemistry. 1 mM dopamine solution was prepared and conjugated with the activated ester group of SAMs using amide formation reaction exposing cis-diol of the dopamine, which further reacted with the boronic acid unit of the BTZ to form a cyclic boronate ester. Loading of the BTZ on the NPG milli rod was confirmed by TGA and solution total loading of the BTZ was found to be 243.32 ± 6.7 µg (n=3) as shown in Figure 3.12.

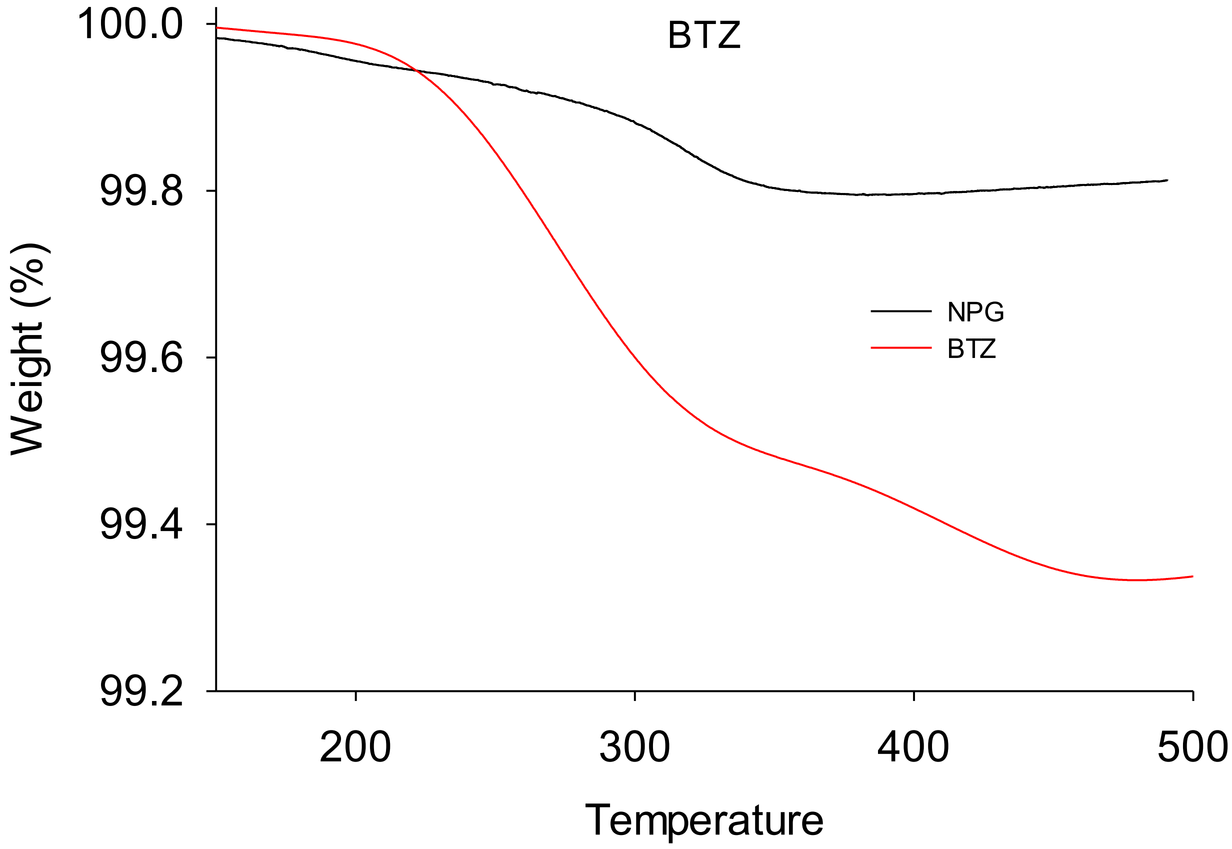

Figure 3.12 Thermogravimetric curve of dopamine modified NPG (black line) and BTZ-dopamine modified NPG rod (red)

The release behavior of BTZ from NPG was assessed at the buffer solution of two different pH (7.4 and 5.5). the release profiles of BTZ from NPG milli rod in buffer at different pH are demonstrated in Figure 3.13. BTZ release was monitored up to 9 days.

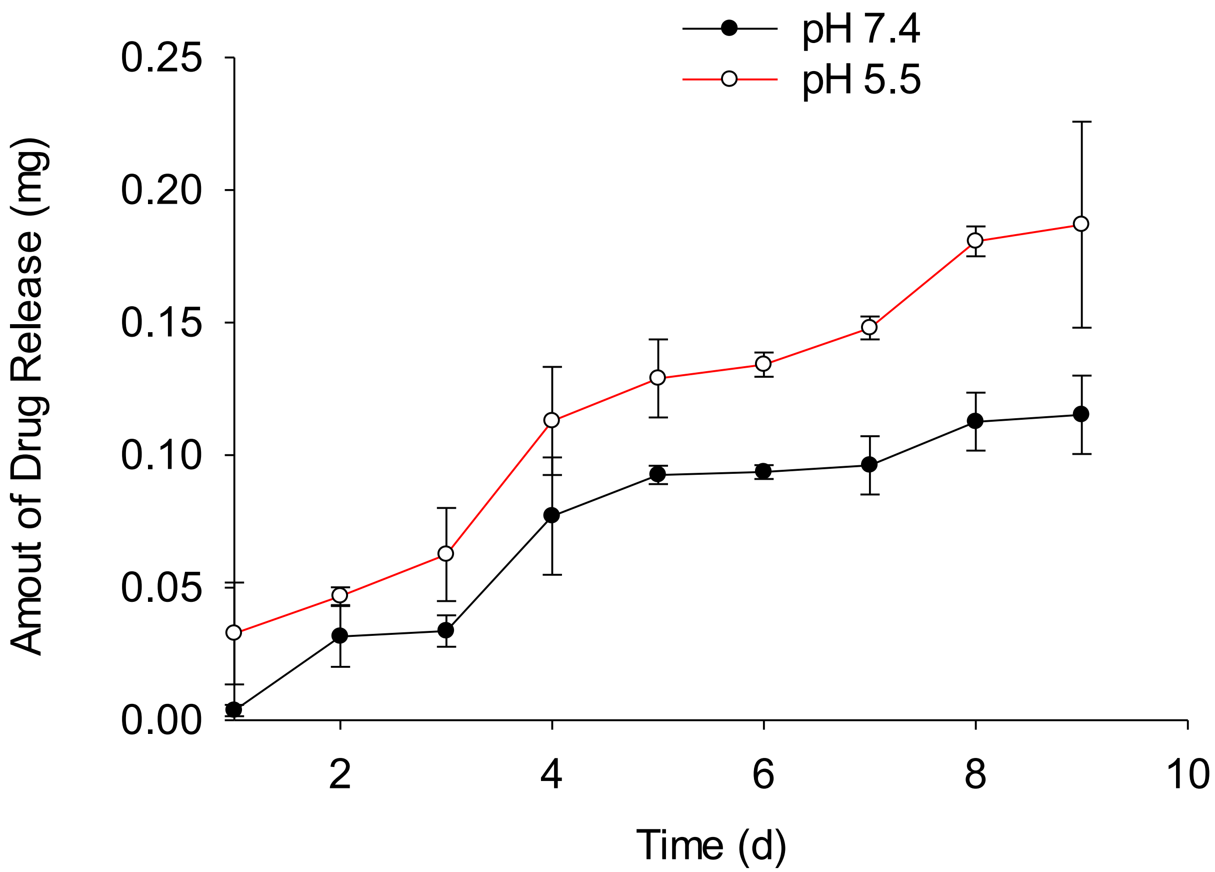

Figure 3.13 Cumulative release of drugs as a function of time. Release of the BTZ at pH 5.5 (red line), and pH 7.4 (black line). (37 °C, 10 mM buffer). The error bars represent the standard deviation for n=3 experiments.

The cumulative drug release of the BTZ at pH 5.5 was 187 ± 39 µg (n=3) vs at pH 7.4 was 115.2 ± 15.0 µg (n=3) over 9 days period of the time. The NPG-dopamine-BTZ conjugate might have great potential as a tumor-targeted proteasome inhibitor for tumor specific drug delivery and effective cancer treatment.

5. CHAPTER IV. SELECTIVE CAPTURE OF GLYCOPROTEIN BY BORONIC ACID MODIFIED NANOPOROUS GOLD

In this study, the interactions of glycan or glycoproteins with boronic acid are used to develop an NPG monolith substrate for the isolation of glycoproteins. NPG monolith can be used as the substrate for the chromatographic separation and extraction of biomolecules after modification of the surface by a suitable self-assembled monolayer. The surface modified NPG monolith is free-standing, has intact pore size within the range of nanoscales and the pore size can be tuned according to the necessity of the experiment. NPG monolith is a nanostructured material produced by the removing less noble metal(s) from low carat gold alloys generally using selective dissolution by immersing in the concentrated nitric acid. The microstructure of NPG monolith has interconnected bicontinuous ligaments forming pores in the nanoscale range.

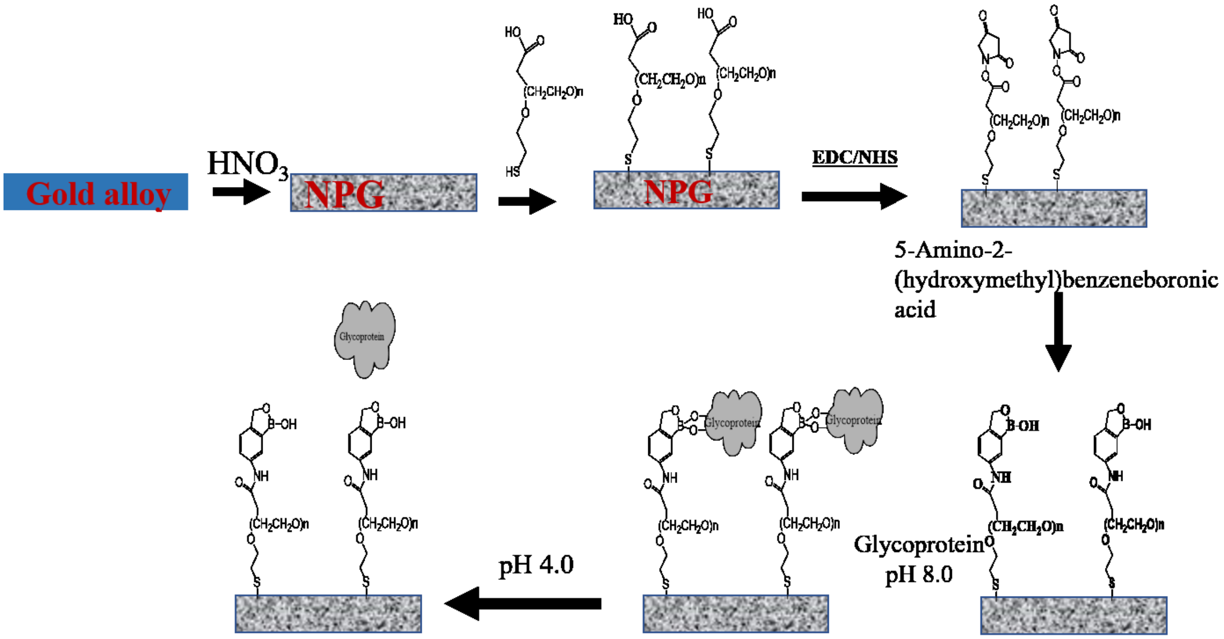

Scheme 4. Schematic diagram of selective capture and release of glycoprotein from boronic acid modified nanoporous gold monolith

4.1 *Fabrication and characterization of nanoporous gold monolith*: NPG monoliths were synthesized by selective dealloying of less noble metal from the gold alloy in concentrated nitric acid as shown in scheme 5. NPG monoliths were stored in pure ethanol. Surface characterization of the NPG wire was performed by SEM. The NPG wire was also broken into smaller pieces and the cleaved fragments imaged using SEM to characterize the bulk of the NPG wire and to confirm interior porosity. Figure 4.1a shows the NPG monolith after dealloying. Figure 4.1b shows the AFM imaging of NPG monolith surface. The average pores size on the surface of the NPG monolith is determined as 32±5 nm (n=40) and the average pores size seen in the cross section of the NPG wire was found 55±10 nm (n=40). These pore dimensions make the NPG wire highly suitable materials for loading of glycoprotein following modification with activated HS-PEG-COOH. The specific surface area of the monolith was reported previously from our lab to be 6.9 ± 0.5 m^2g^{-1} (n=3) [139] and the pore size distribution was also reported using BJH analysis and was found to predominantly in the range of 80-120 nm [139]. Scanning electron microscopy image of the dealloyed NPG monoliths reveals interconnected ligaments and pores in both exterior and interior part of the monolith as shown in Figure 4.1. AFM image was taken to show the morphology of the nanoporous gold as shown in figure 4.1 (b). The height distribution shows the ligament distribution of the nanoporous gold.

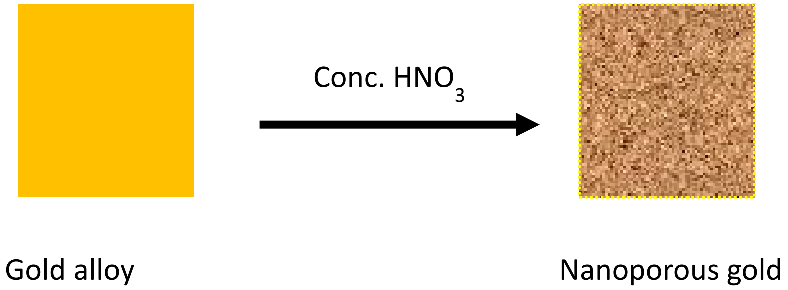

Scheme 5. Schematic diagram of dealloying of nanoporous gold to form nanoporous gold monolith

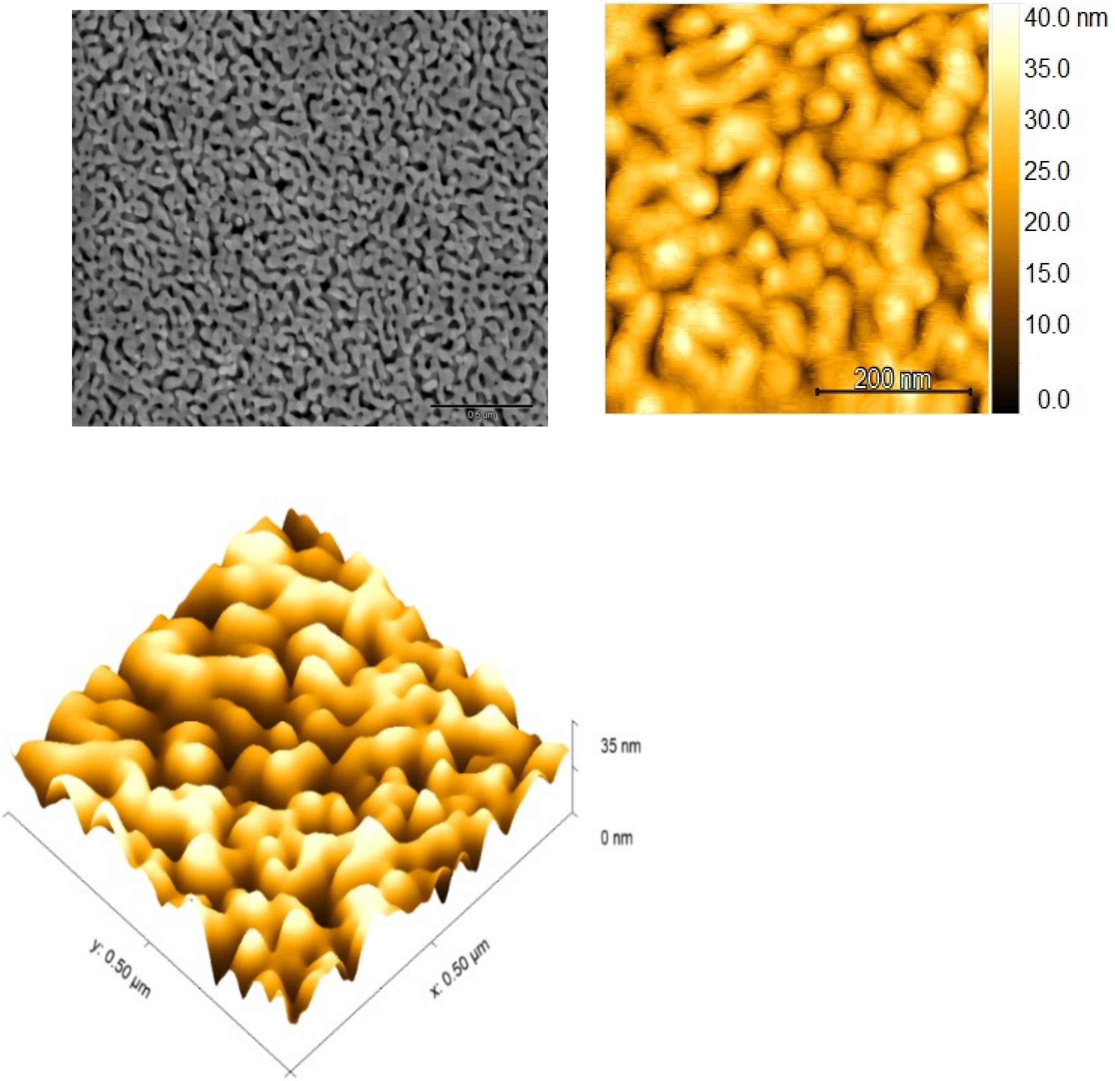

Figure 4.1 SEM and AFM images of the top side view of the NPG monolith

The pore size and the inter-ligament distance was easily tunable by varying the dealloying condition and the nature of the alloy of gold (i.e. alloy composition). Our lab also developed an electrochemical method of annealing NPG electrode by potential cycling for numbers of times [4]. The pore size of the NPG electrode was increased by annealing after formation of the NPG. The average pore size of the NPG monolith was controllable by changing the temperature of dealloying condition. When the dealloying of gold alloy was done at very low temperature (-20 °C), the pore size of the NPG monolith was less than 30 nm, the pore size distribution of the room temperature dealloying are between 40-100 nm and the pore size distribution of the high temperature dealloyed NPG monolith are more than 100 nm although the time of dealloying are same and the completion of the dealloying process was confirm by EDX measurement. Figure 4.2 shows the SEM images of the NPG monolith dealloyed at different temperatures at same level of magnification of the SEM image.

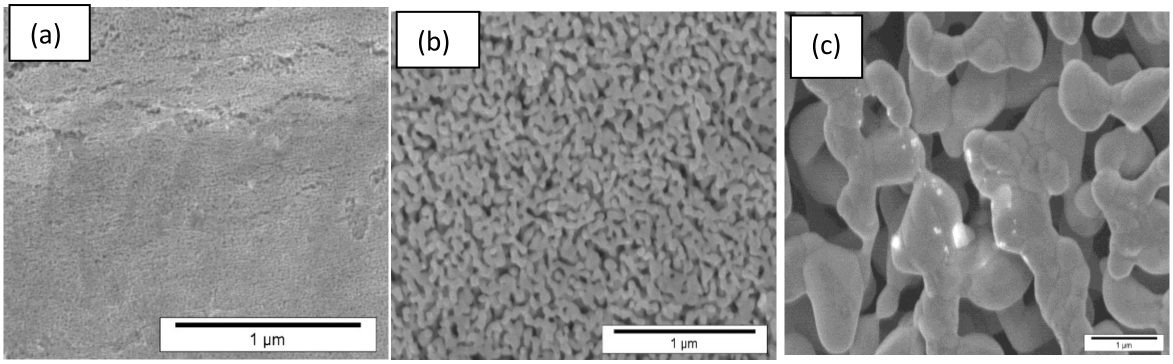

Figure 4.2 SEM image of the NPG monolith dealloyed at different temperature (a) – 20 °C (b) room temperature and (c) at 60 °C

4.2 *Atomic force microscopy analysis of the immobilized glycoprotein on ultra-flat gold surfaces*: Atomic force microscopy was used for the determination of thickness of SAM on the flat gold surface by scanning across the substrate (Figure 4.3). Ultra-flat gold surfaces were prepared by the sputtering of gold onto mica surfaces followed by annealing at 350 °C for 3 hours. Tapping mode AFM was used to image the flat gold, and the SAMs of HS-PEG-COOH before and after their interaction with glycoprotein. Poly(ethylene glycol) (PEG) SAMs are extensively used to modify substrates to prevent nonspecific protein adsorption and to increase the hydrophilicity [140]. The surface roughness of the flat gold surface increased after immobilization of SAM and further increased after immobilization of glycoprotein. The average roughness of flat gold surface was observed 0.85±0.17 nm. After formation of the self-assembled monolayer of the HS-PEG-COOH, the roughness of the flat gold surface increased to 1.5±0.07 nm and the roughness further decreased after elution of glycoprotein from the elution buffer on the flat gold surface by incubating to the buffer of pH 4.0 to the original value.

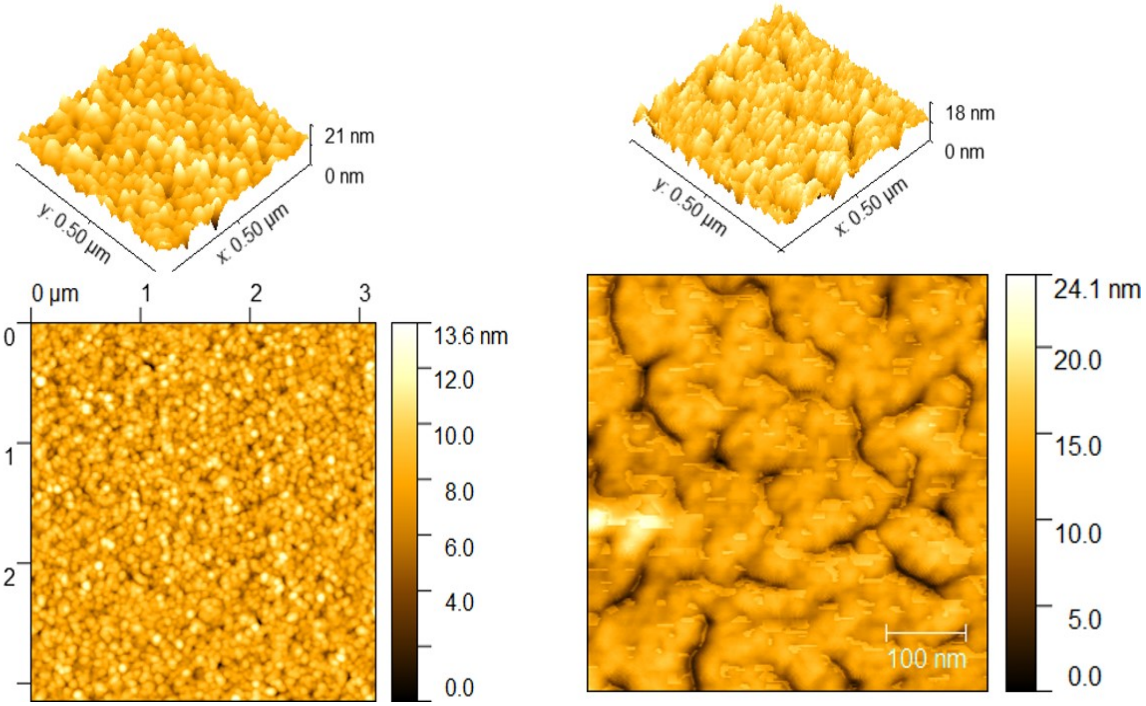

Figure 4.3 Tapping mode-AFM images of the bare gold and ovalbumin functionalized flat gold surface

4.3 *Electrochemical and optical characterization of interaction between boronic acid and glycoprotein*:

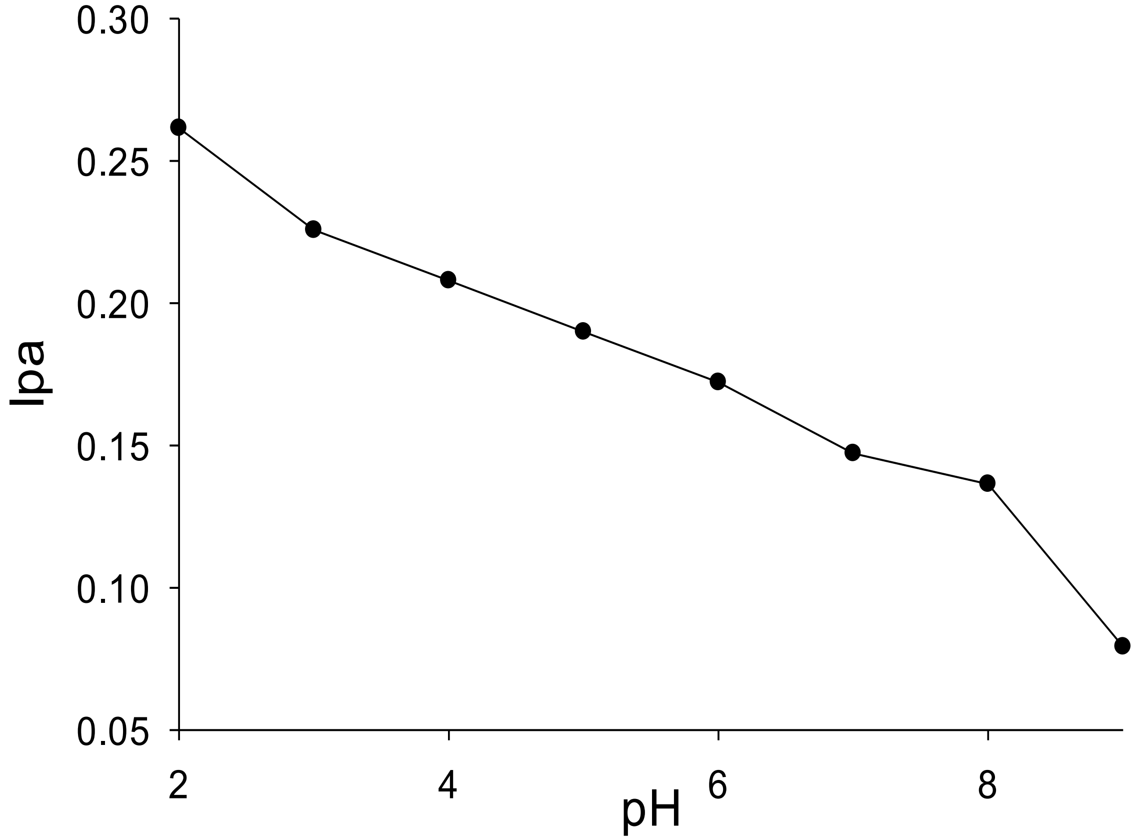

Figure 4.4. Plot of anodic peak current (Ipa) vs the pH of the electrolyte solution for the pKa estimation from boronic acid modified gold.

The surface pK_a of SAMs on the gold surface may differ from the solution pK_a. This may have a large effect on the sensitivity and selectivity in different solutions. Different methods such as contact angle titration, chemical force titration using AFM, quartz crystal microbalance, surface potential, electrochemical desorption, and spectroscopy has been used to determine the surface pK_a [141]. In the electrochemical method, buffer solutions with different pH values, and an anionic electrochemical probe to investigate the surface pKa of the carboxyl SAMs is required. The terminal carboxyl groups exhibit pH dependence, when the pH in the solution is high enough, the SAMs surface charge will be negative. $K_3Fe(CN)_6$ is used as a probe to determine its interaction with SAM surface in different charge situation. The HS-PEG-COOH (MW 1k) was used to present the special end group of SAM to determine the surface pKa. The SAM with -COOH terminal group inhibits the electron transfer between the electroactive probe and the electrode when they possess the same negative charge. The pH-dependence of the $K_3Fe(CN)_6$ probe current peak in CV scans was observed when the pH of the bulk solution changed as shown in figure 4.4. The peak current of $K_3Fe(CN)_6$ changes with pH value of the bulk solutions. The surface pKa was determined using following equation [101].

$$pKa = pH + \log[(\, i_{AH} - I_{A-})/(i - i_{A-}) - 1]$$

Where i_{A-} and i_{AH} are currents of the probe on the SAM fabricated by A^- and AH structures, respectively. The current i is the total apparent current of the probe and i_{A-} and i_{HA} were determined by the average values at high pH (> 7) and low pH (< 7). The surface pK_a estimated by the above method was 7.43.

Electrochemical impedance spectroscopy (EIS), an effective method for probing the features of a surface modified electrode and localized surface plasmon resonance (LSPR) was employed to monitor the step wise construction of the boronic acid modified gold surface and its interaction with glycoprotein. Fig 4.5 illustrates the Nyquist diagrams of the boronic acid modified gold electrode in different conditions which were conducted in pH 8.0 PBS containing 5 mM $[Fe(CN)_6]^{3-/4-}$ solution at frequencies from 1 Hz to 1 MHz Bare gold exhibited a small semicircle at high frequencies, suggesting a very low charge transfer resistance (R_{ct}). After the immobilization of the HS-PEG-COOH into a SAM on the gold surface, a semicircle with a R_{ct} value of around 1000 Ω was observed. Similarly, a R_{ct} vale was found around 3000 Ω, and 7000 Ω after immobilization of benzoboroxole and fetuin indicating that the modified film has a progressively larger obstruction effect and a high resistance to the redox probe. When the embedded glycoprotein was eluted using elution buffer, The R_{ct} reduced significantly back to about 3500 Ω suggesting that the immobilized glycoprotein can be eluted with maximum capacity by reducing the pH of the surroundings.

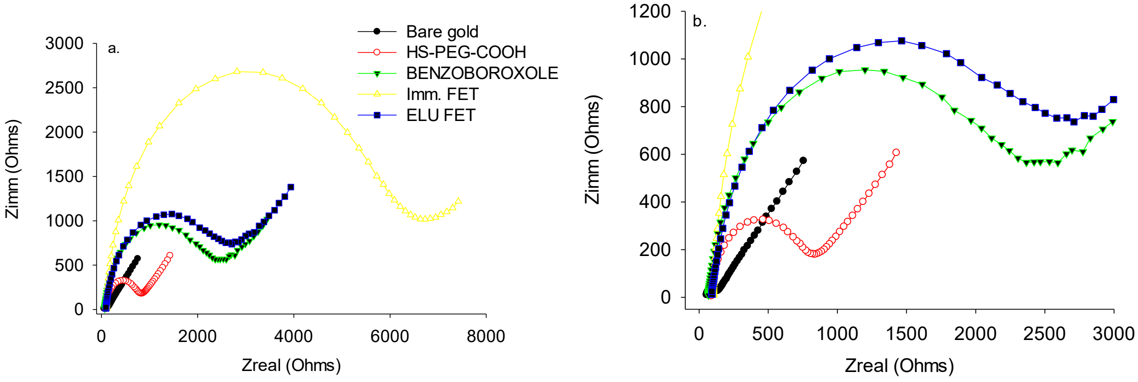

Figure 4.5. (a) Nyquist plot for the modified gold electrode at different condition: bare gold wire (black line); HS-PEG-COOH immobilized gold wire (red line) ; boronic acid modified gold wire (green line); fetuin immobilized gold wire (yellow line); and gold wire after elution of fetuin (blue line). EIS measurements were done in 5 mM solution of the redox probe at formal potential at 0.2 V bias potential. (b) Nyquist plot for the reduced scale.

The selectivity of the boronic acid modified NPG monolith towards glycoprotein was evaluated by testing glycoprotein (ovalbumin) and non-glycoproteins (bovine serum albumin) as model samples using EIS and CV as shown in figure 4.5 and figure 4.6, respectively. The boronic acid functionalized gold wire was prepared by the formation of carboxy terminal self-assembled monolayer of the thiolated PEG followed by the activation using EDC/NHS chemistry. To minimize the non-specific adsorption and reaction potentially caused by the free activated esters, 1 % (v/V) ethanolamine solution prepared in the ethanol solution prior to the capture of the Ova or BSA to cap the unused reactive ester and convert them to less reactive hydroxyl terminal ends which are not capable of covalently immobilizing proteins. Both EIS and CV showed significant amounts of Ova captured as determined by the large increase of the R_{ct} value in the Nyquist plot as shown in Figure 4.5 in comparison with the incubation of the modified NPG electrode in the BSA solution. The interaction of boronic acids with the glycans of glycoproteins provides a tool for efficiently reducing the complexity of biological samples containing many proteins. The boronate interaction can also be used for the straightforward and selective quantification of glycoproteins in complex matrices by electrochemical detection.

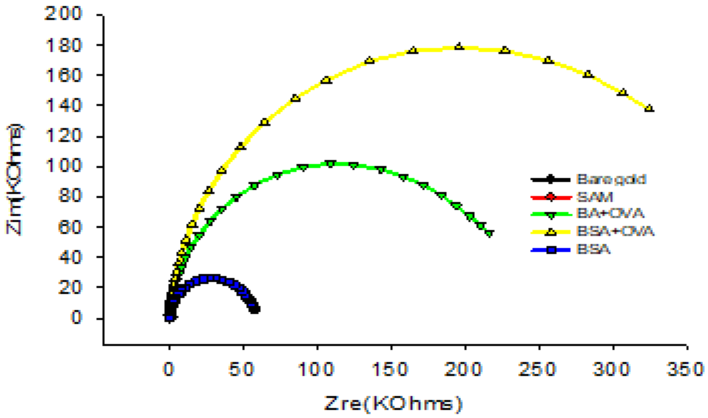

Figure 4.6 Nyquist plots for the modified gold electrode in different conditions: bare gold wire (black line); HS-PEG-COOH immobilized gold wire (red line); boronic acid and Ovalbumin immobilized gold wire (green line); BSA + Ova immobilized gold wire (yellow line); and BSA incubated modified gold wire (blue line). EIS measurements were done in 5 mM of the redox probe at formal potential at 0.2 V bias potential vs reference electrode.

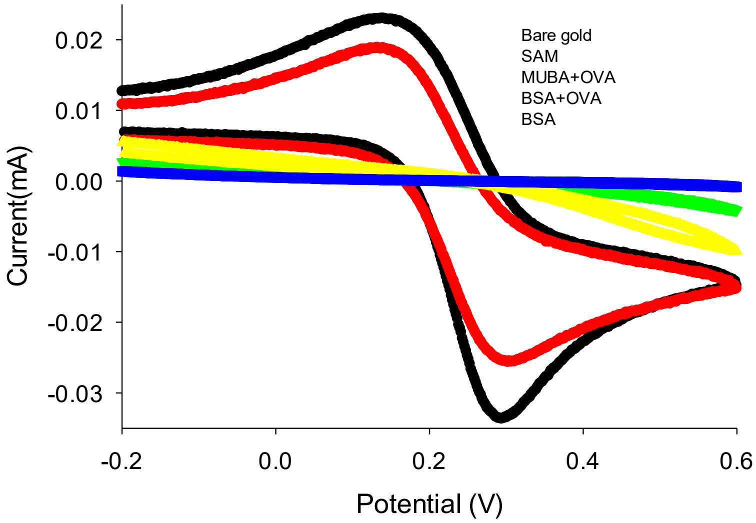

Figure 4.7 Cyclic Voltammetry for the modified gold electrode at different condition: bare gold wire (black line); HS-PEG-COOH immobilized gold wire (red line) ; boronic acid and ovalbumin immobilized gold wire (green line); BSA + Ova immobilized gold wire (yellow line); and BSA incubated modified gold wire (blue line). CV measurements were done in 5 mM of the redox probe over a potential range of -0.2 V to +0.6 V at a scan rate of 50 mV/sec.

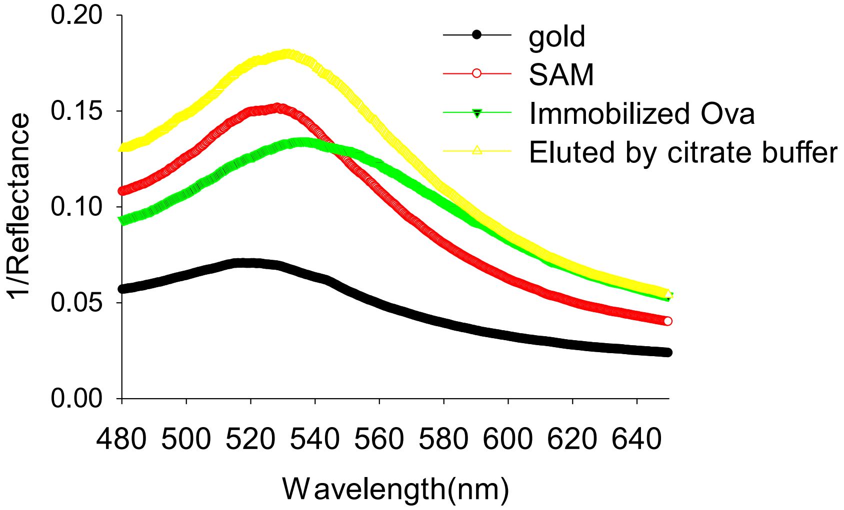

Figure 4.8. Localized surface plasmon resonance spectra when thin film of gold was modified by different reagents: bare god thin film (black line); HS-PEG-COOH modified

surface (red line); Immobilized Ova (green line); and spectra after elution of Ova (yellow line). Data are plotted as 1/reflectance versus wavelength.

4.4 *Analysis of the glycoprotein immobilized glycoprotein on the NPG monoliths*: Thermogravimetric analysis (TGA) was used to characterize the loading of the glycoprotein onto the NPG monolith. TGA is a destructive method, which allows for the quantitative measurement of the change in the weight of the analyzed material as a function of temperature and time as the temperature is ramped at a constant rate. Modified NPG monoliths were air-dried and placed in the platinum weighing pan and heated inside the thermogravimetric analyzer from room temperature to 100 °C and held for 10 min for complete drying of the sample then heated from room temperature to 600 °C at a ramping rate of 20 °C min^{-1}. Our lab reported lectin-carbohydrate interactions on the modified nanoporous gold by thermogravimetric analysis [139]. TGA was used to determine the amount of loaded carbohydrate molecule on NPG monolith, and loaded lectin was also accessed using TGA. In this work, NPG monoliths were successfully modified by self-assembled monolayer of the thiolated PEG molecules confirmed by the mass losses obtained from the TGA analysis. Formation of the SAM was also monitored by a flow-through method as well as simple incubation of the freshly prepared NPG monolith in the 1 mM SAM solution.

4.5 *Capture and elution of the glycoprotein on the nanoporous gold modified NPG monolith by solution depletion method*: Solution depletion is one of the simplest methods to study protein adsorption. One measure a concentration change in the bulk solution prior to and adsorption (Δc_p). The protein concentration measuring techniques are numerous: UV absorption, fluorescence, colorimetric methods, and many others, including the use of radioisotopes labeled or fluorescently labeled proteins [142]. NPG monoliths can be used as the adsorbents [143-145]. The spectroscopic techniques for the protein studies depend the interaction of the light with protein molecules. The magnitude of the spectroscopic signal can often be related to the amount of protein. The protein concentration is determined by measuring the UV adsorption at 280 nm before and after the immobilization

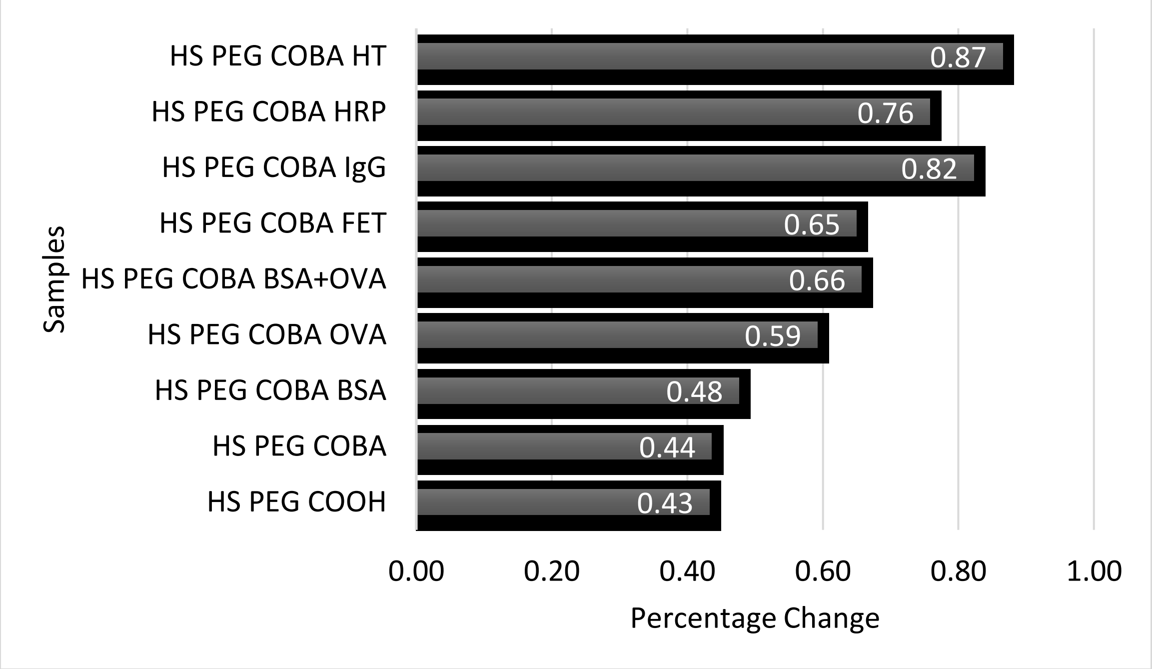

Figure 4.9 Percentage mass loss of the modified nanoporous gold of the different sample of the modified nanoporous gold monolith determined by TGA analysis.

on the modified NPG monolith. The protein solutions were prepared in the phosphate buffer at pH 8.0 with concentration of 0.5 mg/ml. Ovalbumin (Ova), immunoglobin G (IgG), holo-transferrin (HT), Fetuin (Fet), asialofetuin (Asf), horseradish peroxidase (HRP) are the glycoproteins and bovine serum albumin (BSA) are non-glycoproteins, and these are the proteins tested by the solution depletion method as shown in Figure 4.9. The absorbance of the solution was measured before and after the incubation on the modified NPG as well as after the elution from acetate buffer. The concentration of the protein's solutions was calculated by Beer Lambert law [146], describe the relationship between absorbance (A), the molar solution concentration (c) in molarity , and the pathlength of lights takes to get to the sample (l) in centimeters. Absorbance is directly proportional to the concentration and length via A = Ɛcl where Ɛ (L mol^{-1} cm^{-1}) is the wavelength dependent molar absorptivity coefficient and it is constant for a particular substance.

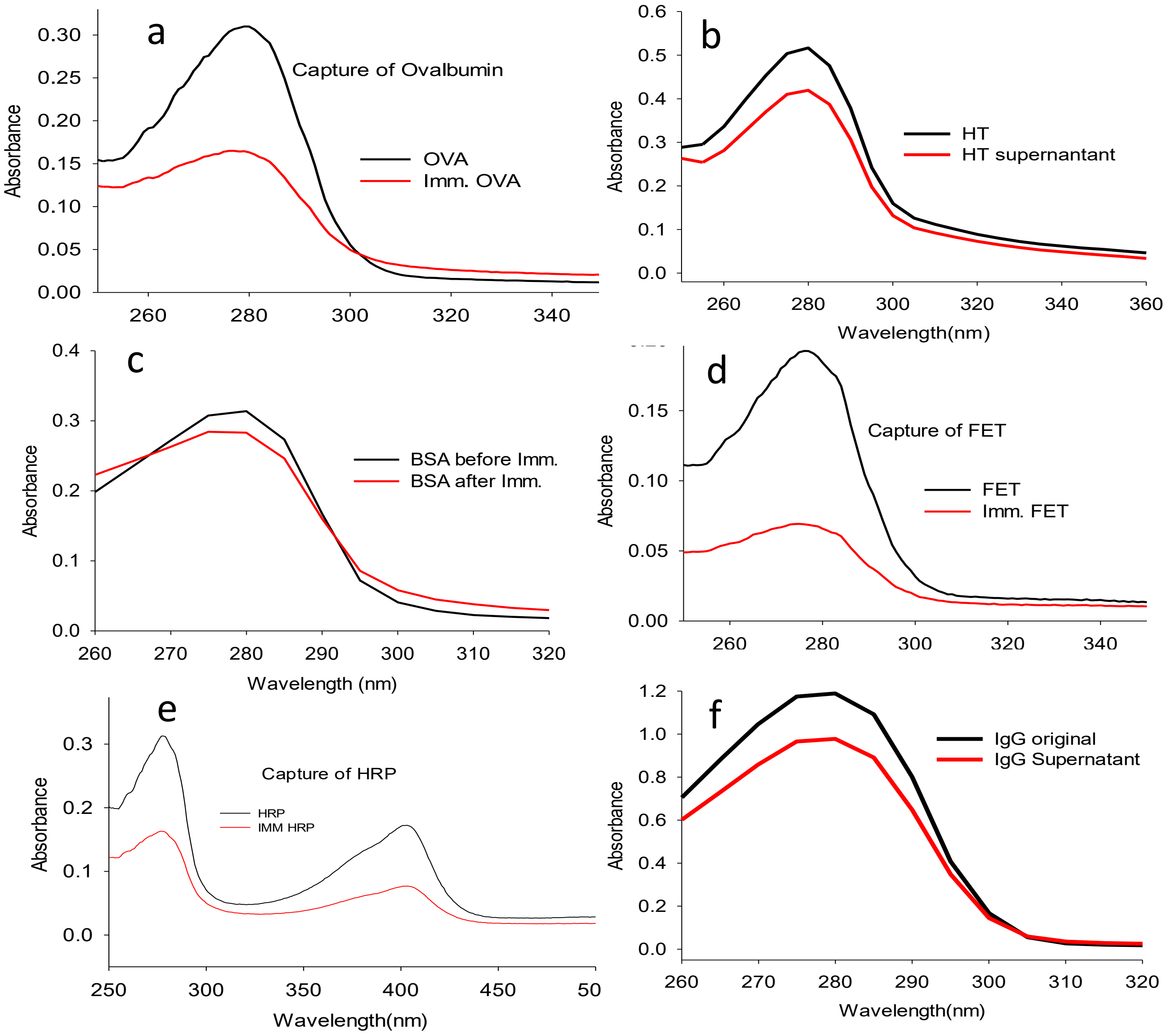

Figure 4.10 UV-vis scan of protein solution prior to and after the incubation on the modified nanoporous gold monolith; (a) Ovalbumin, (b) Holo-transferrin, (c) Bovine serum albumin, (d) Fetuin, (e) Horseradish peroxidase, and (f) immunoglobin G.

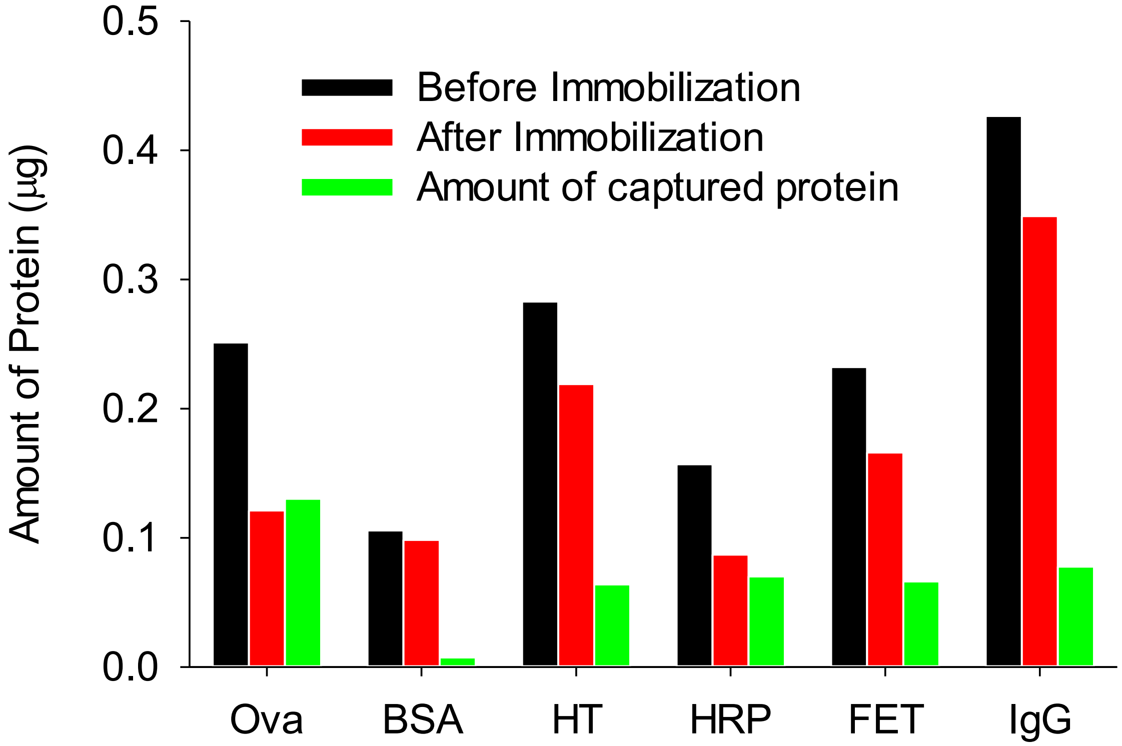

Figure 4.11 Spectroscopic determination of captured of glycoproteins; Ovalbumin (Ova) , Holotransferrin (HT), Horseradish peroxidase (HRP), Fetuin (FET), Immunoglobin G (IgG) and non glycoprotein; Bovine serum albumin (BSA).

The quantitative calculation of the selective capture of the glycoprotein from the boronic acid modified NPG monolith was shown in figure 4.10 from solution depletion method. Captue of the glycoproteins such as Ovalbumin, Holo-transferrin, Fetuin, Horseradish peroxidase, and immunoglobin G and non glycoprotein Bovine serum albumin was measured by absorbance measurement as shwn in figure 4.9. Using Beers Law, the amount of the glycoprotein capture was shown in the bar diagram of figure 4.10. The glycoprotein shows that the significant amount of the protein were captured on the modified structure, whereas the the non glycoprotein shows almost no capture to the modified monolith.

4.6 *Selective enrichment of uridine*: Boronic acid modified nanoporous gold monolith was used to selective capture nucleosides such as uridine. Uridine is a glycosylated pyrimidine analog containing uracil attached to a ribose ring (or more specifically, a ribofuranose) via a β-N_1-glycosidic bond. Nucleosides are the building blocks of nucleic acids [147]. However, the direct analysis of nucleosides from real samples is seriously hampered by their sub-stoichiometric nature due to serious matrix interference [148]. Therefore, selectively enriching target nucleosides and eliminating any matrix effect are important for the analysis. Boronic acids can covalently bind cis diol containing molecules in aqueous media, and these cyclic esters dissociate in acidic pH. In this study, we reported the modification of nanoporous gold by boronic acid via conjugation of carboxyl terminal SAMs with 5-amino-2-(hydroxymethyl)benzeneboronic acid. Boronic acid modified nanoporous gold was incubated on the 5 mM uridine solution for 3 hours and captured uridine was eluted by phosphate buffer of pH 4.0 and absorbace of the solution before and after immobilization as well the absorbance of the eluted solution was shown in Figure 4.11.

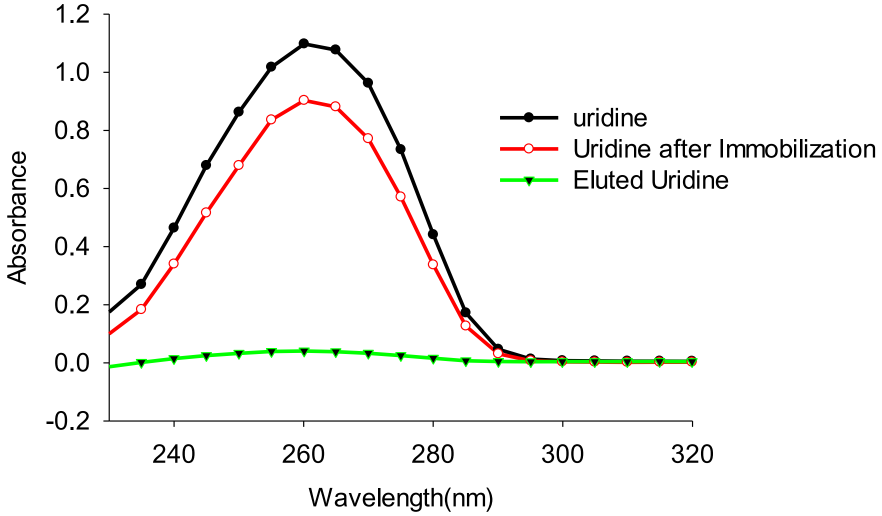

Figure 4. 12 The UV adsorption spectra of Uridine; before immobilization (black line), after immobilization (red line) and eluted uridine solution (green line)

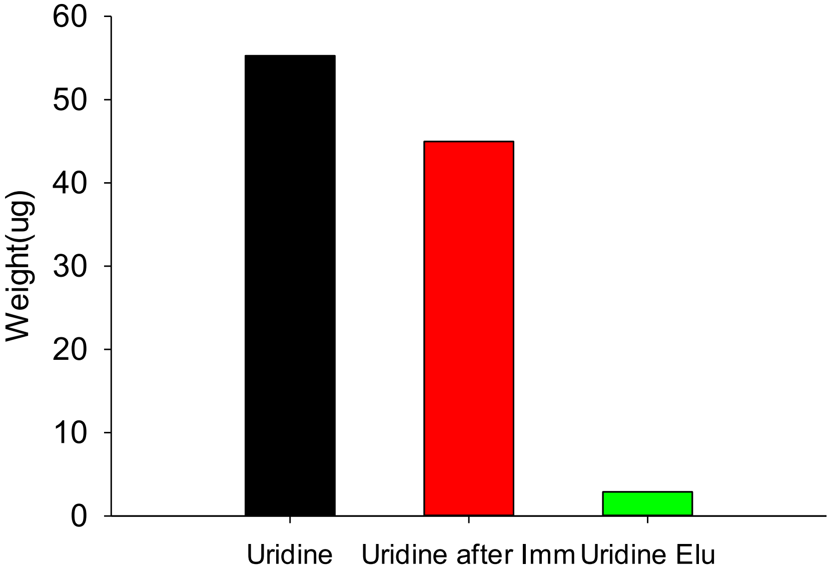

Figure 4.13 Spectroscopic measurement of the amount of uridine capture and release from the boronic acid modified nanoporous gold

In summary, a novel boronic acid functionalized NPG was successfully prepared via a formation of the self-assembled monolayer of pegylated SAMs followed by EDC/NHS chemistry to the amine terminal boronic acid derivatives. The obtained material exhibits favorable pH tolerance range as well as good stability over the range of the temperature. Due to its excellent chemical stability, abundant boronic acid active sites due to porous structure, boronic acid modified NPG provide a new approach for the efficient enrichment and separation of the glycoproteins, nucleosides and many other molecules containing cis-diol unit on it.

5. CHAPTER V FABRICATION OF LOCALIZED PLASMON RESONANCE SPECTROSCOPY ACITIVE THIN FILM OF NANOPOROUS GOLD FOR BIOSENSING

Localized surface plasmon resonance (LSPR) spectroscopy is the one of the preferred sensing platforms for the detection of biomolecules with high sensitivity and low cost. It is well known that LSPR strongly depends on the refractive index of the surrounding medium (substrate, solvent, and adsorbates) of the surface/nanostructure [149-151]. Adsorption of molecules in the nanostructured surface can lead to detectable changes in both the peak wavelength and intensity of the LSPR resonance. A material must have a negative real and small positive imaginary dielectric constant to support surface plasmon resonance (SPR). In LSPR, light interacts with nanometers sized particles or features that are much smaller than the wavelength of the incident light and this generates a plasmon that is a local oscillation of electrons around the particle or nanoscale feature. Similar to SPR, LSPR is sensitive to changes in the local refractive index environment and can be detected by a measurement of the shift of the peak wavelength [152]. We reported a practical approach to fabricate thin films of nanostructured gold on silicon wafer by roughening the Si surface before Au sputtering and deposition. The roughening process creates defects in the morphology of the Si wafer, which increases the number of sites for the nucleation and propagation and the adhesion of the Au film during the sputtering process [153].

5.1 *Fabrication of nanostructured gold film (NGF) preparation*: NGFs were prepared using one-step and two step chronoamperometry (CA) technique. The surface of the silicon wafer was scratched and etched before the sputtering of the thin film of gold. The stability of the as sputtered gold thin film on the surface of the modified silicon wafer was tested next day after deposition and the thin film of gold was found stable after modification and the test for stability was done by thumb, and tape in both dry and wet condition. After fabrication of stable thin film of gold coated silicon wafer, two step chronoamperometry technique was applied to form the LSPR sensitive nanostructured gold film by providing the potential of -1.2V for 60 sec followed by -1.6 V for 30 sec. The process of the fabrication of the nanostructured thin film is shown in scheme 6. Another method that will result in a thin film of nanoporous gold is deposition of gold alloy (30% gold and70% silver) followed by dealloying in concentrated nitric acid.

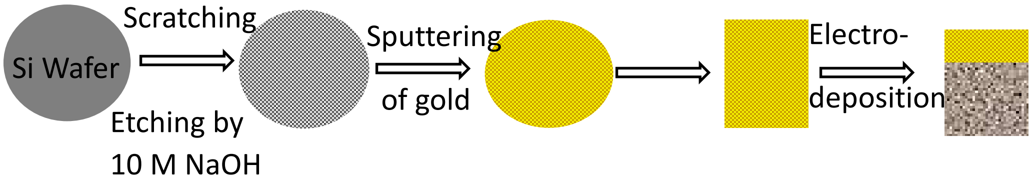

Scheme 6. Schematic diagram of fabrication of LSPR sensitive thin film of nanostructured gold

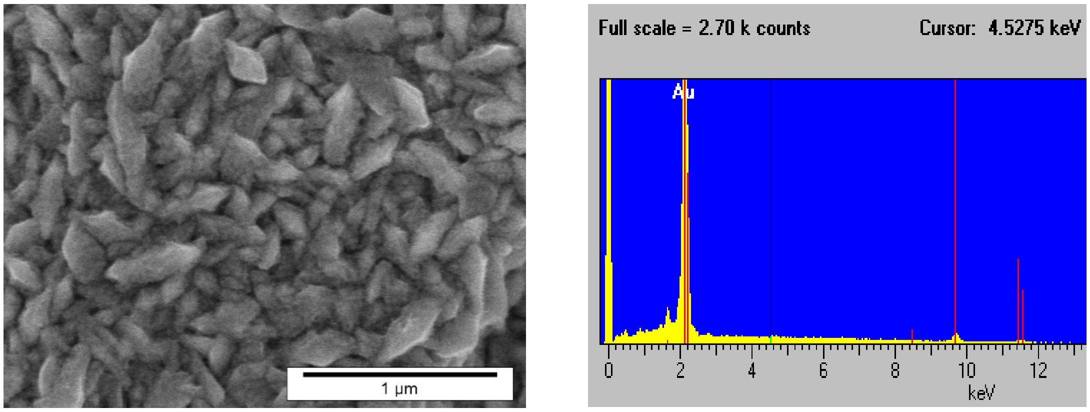

Figure 5.1 (a) SEM of the thin film of the nanoporous gold on the surface of the silicon wafer prepare using two step chronoamperometry technique (-1.2 V for 60s followed by -

1.6 V for 30s in 50 mM Kau(CN)$_2$. (b) EDX measurement of the thin film of the nanoporous gold.

Figure 5.1(a) is an SEM of the thin film of the nanoporous gold on the surface of the silicon wafer prepare using two step chronoamperometry technique (-1.2 V for 60s followed by -1.6 V for 30s in 50 mM Kau(CN)$_2$. It shows randomly oriented brick-like nanostructures with the range of the nanometers scale. The average length of the around 200 nm and width of the 100 nm. Figure 5.2 (b) is the EDX measurement of the thin film of the gold showing the nanostructure is fabricated only from gold.

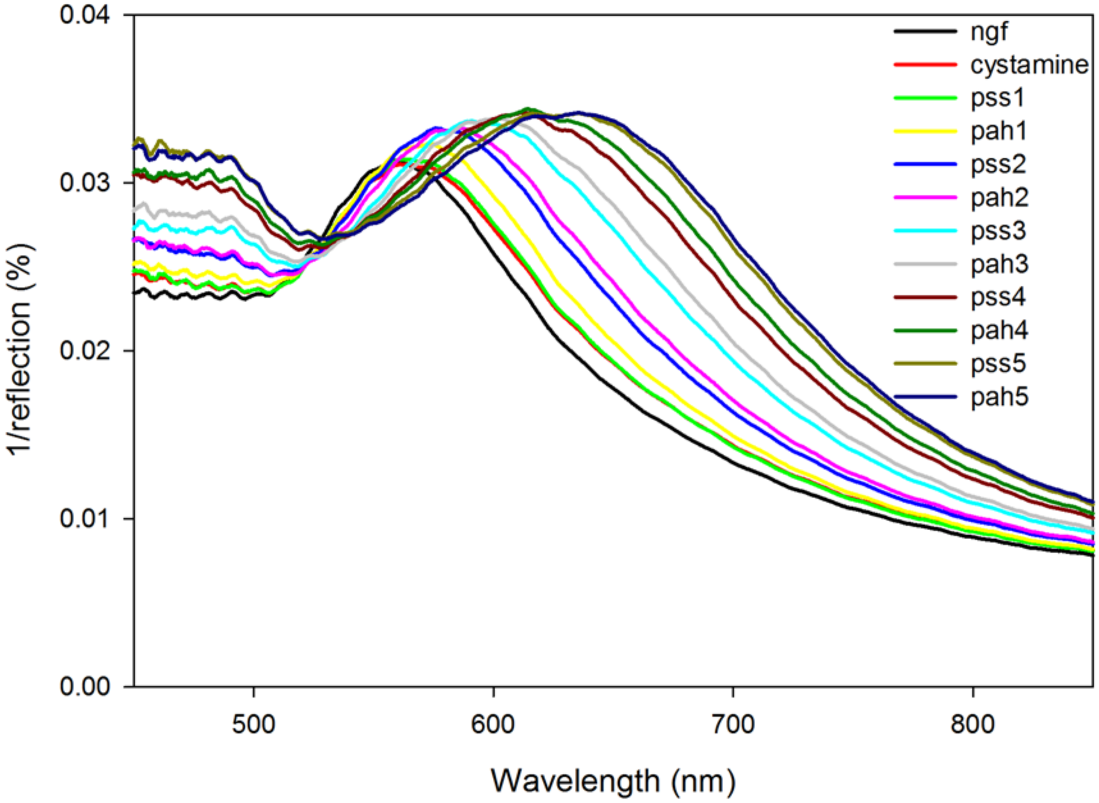

Figure 5.2 LSPR spectra of thin film of the nanostructured gold after the formation of bilayers of polyelectrolyte polymers PSS and PAH

The change in peak wavelength and intensity of LSPR sensitive nanostructured thin film of gold on the silicon wafer is a linear function of number of molecules adsorbed on the surface of the film. Figure 5.2 shows the linear increase of the peak wavelength and the inverse reflectance over a wide range of the wavelength with the thickness of the adsorbate. To control the thickness in the vicinity of the thin film, positively and negatively charged polyelectrolyte polymers were electrostatistically assembled in layer-by-layer (LBL) fashion on the surface after immobilization cysteamine on the gold surface. We started by prepared SAMs of 1 mM cysteamine on the surface to create a positive charge followed by the LBL assembly of PSS and PAH. Each polymer bilayer adds a thickness of 2 nm. Figure 5.2 shows the red shift in LSPR spectra with addition of the successive bilayers.

The response of the LSPR sensitive thin film with the change of the refractive index for biosensing will be determined by simple equation [154-155]:

$$\Delta\lambda_{max} = m\Delta\eta[1-\exp(-2d/l_d)]$$

Where $\Delta\lambda_{max}$ is a shift in wavelength, m is the bulk RIS, $\Delta\eta$ is a change in refractive index, l_d is the decay length, and d is thickness of the adsorbate. Using the equation mentioned above, the value of the l_d was estimated to be 27 nm, which is within the range of the of literature values of 10-30 nm for different types of nanostructured material active for the plasmonic resonance [156].

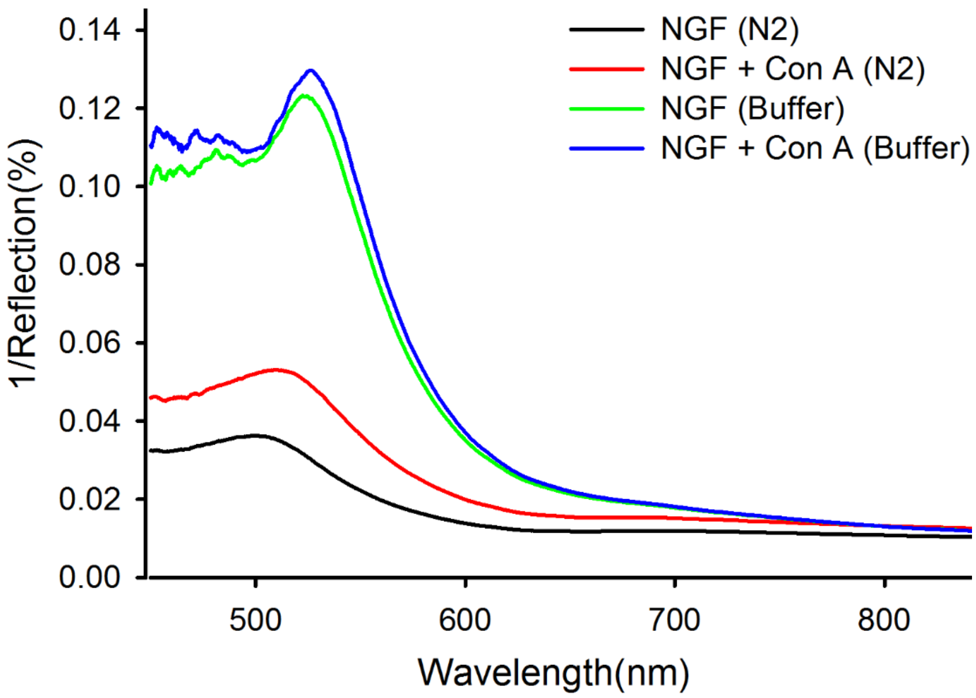

Figure 5.3 LSPR spectra illustrating the response from the transducer before (black line), and after the adsorption of Con A(red) line in dry condition (under nitrogen gas) and before (green line) and after adsorption of Con A under wet conditions.

To illustrate the ability of the material as an effective transducer for the biosensing, adsorption of protein (Con A) on the surface was monitored by LSPR spectra in both dry condition and wet condition respectively as shown in Figure 5.3. The peak wavelength of the spectra shift from 520 nm to 529 nm after adsorption of the Con A on the surface after washing and drying by nitrogen gas, similarly, the wavelength of the spectra shift from 556 nm to 558 nm with significant increase of the inverse reflectance when the spectra was measured on the solution phase.

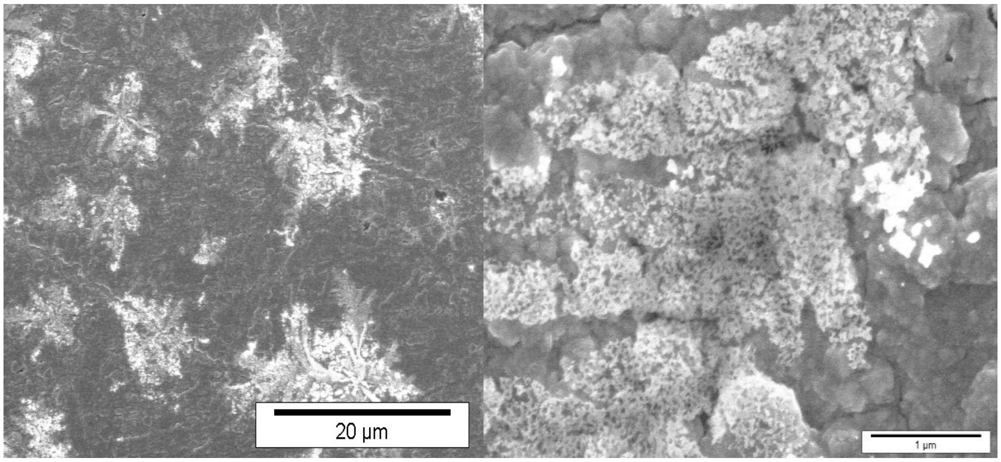

Figure 5.4 SEM image of the thin film of nanoporous gold on the surface of the sputtered gold.

Another method for the fabrication of the plasmonic active thin film of the nanoporous gold on the silicon (NGFs) uses a one-step chronoamperometry (CA) technique. The surface of the silicon wafer was scratched and etched before the sputtering of the thin film of gold. The stability of the as sputtered gold thin film on the surface of the modified silicon wafer was tested next day after deposition and the thin film of gold was found stable after modification and the test was done by thumb, and tape in both dry and wet condition as mentioned above in 5.1. A mixture of 15 mM $KAu(CN)_2$ and 35 mM $KAg(CN)_2$ solutions was prepared in 0.25 M Na_2CO_3 and one step chronoamperometry technique was applied to form the LSPR sensitive nanostructured gold film by providing the potential of -1.0 V for 90 sec followed by the chemical dealloying by concentrated nitric acid . SEM image of the NPG thin film is shown in Figure 5.4. which showed the LSPR active nanostructured gold. The change in peak plasmon resonance wavelength of the NPG thin film is a linear function of the refractive index of the surrounding solution. To observe this result, we injected different organic solvent from low refractive index to high refractive index from methanol to DMF as shown in Figure 5.5 and the corresponding shift in peak wavelength or reciprocal reflectance as a function of refractive indices of the liquids was plotted. The data were fitted using linear regression and the slope of straight lines gives the refractive index sensitivity (RIS) of NPG thin film as shown in Figure 5.6. The RIS of the thin film of the NPG was found to be 572.4 nm/RIU, which is very high in comparison of solution phase gold nanoparticles ranges from 44-288 nm/RIU [157] as well as greater than the other nanoparticles prepared by electrochemical methods [158].

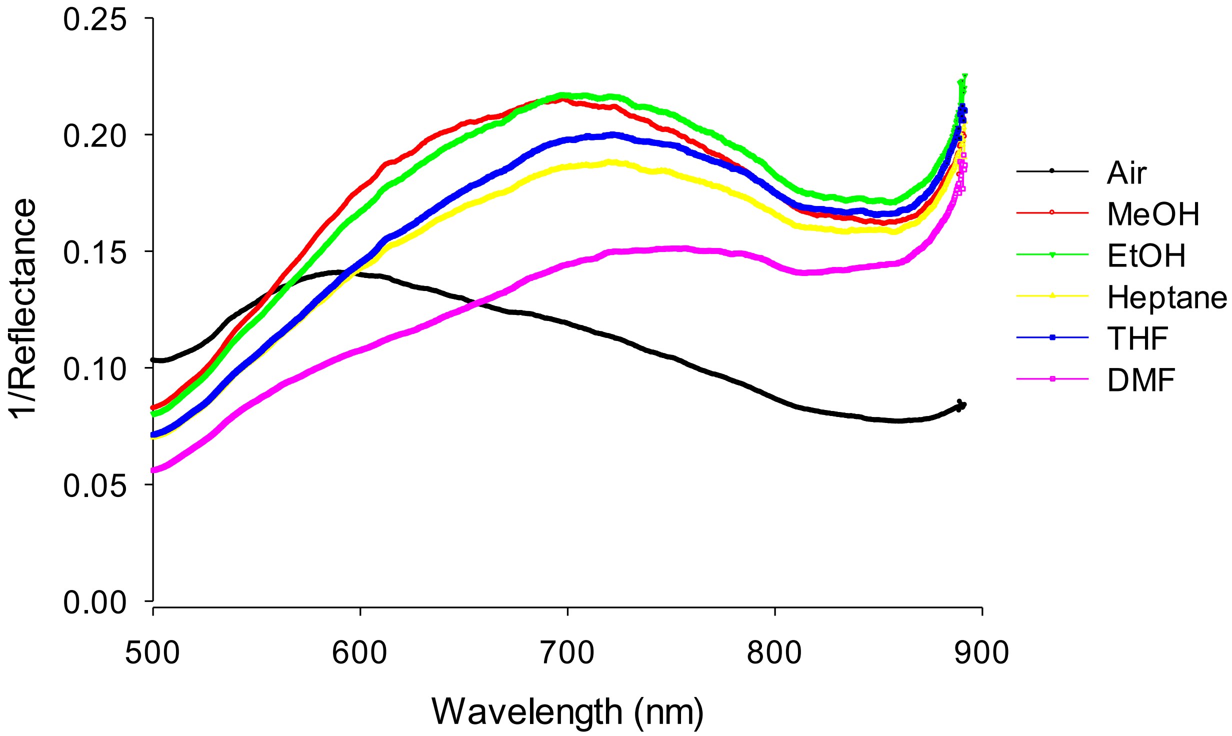

Figure 5.5. LSPR spectra of thin film of nanoporous gold on the silicon wafer when immersed in organic solvents of different refractive index.

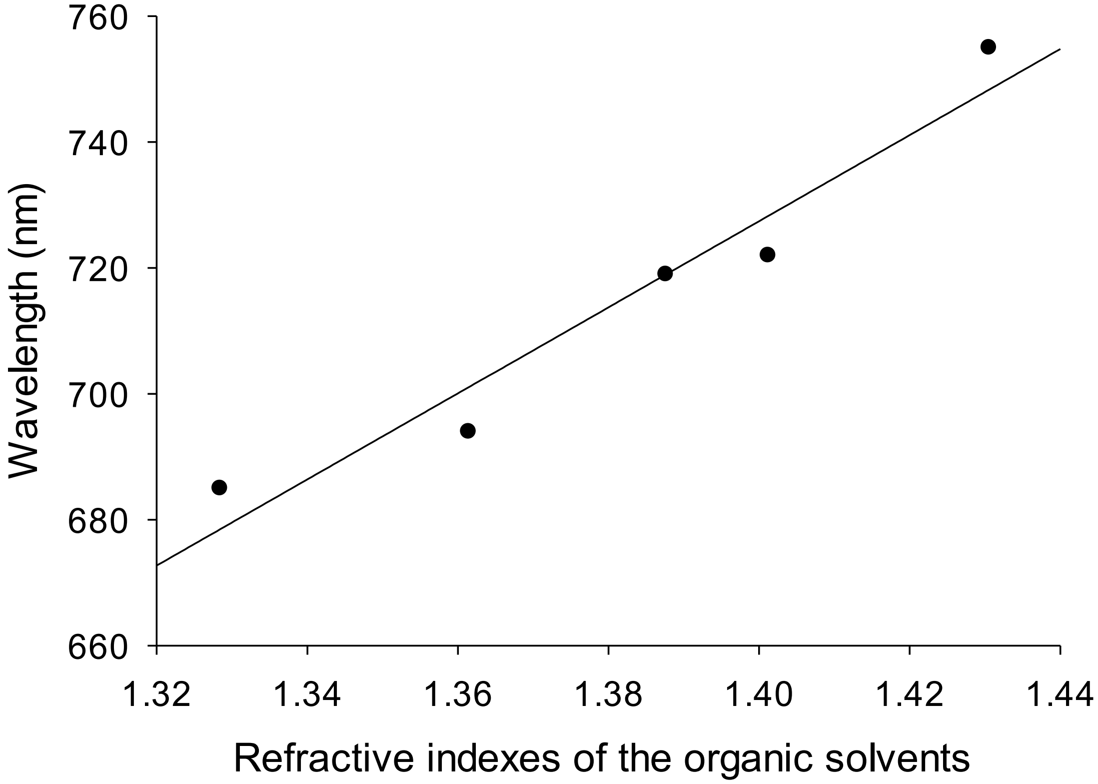

Figure 5.6. Plot of peak wavelength vs. refractive index of the organic solvent. The data were fitted using linear regression and the slope od straight lines give bulk RIS of NPG thin film is 572.368 nm/RIU for wavelength and reciprocal reflectivity, respectively.

6. CHAPTER VI. ELECTROCHEMICAL FABRICATION OF HIERARCHICAL BIMODAL GOLD ELETRODE FOR ELECTROCHEMICAL SENSING

6.1 *Fabrication of hierarchical nanoporous gold electrode*: The HNPG electrodes were prepared by combining both electrochemical and chemical dealloying methods. The method for the fabrication of HNPG electrode is shown in scheme 6. The alloy of gold and silver in the composition of $Au_{10}Ag_{90}$ (at %) was form by electrochemical alloying on the gold wire. Alloys of gold and silver were prepared by electrodeposition of gold and silver alloys onto the gold wire electrodes (diameter 0.2 mm, length 5.0 mm) from the mixture of the 5mM $KAu(CN)_2$ and 45 mM of $KAg(CN)_2$ in 0.25 M Na_2CO_3 solution for 10 minutes at -1.0 V (vs. Ag/AgCl). The silver of the gold-silver alloy was partially leached away by electrochemical dealloying at +0.6 V for 10 minutes in 1M HNO_3 with residual Ag of ~40%. Subsequently, the np-AgAu was annealed in the air for 3 hours at 600 °C in a furnace (47900 furnaces, Barnstead Thermolyne). The residual silver in the coarsened porous alloy was further selectively removed by a second step of dealloying, leading to the formation of HNPG with macro and mesopores distribution of average pore size of 1.32 ± 0.36 µm and 50 ± 16 nm, respectively. The distribution and the measurement of the pore sizes with the different conditions were carefully measured. To characterize the functionality of our electrode, electrochemical characterization was done using cyclic voltammetry in the ferro/ferric cyanide redox probe solution and here we compared the surface area of the different nanoporous gold electrodes with the identical conditions. In a cyclic voltammogram between 0.2 V and 1.6 V, the hierarchical sample exhibits a higher surface area as shown in Figure 6.2. The two key aspects of the HNPG design is to achieve both a large specific area for the functionalization and a transport pathway through the larger pores for the faster and more complete immobilization. The large surface area was achieved by the small pore sizes in the HNPG structure and diffusion of the molecules throughout the bulk of the structure was achieved by larger pores present in the material which facilitate fast and complete immobilization of different molecules including some large molecules like protein. The immobilization time and the number of BSA molecules was calculated from monitoring the absorbance of 2 mL of 0.5 mg mL^{-1} of BSA in the as prepared nanoporous gold wire shown in Figure 6.3 (a) with the hierarchical NPG electrode Figure 3(b). The number of the BSA molecules immobilized on the conventional NPG was calculated was 1.59×10^{13} molecules vs the number of molecules immobilized on the HNPG was calculated as 3.55×10^{13} molecules. Along with the modified structure of the HNPG electrode, formation of the well-packed and ordered self-assembled monolayer of the small molecules or the large molecules like proteins offer a flexible and effective approach for the functionalization of the free surface of the nanoporous materials that can be used for the desired modification and for effective use with better sensitivity for biosensing.

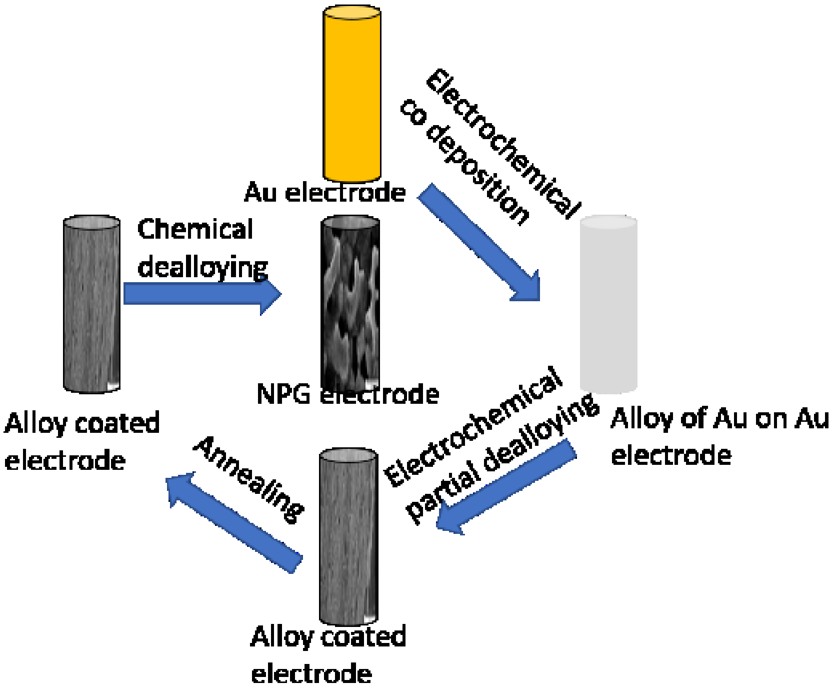

Scheme 7. Schematic diagram of the fabrication of the hierarchical nanoporous gold electrode

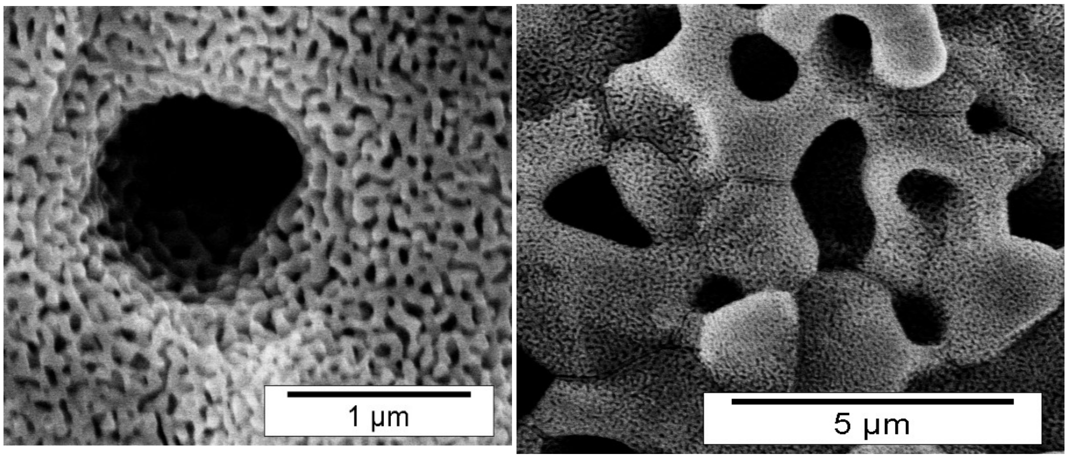

Figure 6.1 SEM image of HNPG electrode at different magnification showing mesoporous and nanoporous structure

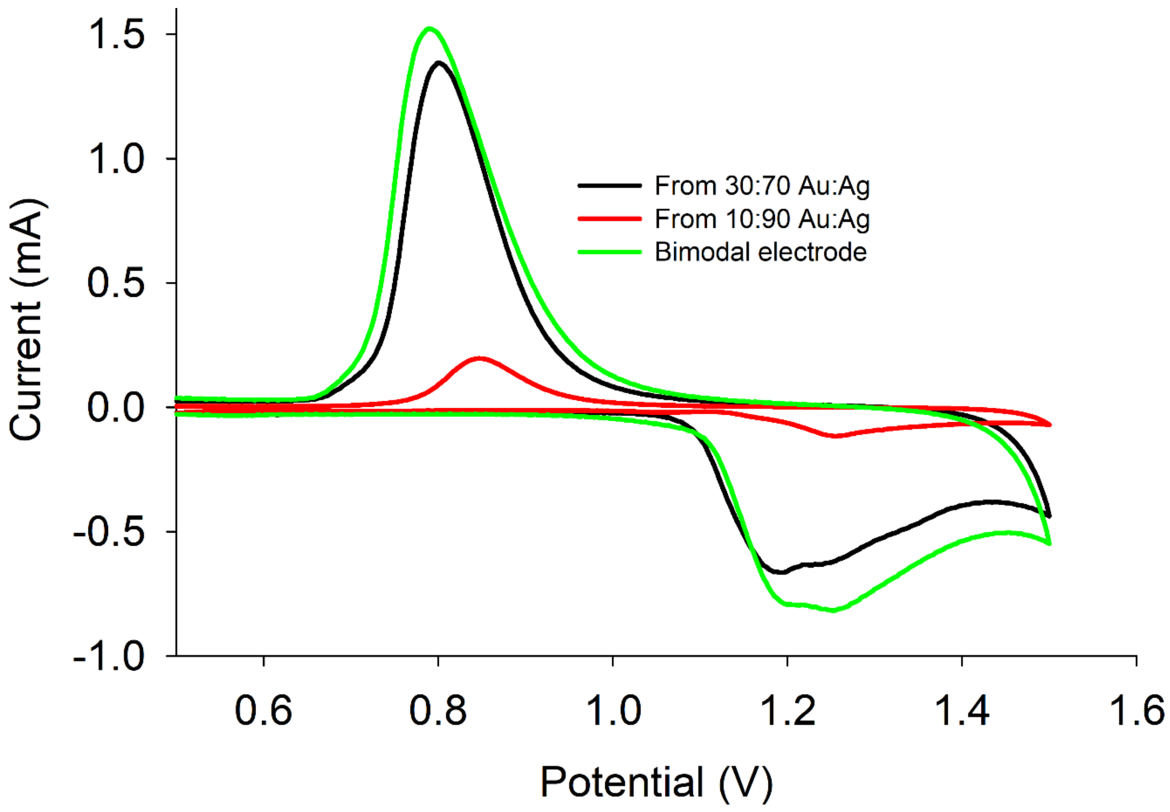

Figure 6.2 Cyclic voltammogram of NPG electrode NPG electrode from the dealloying of the gold alloy of the gold and silver at 30:70 ratio (black line), 10:90 ratio (red line) and

the bimodal gold electrode from 10:90 ratio (green Line) from 0.5 V to 1.6 V with a scan rate of 50 mV/sec in 0.5 M H_2SO_4 .

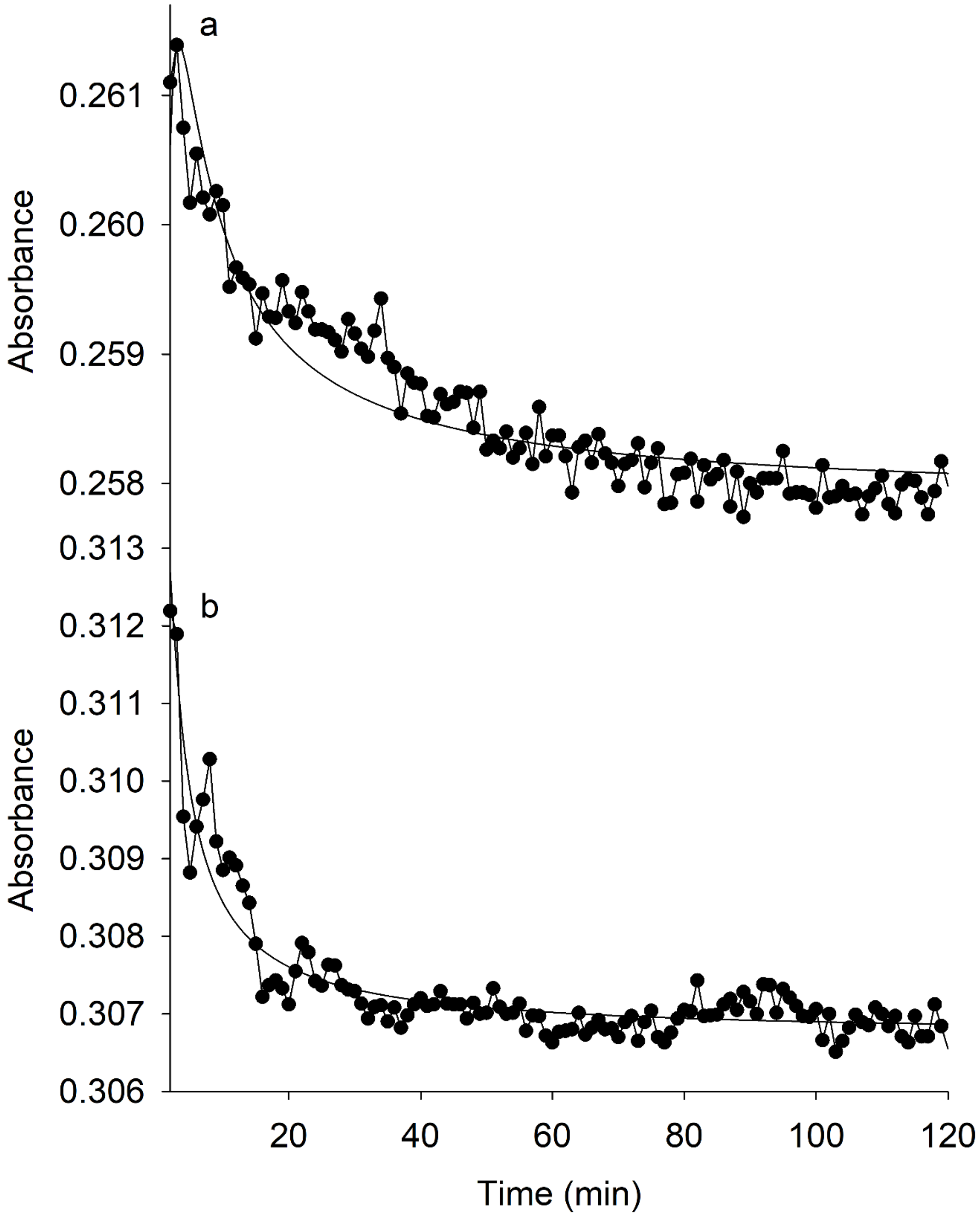

Figure 6.3 UV-Visible Spectrometric absorbance measurement of the 0.5 mg/ml of the BSA solution using a) Nanoporous gold electrode and b) Hierarchical bimodal gold

electrode at wavelength 280 nm. The absorbance was measured immediately dipping the NPG wire in the cuvette containing protein solution

7. CHAPTER VII MISCELLANEOUS WORK

7.1 *Fabrication and characterization of nanoporous gold beads*: The increase in surface area with increasing porosity the gold is the key factor that influence efficiency for loading of molecules and proteins. Porous gold beads were easily prepared by a templating method and showed uniform pore size distribution and large surface area [159]. Templating is the simple approach to incorporate and control porosity. Inorganic or organic materials that are removed in a final step can be used as templates for the formation of nanostructured porous materials. Templating followed by dealloying provides a versatile approach to creating materials with hierarchical porosities. Nanoporous gold beads were reported as made using polystyrene beads of the textural pores serving as templates [160]. We prepared nanoporous gold beads of controlled particle size by using rapid co-reduction of $HAuCl_4$ and $AgNO_3$ by $NaBH_4$, a very strong reducing agent, with constant stirring at a rate of 2000 rev/min followed by dealloying in concentrated HNO_3 overnight. The nature and pore size distribution of the beads were dependent on the ratio of gold and silver salt and the optimal ratio of gold and silver salt molar ratio was maintained as 30:70. The optical images as well as from the scanning electron microscopy are shown in Figure 7.1 along with EDX determination of the elemental composition. The composition of gold was found to be around 15 mol% when the alloy of the gold beads was form.

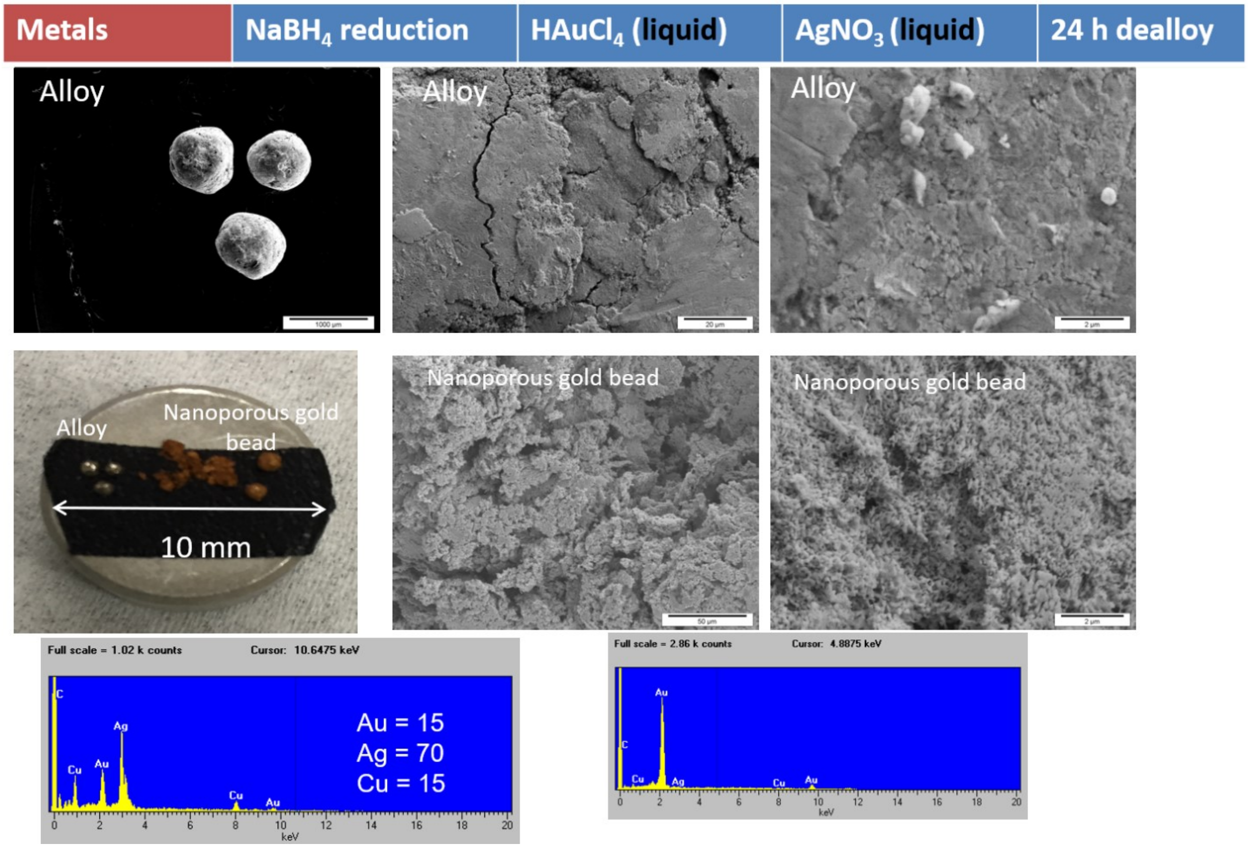

Figure 7.1 Images and EDX measurement of nanoporous gold bead

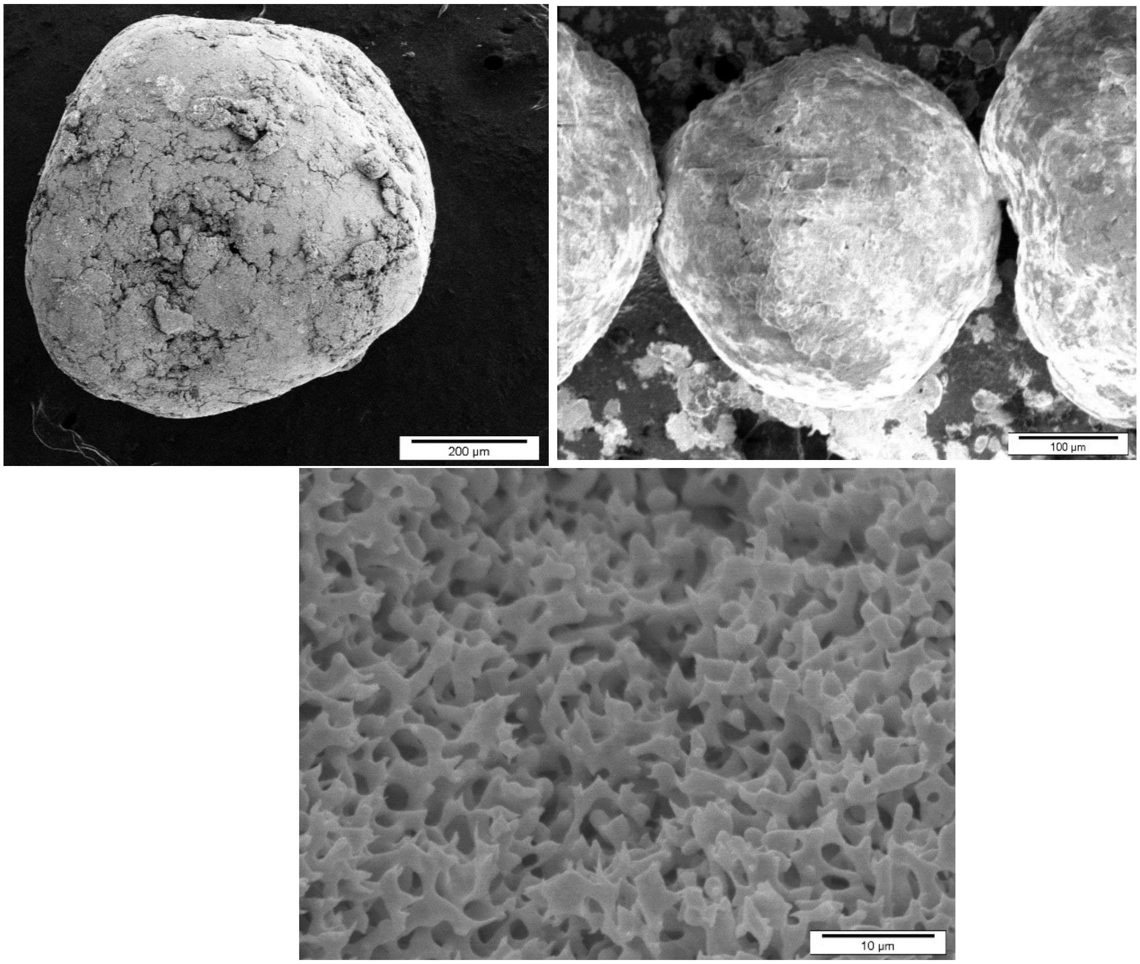

Figure 7.2. High magnification SEM image of nanoporous gold beads

7.2 *Electrochemical study of carbohydrate-protein interaction*: Recognition of glycoconjugates is an important event in biological systems, in the form of carbohydrate-protein interactions. It is a well-known fact that most cells are covered with carbohydrates attached to glycolipids and membrane glycoproteins. Glycans are also present on many of the circulating glycoproteins from the serum. Glycans are capable of forming many different combinatorial structures, including branched ones, from a small number of sugar units [161]. The monosaccharides are joined together via glycosidic bonds between the anomeric hydroxyl group of one monosaccharide and any of the hydroxyl functions of the second monosaccharide, with loss of a molecule of water. The identification and the detection of proper multivalent carbohydrate scaffolds has become the prerequisite to the study and characterization of carbohydrate-protein interactions. SAMs can be used to control the density and orientation of attached carbohydrates, or to position them in patterns, in ways that aid the study of multivalent interactions with their binding partners. SAMs have been applied to surface-based real-time, label-free analysis methods. For example, a Huisgen 1,3-dipolar cycloaddition click chemistry was employed to immobilize azido derivatives of mannose, lactose and alpha-galactose and the interaction of these sugars was studied with their specific lectin partners Concanavalin A, *Erythrina Cristagalli* lectin and alpha-galactose binding lectin. The affinity constant of the Con A binding to mannose was $(8.7 \pm 2.8) \times 10^5$ and $(3.9 \pm 0.2) \times 10^6$ M^{-1} measured from QCM and SPR respectively [162]. Similarly, the affinity constant of the Lactose-ECL and α-Gal binding with polyclonal anti-Gal antibody were determined to be $(4.6 \pm 2.4) \times 10^6$ and $(6.7 \pm 3.3) \times 10^6$ M^{-1}, respectively [162]. The binding of the concanavalin A and cholera toxin to their specific α- mannose and β- galactose derivative functionalized on the gold electrode via SAM was determined by cyclic voltammetry and the association constant for the mannose-Con A was found to be $(5.8 \pm 1.2) \times 10^7$ M^{-1} and $(2.6 \pm 0.5) \times 10^8$ M^{-1} for galactose-CT [163]. 50 mM and 20 mM mixture of the EDC and NHS in MES buffer was employed to immobilize the NH_2- terminal mannose and pentasaccharides to fabricated carbohydrate self-assembled monolayers on the gold electrode. The affinity of Con A binding to mannose and pentasaccharides was measured by EIS and CV, respectively and study confirm that their specificity to their corresponding lectins and nonspecific adsorption on the surface was negligible.

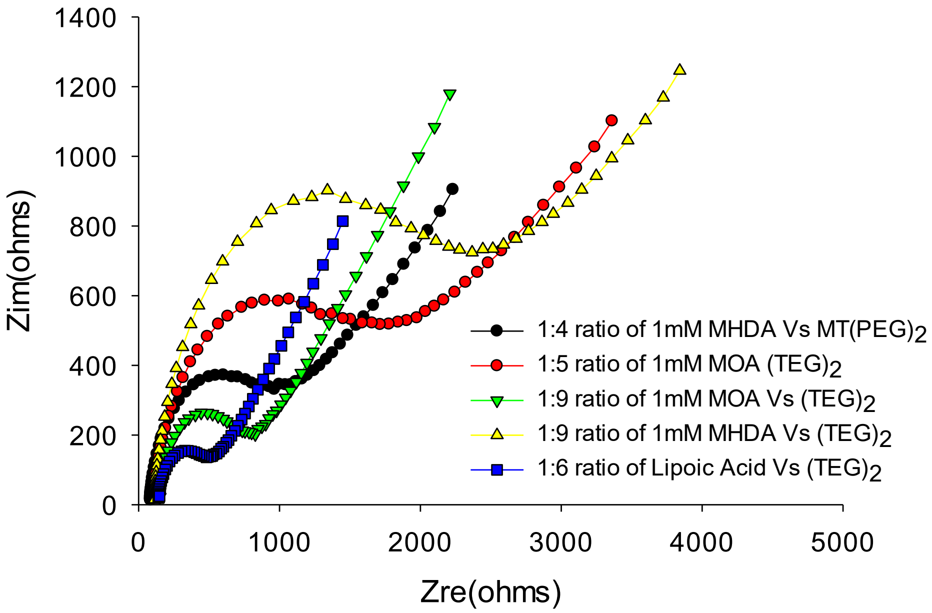

Figure 7.3 EIS measurement of carboxy-terminal mixed SAM modified flat gold wire with 5 mM of [$K_3Fe(CN)6$] and [$K_4Fe(CN)6$] in tris buffer (pH=7.4)

We characterized the formation of carboxylic terminal SAMs on the gold elected using impedance properties of the modified electrode system with spacer. We tested SAMs of MOA, lipoic acid, MHDA with different ratio of SAMs of pegylated hydroxyl terminal thiol as shown in Figure 7.2. After examination the properties of the SAMs on the gold electrode, the carboxylic terminal group of the SAM was activated by the 50 mM EDC and 20 mM NHS in MES buffer to immobilized amine terminal pentasaccharides on it and the interaction of the pentasaccharides with lectin Con A was examined by electrochemical method such as EIS, and LSPR method as shown in Figure 7.3.

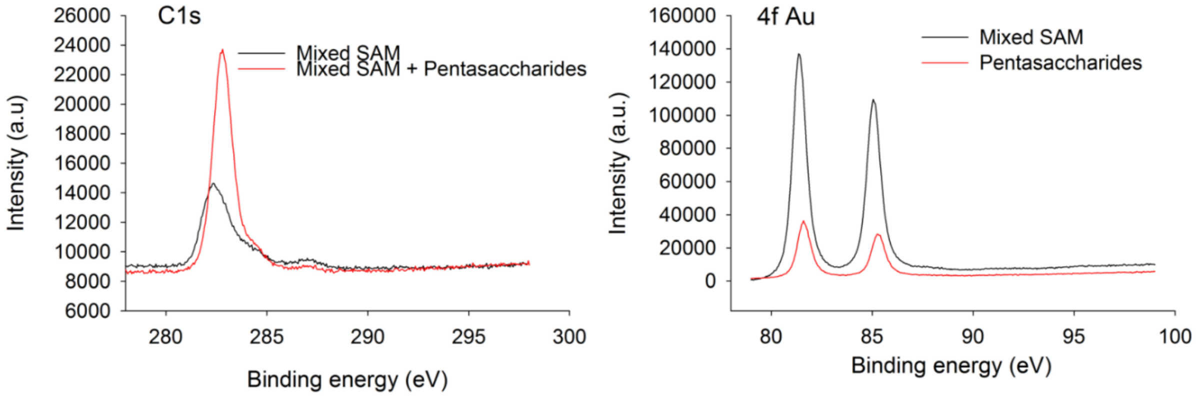

Figure 7.4 XPS spectra of the gold surface (a) survey for the carbon (b) survey for the Au

The formation of the SAMs of the pentasaccharides s was also examined by X-ray

Table 1. Atomic Concentration Table

	C1s	Au4f
Before	49.37	39.78
After	81.06	8.41

photoelectron spectroscopy (XPS) performed at Washington University. The gold surface was immersed in the ethanolic solution of 1 mM of mix SAM of MUDA and pegylated thiol in the ratio of 1:3, and them 0.1 mM of the pentasaccharides was immobilized using EDC/NHS chemistry. XPS is a powerful tool for the investigating the chemical properties of the SAMs, because XPS spectra provide the useful information about the amount of the element present on the surface and the thickness of the monolayer. The XPS spectrum is shown in Figure 7.4. The C 1s core region, a sharp peak at 285.2 eV was observed due to presence of SAMs on the surface. The amount of the carbon content increase significantly from 49.37 to 81.06 after immobilization of the pentasaccharides, which implies the formation of the SAMs of pentasaccharides on the gold surface. On the other hand, as shown in Figure 20 (b), the intensity of the gold peak decreases due to increase in the thickness of the SAMs after immobilization of pentasaccharides.

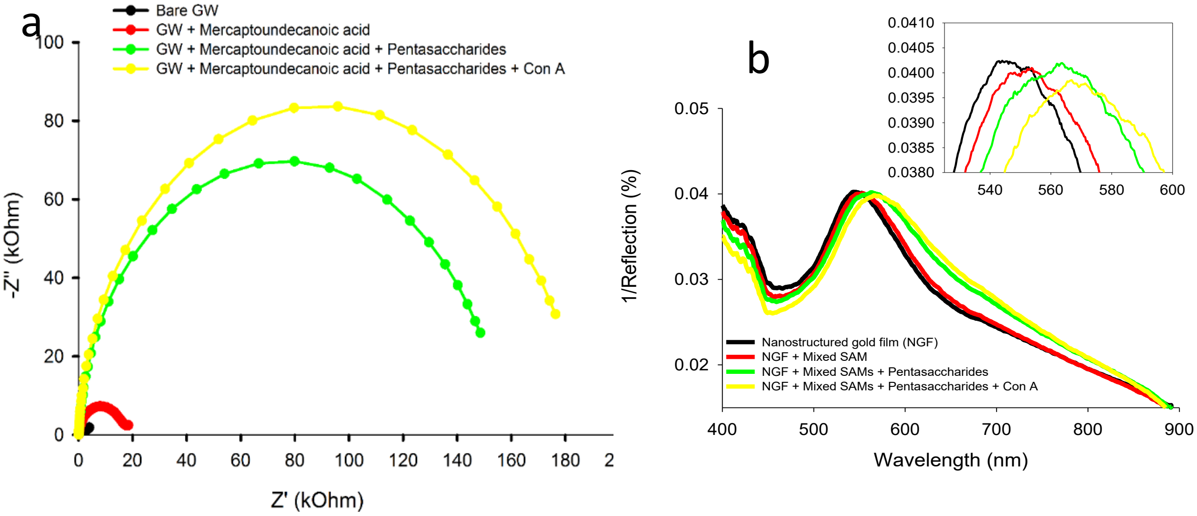

Figure 7.5 (a) Nyquist plot of gold wire: bare gold (black), after formation of SAM (red line), immobilization of pentasaccharides (green line), and interaction with Con A (yellow line) (b) LSPR spectra of: bare gold (black), after formation of SAM (red line) , immobilization of pentasaccharides (green line), and interaction with Con A (yellow line)

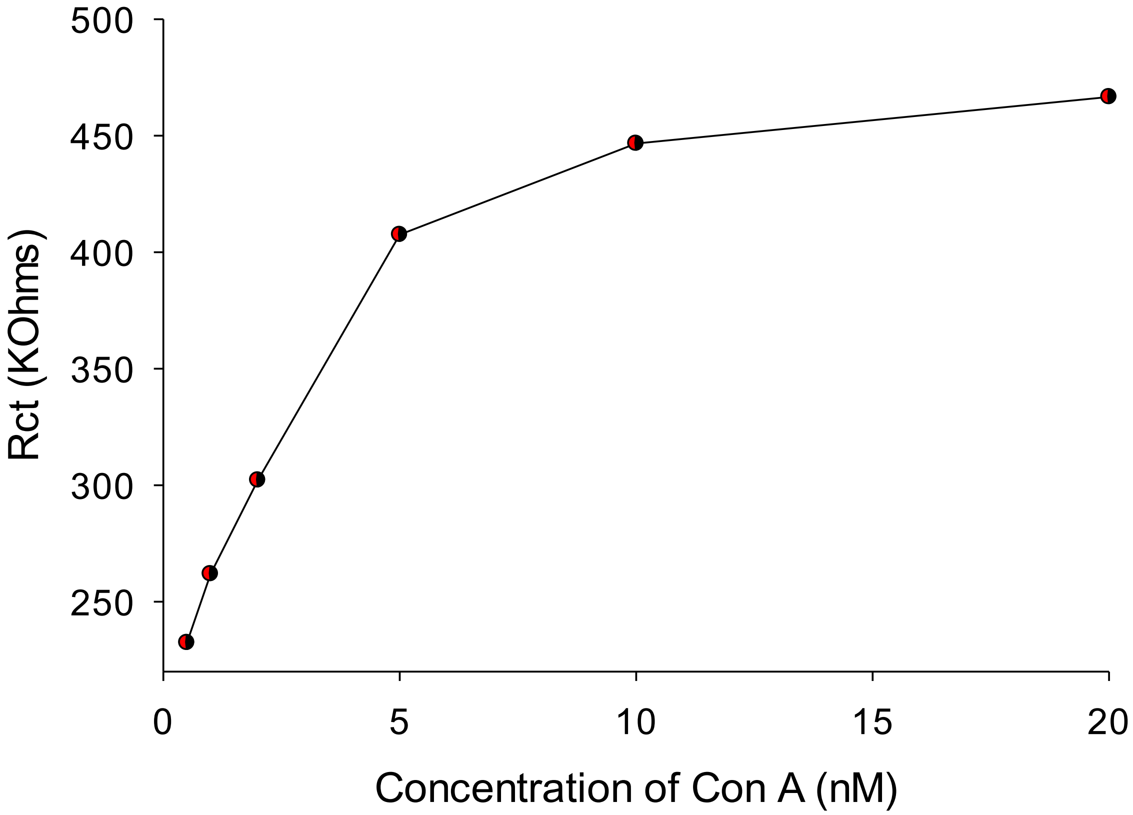

Figure 7.6 Concentration dependent study of interaction of pentasaccharides with Con A from EIS.

The concentration dependent interaction of pentasaccharides with Con A was studied by EIS as shown in Figure 22. The interaction of con A and pentasaccharides shows the linear response from the concentration of 1 nM to 5 nM, with increase in the concentration, the R_{ct} value does not change due to saturation of the active sites present on the surface. In summary, EIS and LSPR were the useful tool to study the interaction between concanavalin A and high mannose pentasaccharides representation lectin-carbohydrate interaction

7.3 *Fabrication and Characterization of monolithic polymer*: The synthesis and properties of porous polystyrene/divinylbenzene based polymer have been investigated for some time. Porous polymer materials have found growing use as stationary phases for chromatographic separations [164]. Polystyrene based polymer played a very important role in the separation of drugs and chiral compounds. The main advantages of this polymer are high pressure tolerance and pH stability, tunable particle/pore size, excellent compactibility with polar and non-polar organic solvents, and a facile fabrication process which resulted in good adaptability for chromatographic purposes such as HPLC, ion chromatography and size exclusion chromatography [165-167]. For chromatography, a well defined pore structure is necessary and this is acomplished using porogenic substances during a polymerisation process. Different kinds of multistep methods such as activated swelling, seeded emulsion polymerization, precipitation polymerisation, template imprinting, and membrane techniques have been used to synthesize these porous polystyrene materials. However, there are some drawbacks connected with conventional ion exchange resins having a bead structure. A significant issue resin beads is the difficulty of uniformly packing the in a thin cell, such as that used in the desalination cell of an

Figure 7.7. Image of monolith A and monolith B

electrodeionization apparatus. The second problem is the large ion exchange band length (H) value with the increase of the flow rate. The rates within the beads may be slower than those of the surface of the beads and third problem associated with polymer beads is the slow ion mobility between the beads. The overall conductivity reduces of the resin beads in the cell is low and reduces the performance of electrodeionization apparatuses [101, 168-169].

The open-celled monolith structure is the reverse of the structure formed by conventional resin beads packed in a column. Monolithic polystyrene-based polymers have been synthesized and their applications in bioseparation and bio-reaction have been demonstrated [170-171]. The use of the polymer monoliths in synthetic organic chemistry has recently become more popular, mainly due to developments in the fields of combinatorial chemistry and parallel synthesis [172]. The polymer supported automated synthesis used in various form of either beads or monolithic form with smaller or large level of porosity and many types of beads are commercially available; however, their uses have limitations. With gel type beads, the majority of the reactive sites are positioned inside a bead, and swelling is normally essential to enable accessibility of reactive sites. This can limit the range of solvents in which supports can be used. With permanently porous beads there is no requirement for pre-swelling and greater solvent compatibility can be achieved; however, the reactive sites inside the porous beads are accessed by diffusion only, which is a slow process. In addition, porous beads are fragile and difficult to manipulatedue due to their propensity for electrostatic charge build up. Furthermore, when using polymer beads in a flow passing around than the beads rather than from the beads which also severely reduce the effficiency [173].

A porous monolith having uniform open-celled structure was prepared by emulsion polymerization by varying the composition of the different monomer as shown in Table 1. The formation of the open-celled monolith structure wsa seen by imaging using SEM as shown in Fgure 7.3. To evaluate the structures more precisely, the size, the pore size distribution and the total pore volume were determined by nitrogen gas adsorption-desorption isotherms using BET analysis. Styrene was used as the main constituent of the polymerization with different ratio of divinyl benzene as a cross linking agent were used for the polymerization with variation of the functionalized monomer to get the activated open-cell monolith as shown in Table 1. Span 80 was used as the emulsifier and α, α'-azobisisobutyronitrile (AIBN) was the initiator of the polymerization. The emulsion polymerization was carried out in water. IR spectra was also measured to confirm the activation of polymer by using fuctionalized monomer like vinyl benzyl chloride, vinyl

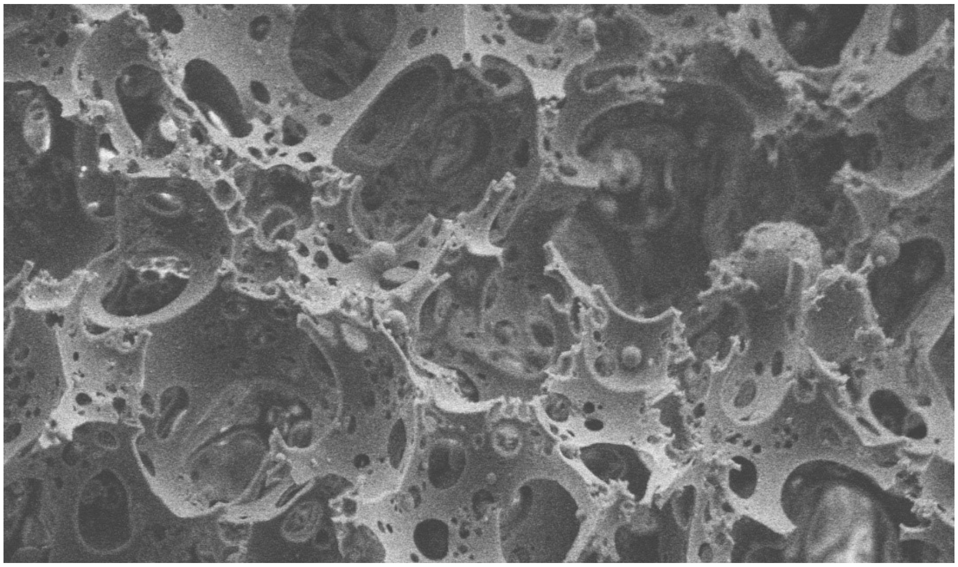

Figure 7.8 SEM image of polymer at high magnification

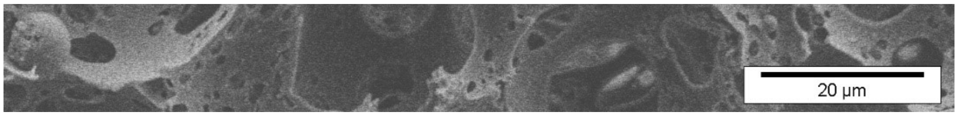

benzoic acid, and pentonic acid to get activated terminal fuctional group like chloride and carboxylic acid.

7.4 *Characterization of Panzagel*: We reported the development of novel polystyrene resin with diethylene glycol derived cross linker and named as Panzagel [174], and investigated the swelling properties, chemical and thermal stabilities, along with pore size distribution. Moreover, Panzagel was implemented as a new material for the for the automated HPLC synthesis of glycans.

Thermal degradation properties of Panzagel was assessed by TGA. Figure 3 shows the thermal decomposition of Panzagel at various temperatures. Panzagel was found thermally stable up to 360 °C. While about 97% weight loss occurs at 460 °C. The thermal decomposition temperature and the SEM images of the polymer didn't show any significant different after treatment with TMSOTf acid. Panzagel treated with TMSOTf decomposed around 85% up to 600 °C leaving behind residue.

The prepared polymer microspheres were observed by scanning electron microscopy as shown if Figure 4. Figure 4(a) and (b) indicates the polymer microspheres with an average size of 158 μm (Average of 30 polymer beads). Nitrogen adsorption/desorption isotherm plots have been used to evaluate the pore volume (Vp) and the surface area (S) of the synthesized materials and the total pore volume was calculated as 0.0033 mL g^{-1} and the BET surface area was 0.84 m^2 g^{-1}.

Upon treatment of 100 mg of resin with 100 μL of TMSOTf, in 1 mL of methylene chloride for 1 h, no decomposition was observed. The thermal stability of the resin did not show significant differences, indicating a chemical structure unaltered by the prolonged contact with acid.

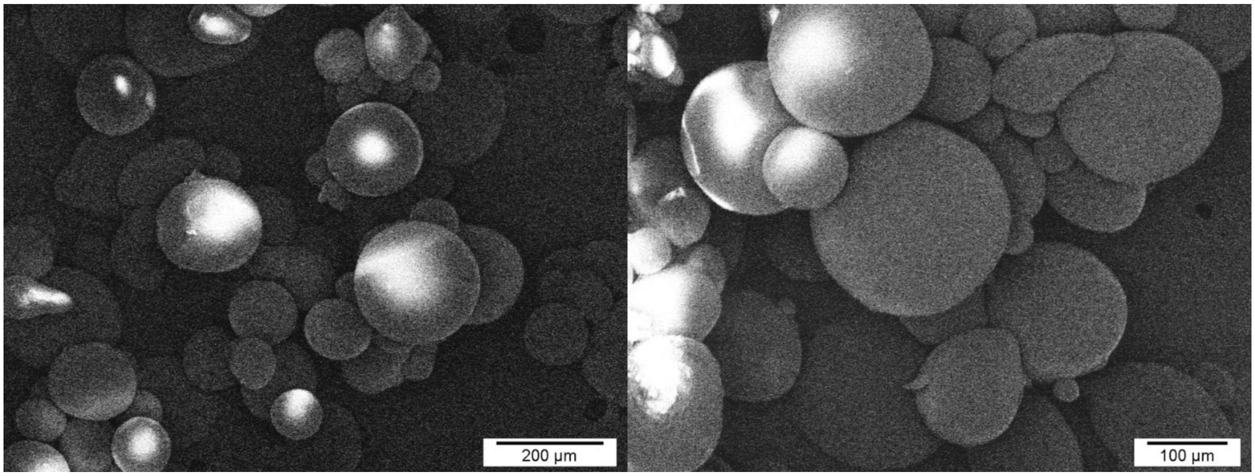

Figure 7.9. SEM image of polystyrene based polymer at: a) 100x and b) 150x magnifications

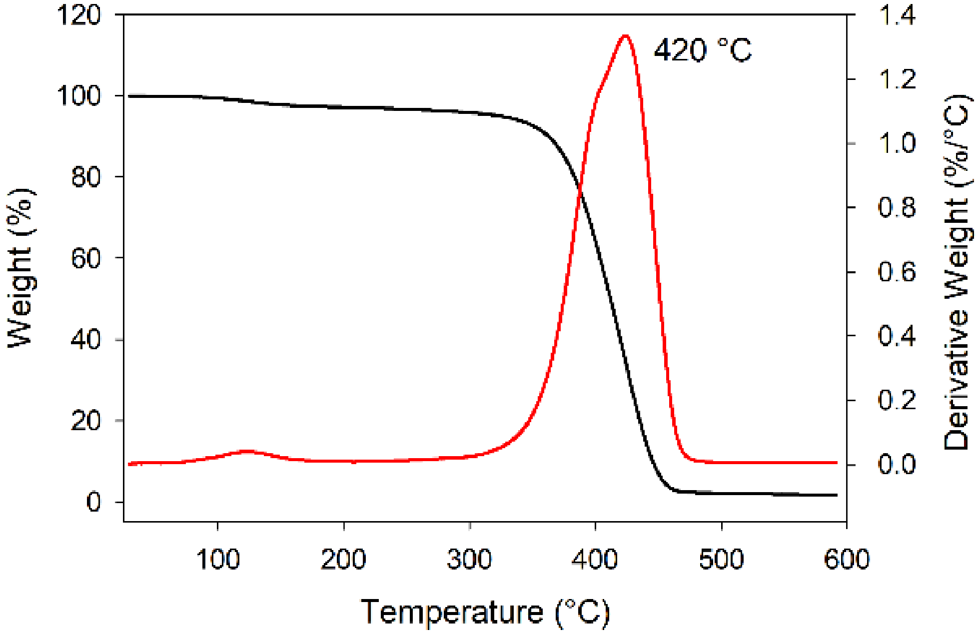

Figure 7.10. Thermogravimetric analysis (TGA) plots (black line) and weight derivatives curve (red line) of Polystyrene divinyl benzene polymer

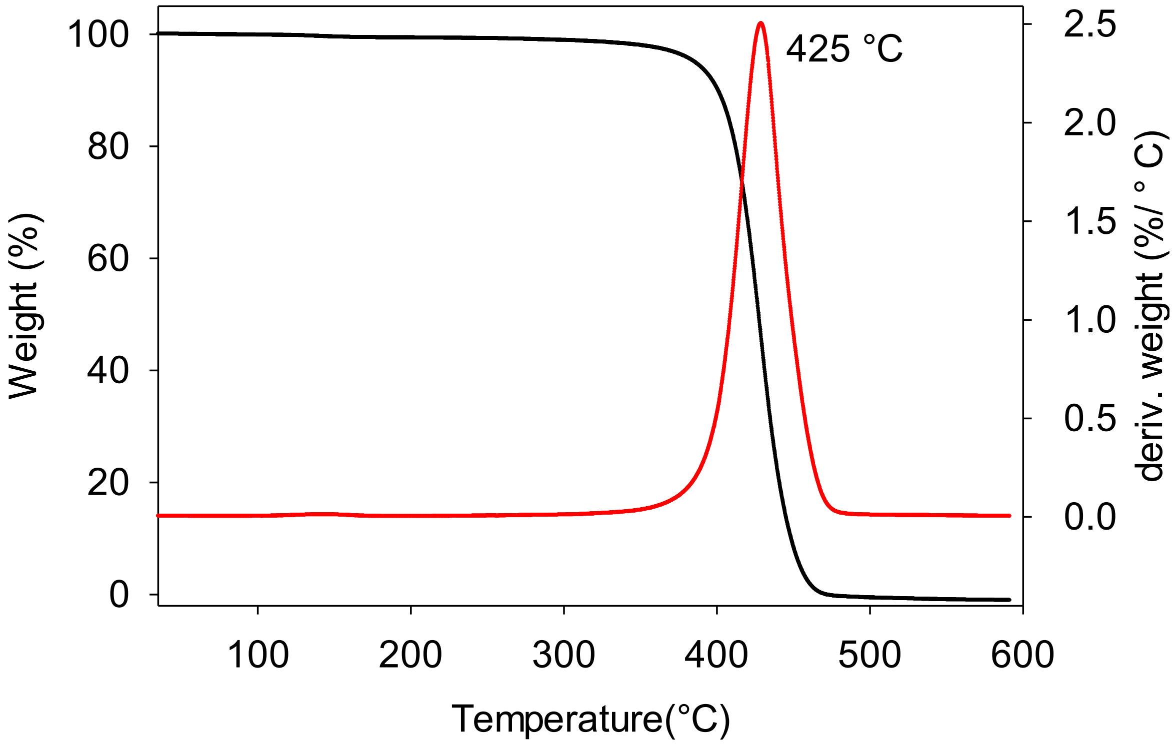

Figure 7.11. Thermogravimetric analysis (TGA) plots (black line) and weight derivatives curve (red line) of Panzagel

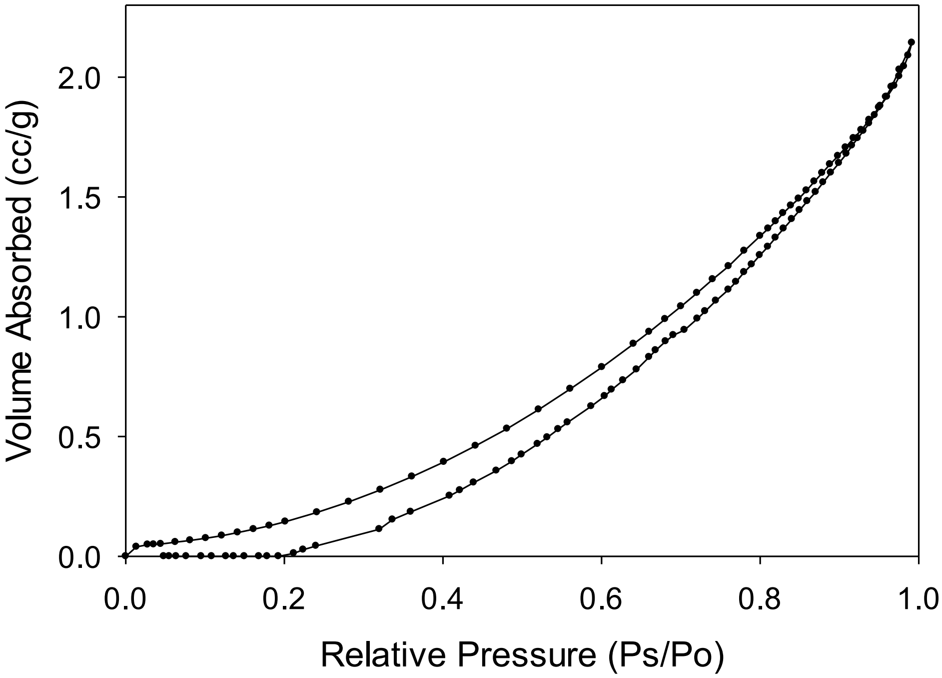

Figure 7.12. BET isotherm of functionalized polymer

Table 2. Polymerization materials and conditions

Styrene (µl)	**DVB (µl)**	**AIBN (mg)**	**Span 80**	**Vinyl Benzyl chloride (ml)**	**Vinyl Benzoic Acid (mg)**	**Pent enoic Acid(ml)**	**Vinyl Aniline (mg)**	**1-decanol (ml)**	**Cyclo hexanol (ml)**
540	15	5	100	-	-	-	-	-	-

220	30	5	100	220	-	-	-	-	-
220	30	5	100	-	220	-	-	-	-
220	30	5	100	-	-	-	220	-	-
220	30	5		-	-	220	-	-	-
500	500	10	100	-	-	-	-	-	2
500	500	10	100	-	-	-	-	2	-
500	500	10	-	-	-	-	-	2	2
500	500	10	-	-	200	-	-	-	4
500	500	10	-	-	-	200	-	4	-
500	500	10	-	-	-	200	-	2	2
500	500	10	-	-	200	-	-	2	2
500	500	10	-	200	-	-	-		4
500	500	10	-	200	-	-	-	2	2
500	500	10	100	-	-	200	-	2	-

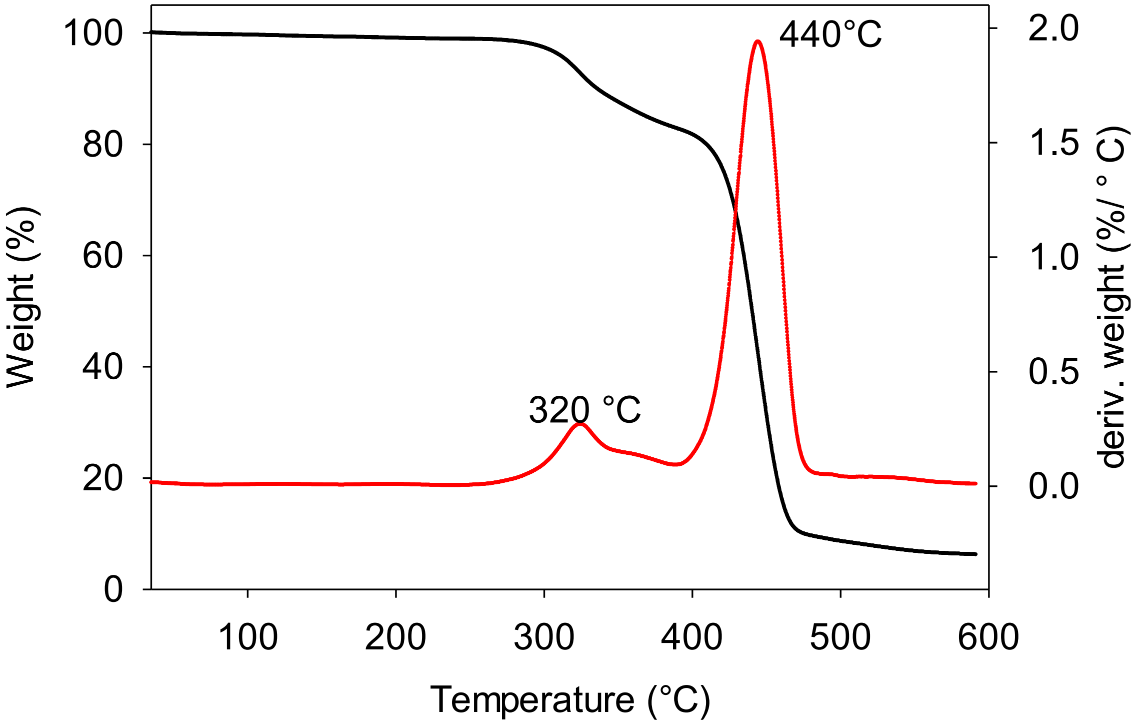

Figure 7.13 Thermogravimetric analysis (TGA) plots (black line) and weight derivatives curve (red line) of the Panzagel after treatment with TMSOTf

Table 3. Swelling experiment in DCM

Polymers	**Weight I (mg)**	**Weight II (mg)**	**ΔW**	**Volume I (ml)**	**Volume II (ml)**	**ΔV**	**ΔV/ΔW**
S+D+De+P	126.24	1009.64	879.4	5.2	4.4	0.8	9.1×10e-4
S+D+De+v	34.38	40.52	1.14	4.4	4.3	0.1	8.7×10e-2
S+D+CY+W+P	87.6	460.20	372.24	2.8	2.2	0.6	1.6×10e-3
S+D+De+P+CY	98.17	645.66	547.49	3	2.5	0.5	9.1×10e-4
S+D+De+VB	81.50	614.46	487.88	4	3.6	0.4	8.2×10e-4
S+D+De+CY+V	57.4	346.07	284.03	3	2.8	0.2	7.3×10e-4

S- styrene, D- divinyl benzene, De- 1-Decanol, P- 4-Pentenoic acid, V- vinyl benzoic acid W- Water, CY- Cyclohexanol, VB- Vinyl Benzyl chloride

Table 3. Swelling experiment in Buffer

Polymers	Weight I (mg)	Weight II (mg)	ΔW	Volume I (ml)	Volume II (ml)	ΔV	ΔV/ΔW
S+D+De+P	45.20	61.23	16.03	3	2.95	0.05	3×10e-3
S+D+De+v	117.44	126.54	9.1	2.95	2.93	0.02	2×10e-3
S+D+CY+W+P	32.22	39.10	6.88	2.95	2.92	0.03	4×10e-3

S- styrene, D- divinyl benzene, De- 1-Decanol, P- 4-Pentenoic acid, V- vinyl benzoic acid W- Water, CY- Cyclohexanol, VB- Vinyl Benzyl chloride

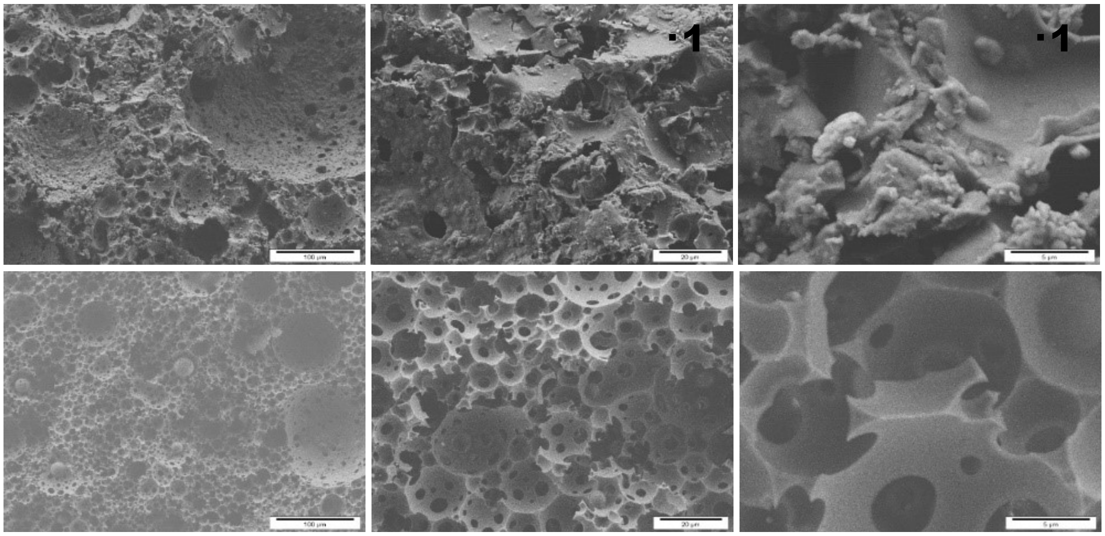

Figure 7.14. Scanning electron micrograph of the porous resin monolith

We synthesized a new monolithic and beads of the ion exchange resin with continuous porous structure by one step and two step polymerization process with different activated functional group, as summarized in Table 2. Swelling experiment shows the relationship between the cross-linking agent to the polymerization process. With increase in the percentage composition of the divinylbenzene, synthesized polymer become hard and shows less swelling as shown in Table 3.

CONCLUSIONS

Here, we have prepared novel and sensitive nanostructured gold in the different form of electrode, beads, nanoparticles, monoliths (plates, milli wire), and thin film on the solid support using both chemical and electrochemical techniques and used them as a transducer and solid support for the electrochemical and LSPR based biosensing as well as drug delivery and protein separation. Co-reduction of gold and silver salt followed by dealloying of the silver were used to fabricated nanoporous gold nanoparticles and nanoporous gold beads. Co-deposition of the gold and silver and selective partial dealloying using electrochemical technique followed by annealing and complete chemical dealloying approaches was used to fabricated hierarchical bimodal gold electrode and used it for electrochemical biosensing. We have found that the method to synthesize LSPR-sensitive thin film of nanostructured gold on the adhesion layer free gold coated silicon wafer followed by two-step chronoamperometry technique having first potential of -1.2 V for 60 sec and second potential -1.6 V for 30 sec and we used if for label free detection of carbohydrate protein interactions showing how LSPR peak shifts with the specific interaction of glycoprotein and lectin and formation of inclusion complex.

We describe the feasibility of using NPG rods as a carrier for the delivery of small drug like doxorubicin and bortezomib. We have demonstrated that DOX can form inclusion complex with thiolated beta cyclodextrin on the surface of the nanoporous gold and BTZ can form pH switchable covalent bond with dopamine modified nanoporous gold; as a result, the form complexes demonstrated pH-dependent slow release of the drugs, in vitro.

The pH-dependent reversible but covalent binding of boronic acid to cis diol contain glycoprotein was another application of the nanoporous gold monolith after modification by boronic acid. We developed to create a solid phase support for the separation and extraction of glycoproteins. NPG monolith were fabricated by dealloying in concentrated nitric acid and then functionalized by activated self-assembled monolayer of pegylated carboxyl terminal thiol. The capture of target glycoproteins was due to the reversible affinity of the cis diol moieties of the glycoproteins to the boronic acid unit of the immobilized boronic acid derivatives. TGA and a UV detected in situ solution depletion method were used to determine to calculate the amount of the glycoprotein on the modified NPG monolith.

We synthesize polystyrene based resin with active functional group and investigated its swelling properties, thermal stability, and pore size distribution. Moreover, the applicability of the resin was then investigated with the fully automated synthesis of oligosaccharides. This was achieved using the same spilt valve introduced recently in the HPLC-based automation and the use of an analytical autosampler. A new solid support available specifically for oligosaccharide synthesis will increase the attractiveness of automated technologies, setting the ground for further improvements

Reference

1. Stine, K. J., Application of porous materials to carbohydrate chemistry and glycoscience. In *Advances in carbohydrate chemistry and biochemistry*, Elsevier: 2017; Vol. 74, pp 61-136.
2. Thommes, M.; Kaneko, K.; Neimark, A. V.; Olivier, J. P.; Rodriguez-Reinoso, F.; Rouquerol, J.; Sing, K. S., Physisorption of gases, with special reference to the evaluation of surface area and pore size distribution (IUPAC Technical Report). *Pure Appl. Chem.* **2015,** *87* (9-10), 1051-1069.
3. Zdravkov, B.; Čermák, J.; Šefara, M.; Janků, J., Pore classification in the characterization of porous materials: a perspective. *Open Chem.* **2007,** *5* (2), 385-395.
4. Sharma, A.; Bhattarai, J. K.; Alla, A. J.; Demchenko, A. V.; Stine, K. J., Electrochemical annealing of nanoporous gold by application of cyclic potential sweeps. *Nanotechnology* **2015,** *26* (8), 085602.
5. Seker, E.; Reed, M. L.; Begley, M. R., Nanoporous Gold: Fabrication, Characterization, and Applications. *Materials* **2009,** *2* (4), 2188-2215.
6. Collinson, M. M., Nanoporous gold electrodes and their applications in analytical chemistry. *ISRN Anal. Chem.* **2013,** *2013*.
7. Matharu, Z.; Daggumati, P.; Wang, L.; Dorofeeva, T. S.; Li, Z.; Seker, E., Nanoporous-Gold-Based Electrode Morphology Libraries for Investigating Structure-Property Relationships in Nucleic Acid Based Electrochemical Biosensors. *ACS Appl. Mater. Interfaces* **2017,** *9* (15), 12959-12966.
8. Sharma, A.; Bhattarai, J. K.; Nigudkar, S. S.; Pistorio, S. G.; Demchenko, A. V.; Stine, K. J., Electrochemical impedance spectroscopy study of carbohydrate-terminated alkanethiol monolayers on nanoporous gold: implications for pore wetting. *J. Electroanal. Chem.* **2016,** *782*, 174-181.
9. Xiao, X.; Li, H.; Wang, M. e.; Zhang, K.; Si, P., Examining the effects of self-assembled monolayers on nanoporous gold based amperometric glucose biosensors. *Analyst* **2014,** *139* (2), 488-494.
10. Wittstock, A.; Zielasek, V.; Biener, J.; Friend, C. M.; Baeumer, M., Nanoporous gold catalysts for selective gas-phase oxidative coupling of methanol at low temperature. *Science* **2010,** *327* (5963), 319-322.
11. Daggumati, P.; Matharu, Z.; Seker, E., Effect of nanoporous gold thin film morphology on electrochemical DNA sensing. *Anal. Chem.* **2015,** *87* (16), 8149-8156.
12. Pandey, B.; Bhattarai, J. K.; Pornsuriyasak, P.; Fujikawa, K.; Catania, R.; Demchenko, A. V.; Stine, K. J., Square-wave voltammetry assays for glycoproteins on nanoporous gold. *J. Electroanal. Chem.* **2014,** *717-718*, 47-60.
13. Xia, Y.; Huang, W.; Zheng, J.; Niu, Z.; Li, Z., Nonenzymatic amperometric response of glucose on a nanoporous gold film electrode fabricated by a rapid and simple electrochemical method. *Biosens. Bioelectron.* **2011,** *26* (8), 3555-3561.
14. Seker, E.; Berdichevsky, Y.; Staley, K. J.; Yarmush, M. L., Microfabrication-compatible nanoporous gold foams as biomaterials for drug delivery. *Adv. Healthcare Mater.* **2012,** *1* (2), 172-176.
15. Pornsuriyasak, P.; Ranade, S. C.; Li, A.; Parlato, M. C.; Sims, C. R.; Shulga, O. V.; Stine, K. J.; Demchenko, A. V., STICS: surface-tethered iterative carbohydrate synthesis. *Chem. Commun.* **2009,** (14), 1834-1836.
16. Daggumati, P.; Appelt, S.; Matharu, Z.; Marco, M. L.; Seker, E., Sequence-specific electrical purification of nucleic acids with nanoporous gold electrodes. *J. Am. Chem. Soc.* **2016,** *138* (24), 7711-7717.

17. Alla, A. J.; FB, D. A.; Bhattarai, J. K.; Cooper, J. A.; Tan, Y. H.; Demchenko, A. V.; Stine, K. J., Selective capture of glycoproteins using lectin-modified nanoporous gold monolith. *J. Chromatogr. A* **2015,** *1423*, 19-30.

18. Yan, X.; Meng, F.; Xie, Y.; Liu, J.; Ding, Y., Direct N_2H_4/H_2O_2 fuel cells powered by nanoporous gold leaves. *Sci. Rep.* **2012,** *2*, 941.

19. Biener, J.; Wittstock, A.; Zepeda-Ruiz, L. A.; Biener, M. M.; Zielasek, V.; Kramer, D.; Viswanath, R. N.; Weissmuller, J.; Baumer, M.; Hamza, A. V., Surface-chemistry-driven actuation in nanoporous gold. *Nat. Mater.* **2009,** *8* (1), 47-51.

20. Lang, X. Y.; Yuan, H. T.; Iwasa, Y.; Chen, M. W., Three-dimensional nanoporous gold for electrochemical supercapacitors. *Scr. Mater.* **2011,** *64* (9), 923-926.

21. Bhattarai, J. K. Electrochemical Synthesis of Nanostructured Noble Metal Films for Biosensing. University of Missouri-St. Louis, 2014.

22. Bhattarai, J. K.; Sharma, A.; Fujikawa, K.; Demchenko, A. V.; Stine, K. J., Electrochemical synthesis of nanostructured gold film for the study of carbohydrate–lectin interactions using localized surface plasmon resonance spectroscopy. *Carbohydr. Res.* **2015,** *405*, 55-65.

23. Cobley, C. M.; Xia, Y., Gold and nanotechnology. *Elements* **2009,** *5* (5), 309-313.

24. Cobley, C. M.; Chen, J.; Cho, E. C.; Wang, L. V.; Xia, Y., Gold nanostructures: a class of multifunctional materials for biomedical applications. *Chem. Soc. Rev.* **2011,** *40* (1), 44-56.

25. Ganesh, N. V.; Fujikawa, K.; Tan, Y. H.; Nigudkar, S. S.; Stine, K. J.; Demchenko, A. V., Surface-tethered iterative carbohydrate synthesis: a spacer study. *J. Org. Chem.* **2013,** *78* (14), 6849-6857.

26. Biener, J.; Nyce, G. W.; Hodge, A. M.; Biener, M. M.; Hamza, A. V.; Maier, S. A., Nanoporous plasmonic metamaterials. *Adv. Mater.* **2008,** *20* (6), 1211-1217.

27. Xiao, X.; Si, P.; Magner, E., An overview of dealloyed nanoporous gold in bioelectrochemistry. *Bioelectrochemistry* **2016,** *109*, 117-126.

28. Jia, F.; Yu, C.; Zhang, L., Hierarchical nanoporous gold film electrode with extra high surface area and electrochemical activity. *Electrochemistry Communications* **2009,** *11* (10), 1944-1946.

29. Hou, J.; Xu, C.; Zhao, D.; Zhou, J., Facile fabrication of hierarchical nanoporous AuAg alloy and its highly sensitive detection towards dopamine and uric acid. *Sensors and Actuators B: Chemical* **2016,** *225*, 241-248.

30. Lee, M. N.; Santiago-Cordoba, M. A.; Hamilton, C. E.; Subbaiyan, N. K.; Duque, J. G.; Obrey, K. A. D., Developing Monolithic Nanoporous Gold with Hierarchical Bicontinuity Using Colloidal Bijels. *The Journal of Physical Chemistry Letters* **2014,** *5* (5), 809-812.

31. Chae, W.-S.; Yu, H.; Ham, S.-K.; Lee, M.-J.; Jung, J.-S.; Robinson, D. B., Bimodal porous gold opals for molecular sensing. *Electronic Materials Letters* **2013,** *9* (6), 783-786.

32. Walsh, D.; Arcelli, L.; Ikoma, T.; Tanaka, J.; Mann, S., Dextran templating for the synthesis of metallic and metal oxide sponges. *Nature Materials* **2003,** *2* (6), 386-390.

33. Ulman, A., Formation and structure of self-assembled monolayers. *Chemical reviews* **1996,** *96* (4), 1533-1554.

34. Hakkinen, H., The gold-sulfur interface at the nanoscale. *Nat Chem* **2012,** *4* (6), 443-455.

35. Laibinis, P. E.; Whitesides, G. M.; Allara, D. L.; Tao, Y. T.; Parikh, A. N.; Nuzzo, R. G., Comparison of the structures and wetting properties of self-assembled monolayers of n-alkanethiols on the coinage metal surfaces, copper, silver, and gold. *Journal of the American Chemical Society* **1991,** *113* (19), 7152-7167.

36. Mrksich, M.; Whitesides, G. M., Using self-assembled monolayers to understand the interactions of man-made surfaces with proteins and cells. *Annu. Rev. Biophys. Biomol. Struct.* **1996,** *25*, 55-78.

37. Love, J. C.; Estroff, L. A.; Kriebel, J. K.; Nuzzo, R. G.; Whitesides, G. M., Self-assembled monolayers of thiolates on metals as a form of nanotechnology. *Chemical reviews* **2005,** *105* (4), 1103-1170.

38. Evans, S. D.; Sharma, R.; Ulman, A., Contact angle stability: Reorganization of monolayer surfaces? *Langmuir* **1991,** *7* (1), 156-161.

39. Häkkinen, H., The gold–sulfur interface at the nanoscale. *Nature chemistry* **2012,** *4* (6), 443.

40. Pensa, E.; Cortes, E.; Corthey, G.; Carro, P.; Vericat, C.; Fonticelli, M. H.; Benitez, G.; Rubert, A. A.; Salvarezza, R. C., The chemistry of the sulfur–gold interface: in search of a unified model. *Accounts of chemical research* **2012,** *45* (8), 1183-1192.

41. Mameka, N.; Lührs, L.; Heissler, S.; Gliemann, H.; Wöll, C., Tailoring the Strength of Nanoporous Gold by Self-Assembled Monolayers of Alkanethiols. *ACS Applied Nano Materials* **2018,** *1* (12), 6613-6621.

42. Patel, D. A.; Weller, A. M.; Chevalier, R. B.; Karos, C. A.; Landis, E. C., Ordering and defects in self-assembled monolayers on nanoporous gold. *Applied Surface Science* **2016,** *387*, 503-512.

43. Bhattarai, J. K.; Neupane, D.; Mikhaylov, V.; Demchenko, A. V.; Stine, K. J., Self-Assembled Monolayers of Carbohydrate Derivatives on Gold Surfaces. *Carbohydrate* **2017**, 63.

44. Tabasum, S.; Noreen, A.; Kanwal, A.; Zuber, M.; Anjum, M. N.; Zia, K. M., Glycoproteins functionalized natural and synthetic polymers for prospective biomedical applications: A review. *International journal of biological macromolecules* **2017,** *98*, 748-776.

45. You, M.; Yang, S.; Tang, W.; Zhang, F.; He, P.-G., Ultrasensitive electrochemical detection of glycoprotein based on boronate affinity sandwich assay and signal amplification with functionalized SiO2@ Au nanocomposites. *ACS applied materials & interfaces* **2017,** *9* (16), 13855-13864.

46. Lü, C.; Li, H.; Wang, H.; Liu, Z., Probing the interactions between boronic acids and cis-diol-containing biomolecules by affinity capillary electrophoresis. *Analytical chemistry* **2013,** *85* (4), 2361-2369.

47. Su, J.; Chen, F.; Cryns, V. L.; Messersmith, P. B., Catechol polymers for pH-responsive, targeted drug delivery to cancer cells. *Journal of the American Chemical Society* **2011,** *133* (31), 11850-11853.

48. Bie, Z.; Chen, Y.; Li, H.; Wu, R.; Liu, Z., Off-line hyphenation of boronate affinity monolith-based extraction with matrix-assisted laser desorption/ionization time-of-flight mass spectrometry for efficient analysis of glycoproteins/glycopeptides. *Analytica Chimica Acta* **2014,** *834*, 1-8.

49. Li, H.; Wang, H.; Liu, Y.; Liu, Z., A benzoboroxole-functionalized monolithic column for the selective enrichment and separation of cis-diol containing biomolecules. *Chemical Communications* **2012,** *48* (34), 4115-4117.

50. Rowe, L.; El Khoury, G.; Lowe, C. R., A benzoboroxole-based affinity ligand for glycoprotein purification at physiological pH. *Journal of Molecular Recognition* **2016,** *29* (5), 232-238.

51. Rowe, L.; El Khoury, G.; Lowe, C. R., A benzoboroxole-based affinity ligand for glycoprotein purification at physiological pH. *Journal of Molecular Recognition* **2016,** *29* (5), 232-238.

52. Bhattarai, J. K.; Maruf, M. H. U.; Stine, K. J., Plasmonic-Active Nanostructured Thin Films. *Processes* **2020,** *8* (1), 115.

53. Mendes, P. M.; Jacke, S.; Critchley, K.; Plaza, J.; Chen, Y.; Nikitin, K.; Palmer, R. E.; Preece, J. A.; Evans, S. D.; Fitzmaurice, D., Gold nanoparticle patterning of silicon wafers using chemical e-beam lithography. *Langmuir* **2004,** *20* (9), 3766-3768.

54. Veiseh, M.; Zhang, Y.; Hinkley, K.; Zhang, M., Two-dimensional protein micropatterning for sensor applications through chemical selectivity technique. *Biomedical Microdevices* **2001,** *3* (1), 45-51.

55. Madsen, S. J.; Esfandyarpour, M.; Brongersma, M. L.; Sinclair, R., Observing plasmon damping due to adhesion layers in gold nanostructures using electron energy loss spectroscopy. *ACS photonics* **2017,** *4* (2), 268-274.

56. Leandro, L.; Malureanu, R.; Rozlosnik, N.; Lavrinenko, A., Ultrathin, Ultrasmooth Gold Layer on Dielectrics without the Use of Additional Metallic Adhesion Layers. *ACS Applied Materials and Interfaces* **2015,** *7* (10), 5797-5802.

57. Habteyes, T. G.; Dhuey, S.; Wood, E.; Gargas, D.; Cabrini, S.; Schuck, P. J.; Alivisatos, A. P.; Leone, S. R., Metallic adhesion layer induced plasmon damping and molecular linker as a nondamping alternative. *ACS Nano* **2012,** *6* (6), 5702-5709.

58. Veiseh, M.; Zareie, M. H.; Zhang, M., Highly selective protein patterning on gold– silicon substrates for biosensor applications. *Langmuir* **2002,** *18* (17), 6671-6678.

59. Vashist, S. K.; Raiteri, R.; Tewari, R.; Bajpai, R. P.; Bharadwaj, L. M., Quantification of human immunoglobulin G immobilized on gold-coated silicon chip for biosensing applications. *Journal of Physics: Conference Series* **2006,** *34*, 806-811.

60. Ryu, S. W.; Kim, C. H.; Han, J. W.; Kim, C. J.; Jung, C.; Park, H. G.; Choi, Y. K., Gold nanoparticle embedded silicon nanowire biosensor for applications of label-free DNA detection. *Biosens Bioelectron* **2010,** *25* (9), 2182-5.

61. Qin, D.; Xia, Y.; Whitesides, G. M., Soft lithography for micro- and nanoscale patterning. *Nat. Protocols* **2010,** *5* (3), 491-502.

62. Wu, C.; Sun, H.; Li, Y.; Liu, X.; Du, X.; Wang, X.; Xu, P., Biosensor based on glucose oxidase-nanoporous gold co-catalysis for glucose detection. *Biosensors and Bioelectronics* **2015,** *66*, 350-355.

63. Chen, L.; Lang, X.; Fujita, T.; Chen, M., Nanoporous gold for enzyme-free electrochemical glucose sensors. *Scripta Materialia* **2011,** *65* (1), 17-20.

64. Zhou, C.; Tang, X.; Xia, Y.; Li, Z., Electrochemical fabrication of cobalt oxides/nanoporous gold composite electrode and its nonenzymatic glucose sensing performance. *Electroanalysis* **2016,** *28* (9), 2149-2157.

65. Ge, S.; Jiao, X.; Chen, D., Ultrasensitive electrochemical immunosensor for CA 15-3 using thionine-nanoporous gold–graphene as a platform and horseradish peroxidase-encapsulated liposomes as signal amplification. *Analyst* **2012,** *137* (19), 4440-4447.

66. Sun, X.; Ma, Z., Electrochemical immunosensor based on nanoporpus gold loading thionine for carcinoembryonic antigen. *Analytica Chimica Acta* **2013,** *780*, 95-100.

67. Wei, Q.; Zhao, Y.; Xu, C.; Wu, D.; Cai, Y.; He, J.; Li, H.; Du, B.; Yang, M., Nanoporous gold film based immunosensor for label-free detection of cancer biomarker. *Biosensors and Bioelectronics* **2011,** *26* (8), 3714-3718.

68. Adams, J., The proteasome: a suitable antineoplastic target. *Nature Reviews Cancer* **2004,** *4* (5), 349-360.

69. Chen, D.; Frezza, M.; Schmitt, S.; Kanwar, J.; P. Dou, Q., Bortezomib as the First Proteasome Inhibitor Anticancer Drug: Current Status and Future Perspectives. *Current Cancer Drug Targets* **2011,** *11* (3), 239-253.

70. Stubelius, A.; Lee, S.; Almutairi, A., The Chemistry of Boronic Acids in Nanomaterials for Drug Delivery. *Accounts of chemical research* **2019,** *52* (11), 3108-3119.

71. Zhou, J.; Liu, X.; Zhong, Y.; Wei, R.; Chen, Y.; Zheng, T., Research progress in functionalization on polystyrene-divinylbenzene based microsphere. *Asia-Pacific Journal of Chemical Engineering* **2015,** *10* (1), 15-21.

72. Ley, S. V.; Baxendale, I. R.; Bream, R. N.; Jackson, P. S.; Leach, A. G.; Longbottom, D. A.; Nesi, M.; Scott, J. S.; Storer, R. I.; Taylor, S. J., Multi-step organic synthesis using solid-supported reagents and scavengers: a new paradigm in chemical library generation. *Journal of the Chemical Society, Perkin Transactions 1* **2000,** (23), 3815-4195.

73. Lav, T.-X.; Carbonnier, B.; Guerrouache, M.; Grande, D., Porous polystyrene-based monolithic materials templated by semi-interpenetrating polymer networks for capillary electrochromatography. *Polymer* **2010,** *51* (25), 5890-5894.

74. Xie, S.; Svec, F.; Frechet, J. M. J., Preparation of porous hydrophilic monoliths: effect of the polymerization conditions on the porous properties of poly (acrylamide-co-N,N'-methylenebisacrylamide) monolithic rods. *Journal of Polymer Science, Part A: Polymer Chemistry* **1997,** *35* (6), 1013-1021.

75. Husain, N.; Ndou, T. T.; Muñoz De La Peña, A.; Warner, I. M., Complexation of Doxorubicin with β- and γ-Cyclodextrins. *Applied Spectroscopy* **1992,** *46* (4), 652-658.

76. Di Cagno, M. P., The Potential of Cyclodextrins as Novel Active Pharmaceutical Ingredients: A Short Overview. *Molecules* **2017,** *22* (1), 1.

77. di Cagno, M., The potential of cyclodextrins as novel active pharmaceutical ingredients: a short overview. *Molecules* **2017,** *22* (1), 1.

78. Siriviriyanun, A.; Tsai, Y.-J.; Voon, S. H.; Kiew, S. F.; Imae, T.; Kiew, L. V.; Looi, C. Y.; Wong, W. F.; Lee, H. B.; Chung, L. Y., Cyclodextrin- and dendrimer-conjugated graphene oxide as a nanocarrier for the delivery of selected chemotherapeutic and photosensitizing agents. *Materials Science and Engineering: C* **2018,** *89*, 307-315.

79. Lee, J.-Y.; Park, S.-M., Electrochemistry of Guest Molecules in Thiolated Cyclodextrin Self-Assembled Monolayers: An Implication for Size-Selective Sensors. *The Journal of Physical Chemistry B* **1998,** *102* (49), 9940-9945.

80. Lee, J.-Y.; Park, S.-M., Electrochemistry of guest molecules in thiolated cyclodextrin self-assembled monolayers: An implication for size-selective sensors. *The Journal of Physical Chemistry B* **1998,** *102* (49), 9940-9945.

81. Henke, C.; Steinem, C.; Janshoff, A.; Steffan, G.; Luftmann, H.; Sieber, M.; Galla, H.-J., Self-assembled monolayers of monofunctionalized cyclodextrins onto gold: A mass spectrometric characterization and impedance analysis of host−guest interaction. *Anal. Chem.* **1996,** *68* (18), 3158-3165.

82. Rojas, M. T.; Koeniger, R.; Stoddart, J. F.; Kaifer, A. E., Supported monolayers containing preformed binding sites. Synthesis and interfacial binding properties of a thiolated beta-cyclodextrin derivative. *J. Am. Chem. Soc.* **1995,** *117* (1), 336-343.

83. Domi, Y.; Yoshinaga, Y.; Shimazu, K.; Porter, M. D., Characterization and optimization of mixed thiol-derivatized β-cyclodextrin/pentanethiol monolayers with high-density guest-accessible cavities. *Langmuir* **2009,** *25* (14), 8094-8100.

84. Weisser, M.; Nelles, G.; Wohlfart, P.; Wenz, G.; Mittler-Neher, S., Immobilization kinetics of cyclodextrins at gold surfaces. *J. Phys. Chem.* **1996,** *100* (45), 17893-17900.

85. Bhattarai, J. K.; Neupane, D.; Mikhaylov, V.; Demchenko, A. V.; Stine, K. J., Self-assembled monolayers of carbohydrate derivatives on gold surfaces. In *Carbohydrate*, IntechOpen: 2017; pp 63-97.

86. Bollo, S.; Yánez, C.; Sturm, J.; Nunez-Vergara, L.; Squella, J. A., Cyclic voltammetric and scanning electrochemical microscopic study of thiolated β-cyclodextrin adsorbed on a gold electrode. *Langmuir* **2003,** *19* (8), 3365-3370.

87. Liu, W.; Zhang, Y.; Gao, X., Interfacial supramolecular self-assembled monolayers of C60 by thiolated β-cyclodextrin on gold surfaces via monoanionic C60. *J. Am. Chem. Soc.* **2007,** *129* (16), 4973-4980.
88. Chatterjee, K.; Zhang, J.; Honbo, N.; Karliner, J. S., Doxorubicin cardiomyopathy. *Cardiology* **2010,** *115* (2), 155-162.
89. Swiech, O.; Mieczkowska, A.; Chmurski, K.; Bilewicz, R., Intermolecular Interactions between Doxorubicin and β-Cyclodextrin 4-Methoxyphenol Conjugates. *The Journal of Physical Chemistry B* **2012,** *116* (6), 1765-1771.
90. Peng, L.; Liu, S.; Feng, A.; Yuan, J., Polymeric nanocarriers based on cyclodextrins for drug delivery: host–guest interaction as stimuli responsive linker. *Mol. Pharm.* **2017,** *14* (8), 2475-2486.
91. Siriviriyanun, A.; Tsai, Y.-J.; Voon, S. H.; Kiew, S. F.; Imae, T.; Kiew, L. V.; Looi, C. Y.; Wong, W. F.; Lee, H. B.; Chung, L. Y., Cyclodextrin- and dendrimer-conjugated graphene oxide as a nanocarrier for the delivery of selected chemotherapeutic and photosensitizing agents. *Mater. Sci. Eng. C* **2018,** *89*, 307-315.
92. Husain, N.; Ndou, T. T.; Muñoz De La Peña, A.; Warner, I. M., Complexation of doxorubicin with β- and γ-cyclodextrins. *Appl. Spectrosc.* **1992,** *46* (4), 652-658.
93. Hădărugă, N. G.; Bandur, G. N.; David, I.; Hădărugă, D. I., A review on thermal analyses of cyclodextrins and cyclodextrin complexes. *Environ. Chem. Lett.* **2019,** *17* (1), 349-373.
94. Nasongkla, N.; Shuai, X.; Ai, H.; Weinberg, B. D.; Pink, J.; Boothman, D. A.; Gao, J., cRGD-functionalized polymer micelles for targeted doxorubicin delivery. *Angew. Chem. Int. Ed.* **2004,** *43* (46), 6323-6327.
95. Varki, A.; Gagneux, P., Biological functions of glycans. **2017**.
96. Nilsson, J.; Rüetschi, U.; Halim, A.; Hesse, C.; Carlsohn, E.; Brinkmalm, G.; Larson, G., Enrichment of glycopeptides for glycan structure and attachment site identification. *Nature Methods* **2009,** *6* (11), 809-811.
97. Zhu, R.; Zacharias, L.; Wooding, K. M.; Peng, W.; Mechref, Y., Chapter Twenty-One - Glycoprotein Enrichment Analytical Techniques: Advantages and Disadvantages. In *Methods in Enzymology*, Shukla, A. K., Ed. Academic Press: 2017; Vol. 585, pp 397-429.
98. An, H. J.; Froehlich, J. W.; Lebrilla, C. B., Determination of glycosylation sites and site-specific heterogeneity in glycoproteins. *Current Opinion in Chemical Biology* **2009,** *13* (4), 421-426.
99. Liu, H.; Zhang, N.; Wan, D.; Cui, M.; Liu, Z.; Liu, S., Mass spectrometry-based analysis of glycoproteins and its clinical applications in cancer biomarker discovery. *Clinical Proteomics* **2014,** *11* (1), 14.
100. Pappin, B.; Kiefel, M. J.; Houston, T. A., Boron-carbohydrate interactions. In *Carbohydrates-Comprehensive Studies on Glycobiology and Glycotechnology*, InTech: 2012.
101. Jiang, B.; Qu, Y.; Zhang, L.; Liang, Z.; Zhang, Y., 4-Mercaptophenylboronic acid functionalized graphene oxide composites: Preparation, characterization and selective enrichment of glycopeptides. *Analytica Chimica Acta* **2016,** *912*, 41-48.
102. You, M.; Yang, S.; Tang, W.; Zhang, F.; He, P.-G., Ultrasensitive Electrochemical Detection of Glycoprotein Based on Boronate Affinity Sandwich Assay and Signal Amplification with Functionalized SiO2@Au Nanocomposites. *ACS Applied Materials & Interfaces* **2017,** *9* (16), 13855-13864.
103. Li, D.; Li, Y.; Li, X.; Bie, Z.; Pan, X.; Zhang, Q.; Liu, Z., A high boronate avidity monolithic capillary for the selective enrichment of trace glycoproteins. *Journal of Chromatography A* **2015,** *1384*, 88-96.

104. Alla, A. J.; D' Andrea, F. B.; Bhattarai, J. K.; Cooper, J. A.; Tan, Y. H.; Demchenko, A. V.; Stine, K. J., Selective capture of glycoproteins using lectin-modified nanoporous gold monolith. *Journal of chromatography. A* **2015,** *1423*, 19-30.
105. Xing, R.; Wang, S.; Bie, Z.; He, H.; Liu, Z., Preparation of molecularly imprinted polymers specific to glycoproteins, glycans and monosaccharides via boronate affinity controllable-oriented surface imprinting. *Nat. Protocols* **2017,** *12* (5), 964-987.
106. Kaji, H.; Shikanai, T.; Sasaki-Sawa, A.; Wen, H.; Fujita, M.; Suzuki, Y.; Sugahara, D.; Sawaki, H.; Yamauchi, Y.; Shinkawa, T.; Taoka, M.; Takahashi, N.; Isobe, T.; Narimatsu, H., Large-scale Identification of N-Glycosylated Proteins of Mouse Tissues and Construction of a Glycoprotein Database, GlycoProtDB. *Journal of Proteome Research* **2012,** *11* (9), 4553-4566.
107. Gamblin, D. P.; Scanlan, E. M.; Davis, B. G., Glycoprotein Synthesis: An Update. *Chemical Reviews* **2009,** *109* (1), 131-163.
108. Klein, J. A.; Zaia, J., A Perspective on the Confident Comparison of Glycoprotein Site-Specific Glycosylation in Sample Cohorts. *Biochemistry* **2019**.
109. Clark, G. F., The role of carbohydrate recognition during human sperm–egg binding. *Human Reproduction* **2013,** *28* (3), 566-577.
110. Wang, Q.; Barge, L. M.; Steinbock, O., Microfluidic production of pyrophosphate catalyzed by mineral membranes with steep pH gradients. *Chemistry–A European Journal* **2019,** *25* (18), 4732-4739.
111. de la Fuente, J. M.; Barrientos, A. G.; Rojas, T. C.; Rojo, J.; Cañada, J.; Fernández, A.; Penadés, S., Gold glyconanoparticles as water-soluble polyvalent models to study carbohydrate interactions. *Angewandte Chemie International Edition* **2001,** *40* (12), 2257-2261.
112. de Souza, A. C.; Halkes, K. M.; Meeldijk, J. D.; Verkleij, A. J.; Vliegenthart, J. F.; Kamerling, J. P., Synthesis of gold glyconanoparticles: Possible probes for the exploration of carbohydrate-mediated self-recognition of marine sponge cells. *European Journal of Organic Chemistry* **2004,** *2004* (21), 4323-4339.
113. Bhattarai, J. K.; Neupane, D.; Nepal, B.; Mikhaylov, V.; Demchenko, A. V.; Stine, K. J., Preparation, modification, characterization, and biosensing application of nanoporous gold using electrochemical techniques. *Nanomaterials* **2018,** *8* (3), 171.
114. de Oliveira Figueiroa, E.; Albuquerque da Cunha, C. R.; Albuquerque, P.; de Paula, R. A.; Aranda-Souza, M. A.; Alves, M. S.; Zagmignan, A.; Carneiro-da-Cunha, M. G.; Nascimento da Silva, L. C.; dos Santos Correia, M. T., Lectin-carbohydrate interactions: implications for the development of new anticancer agents. *Current Medicinal Chemistry* **2017,** *24* (34), 3667-3680.
115. Dam, T. K.; Brewer, C. F., Chapter 5 - Multivalent Lectin—Carbohydrate Interactions: Energetics and Mechanisms of Binding. In *Advances in Carbohydrate Chemistry and Biochemistry*, Horton, D., Ed. Academic Press: 2010; Vol. 63, pp 139-164.
116. Lee, R. T.; Lee, Y. C., Affinity enhancement by multivalent lectin–carbohydrate interaction. *Glycoconjugate Journal* **2000,** *17* (7), 543-551.
117. Syed, P.; Gidwani, K.; Kekki, H.; Leivo, J.; Pettersson, K.; Lamminmäki, U., Role of lectin microarrays in cancer diagnosis. *Proteomics* **2016,** *16* (8), 1257-1265.
118. Cummings, R. D.; Etzler, M. E., Antibodies and Lectins in Glycan Analysis. In *Essentials of Glycobiology*, Varki, A.; Cummings, R. D.; Esko, J. D.; Freeze, H. H.; Stanley, P.; Bertozzi, C. R.; Hart, G. W.; Etzler, M. E., Eds. Cold Spring Harbor Laboratory Press

Copyright © 2009, The Consortium of Glycobiology Editors, La Jolla, California.: Cold Spring Harbor (NY), 2009.
119. Totten, S. M.; Adusumilli, R.; Kullolli, M.; Tanimoto, C.; Brooks, J. D.; Mallick, P.; Pitteri, S. J., Multi-lectin Affinity Chromatography and Quantitative Proteomic Analysis Reveal Differential

Glycoform Levels between Prostate Cancer and Benign Prostatic Hyperplasia Sera. *Scientific Reports* **2018,** *8* (1), 6509.
120. Pace, C. N.; Vajdos, F.; Fee, L.; Grimsley, G.; Gray, T., How to measure and predict the molar absorption coefficient of a protein. *Protein Science* **1995,** *4* (11), 2411-2423.
121. Vidaud, C.; Miccoli, L.; Brulfert, F.; Aupiais, J., Fetuin exhibits a strong affinity for plutonium and may facilitate its accumulation in the skeleton. *Scientific Reports* **2019,** *9* (1), 17584.
122. Detampel, P.; Witzigmann, D.; Krähenbühl, S.; Huwyler, J., Hepatocyte targeting using pegylated asialofetuin-conjugated liposomes. *Journal of Drug Targeting* **2014,** *22* (3), 232-241.
123. Haque, M. E.; Debnath, D.; Basak, S.; Chakrabarti, A., Structural changes of horseradish peroxidase in presence of low concentrations of urea. *European Journal of Biochemistry* **1999,** *259* (1-2), 269-274.
124. Suroviec, A. H., Determining surface coverage of self-assembled monolayers on gold electrodes. *Chem. Educ.* **2012,** *17*, 83-85.
125. Zhang, R.; Zhang, Y.; Deng, X.; Sun, S.; Li, Y., A novel dual-signal electrochemical sensor for bisphenol A determination by coupling nanoporous gold leaf and self-assembled cyclodextrin. *Electrochim. Acta* **2018,** *271*, 417-424.
126. Tang, Y.; Tang, D.; Zhang, J.; Tang, D., Novel quartz crystal microbalance immunodetection of aflatoxin B1 coupling cargo-encapsulated liposome with indicator-triggered displacement assay. *Anal. Chim. Acta* **2018,** *1031*, 161-168.
127. Swiech, O.; Mieczkowska, A.; Chmurski, K.; Bilewicz, R., Intermolecular interactions between doxorubicin and β-cyclodextrin 4-methoxyphenol conjugates. *J. Phys. Chem. B* **2012,** *116* (6), 1765-1771.
128. Anand, R.; Ottani, S.; Manoli, F.; Manet, I.; Monti, S., A close-up on doxorubicin binding to γ-cyclodextrin: an elucidating spectroscopic, photophysical and conformational study. *RSC Advances* **2012,** *2* (6), 2346-2357.
129. Liu, T.; Li, X.; Qian, Y.; Hu, X.; Liu, S., Multifunctional pH-disintegrable micellar nanoparticles of asymmetrically functionalized β-cyclodextrin-based star copolymer covalently conjugated with doxorubicin and DOTA-Gd moieties. *Biomaterials* **2012,** *33* (8), 2521-2531.
130. Bekers, O.; Kettenes, J. J. V. D. B.; Van Helden, S. P.; Seijkens, D.; Beijnen, J. H.; Bulti, A.; Underberg, W. J., Inclusion complex formation of anthracycline antibiotics with cyclodextrins; a proton nuclear magnetic resonance and molecular modelling study. *J. Incl. Phenom. Mol. Recognit. Chem.* **1991,** *11* (2), 185-193.
131. Bekers, O.; Beijnen, J.; Otagiri, M.; Bult, A.; Underberg, W., Inclusion complexation of doxorubicin and daunorubicin with cyclodextrins. *J. Pharm. Biomed. Anal.* **1990,** *8* (8-12), 671-674.
132. Yang, N.; Wang, Y.; Zhang, Q.; Chen, L.; Zhao, Y., In situ formation of poly (thiolated chitosan-co-alkylated β-cyclodextrin) hydrogels using click cross-linking for sustained drug release. *J. Mater. Sci.* **2019,** *54* (2), 1677-1691.
133. Yang, T.; Huang, J. L.; Wang, Y. T.; Zheng, A. Q.; Shu, Y.; Wang, J. H., β-cyclodextrin-decorated carbon dots serve as nanocarriers for targeted drug delivery and controlled release. *ChemNanoMat* **2019,** *5* (4), 479-487.
134. Alvarez, J.; Liu, J.; Román, E.; Kaifer, A. E., Water-soluble platinum and palladium nanoparticles modified with thiolated β-cyclodextrin. *Chem. Commum.* **2000,** (13), 1151-1152.
135. Hu, X.; Chai, Z.; Lu, L.; Ruan, H.; Wang, R.; Zhan, C.; Xie, C.; Pan, J.; Liu, M.; Wang, H.; Lu, W., Bortezomib dendrimer prodrug-based nanoparticle system. *Adv. Funct. Mater.* **2019,** *29* (14), 1807941.

136. Yamanoi, T.; Oda, Y.; Katsuraya, K.; Inazu, T.; Hattori, K., Synthesis, structure, and evaluation of a β-cyclodextrin-artificial carbohydrate conjugate for use as a doxorubicin-carrying molecule. *Bioorg. Med. Chem.* **2016,** *24* (4), 635-642.

137. Oda, Y.; Yanagisawa, H.; Maruyama, M.; Hattori, K.; Yamanoi, T., Design, synthesis and evaluation of d-galactose-β-cyclodextrin conjugates as drug-carrying molecules. *Bioorg. Med. Chem.* **2008,** *16* (19), 8830-8840.

138. Liu, Y.; Dai, Z.; Wang, J.; Tu, Y.; Zhu, L., Folate-targeted pH-sensitive bortezomib conjugates for cancer treatment. *Chemical Communications* **2019,** *55* (29), 4254-4257.

139. Alla, A. J.; d'Andrea, F. B.; Bhattarai, J. K.; Cooper, J. A.; Tan, Y. H.; Demchenko, A. V.; Stine, K. J., Selective capture of glycoproteins using lectin-modified nanoporous gold monolith. *Journal of Chromatography A* **2015,** *1423*, 19-30.

140. Cerruti, M.; Fissolo, S.; Carraro, C.; Ricciardi, C.; Majumdar, A.; Maboudian, R., Poly(ethylene glycol) Monolayer Formation and Stability on Gold and Silicon Nitride Substrates. *Langmuir* **2008,** *24* (19), 10646-10653.

141. Gooding, J. J.; Hale, P. S.; Maddox, L. M.; Shapter, J. G., Surface pKa of self-assembled monolayers. *Journal of chemical education* **2005,** *82* (5), 779.

142. Hlady, V.; Buijs, J.; Jennissen, H. P., [26] Methods for studying protein adsorption. In *Methods in Enzymology*, Academic Press: 1999; Vol. 309, pp 402-429.

143. Zhang, C.; Zeng, G.; Huang, D.; Lai, C.; Huang, C.; Li, N.; Xu, P.; Cheng, M.; Zhou, Y.; Tang, W., Combined removal of di (2-ethylhexyl) phthalate (DEHP) and Pb (II) by using a cutinase loaded nanoporous gold-polyethyleneimine adsorbent. *Rsc Advances* **2014,** *4* (98), 55511-55518.

144. Tan, Y. H.; Davis, J. A.; Fujikawa, K.; Ganesh, N. V.; Demchenko, A. V.; Stine, K. J., Surface area and pore size characteristics of nanoporous gold subjected to thermal, mechanical, or surface modification studied using gas adsorption isotherms, cyclic voltammetry, thermogravimetric analysis, and scanning electron microscopy. *Journal of materials chemistry* **2012,** *22* (14), 6733-6745.

145. Stine, K. J.; Jefferson, K.; Shulga, O. V., Nanoporous gold for enzyme immobilization. In *Enzyme Stabilization and Immobilization*, Springer: 2017; pp 37-60.

146. Hardesty, J. H.; Attili, B., Spectrophotometry and the Beer-Lambert Law: An Important Analytical Technique in Chemistry. *Collin College, Department of Chemistry* **2010**.

147. Rose, M. E.; Longstaff, C.; Dean, P. D., Negative ion fast atom bombardment mass spectrometry. In situ reactions of boronic acids with triols and related compounds, sugars and nucleosides. *Biomedical mass spectrometry* **1983,** *10* (9), 512-527.

148. Cheng, T.; Li, H.; Ma, Y.; Liu, X.; Zhang, H., Synthesis of boronic-acid-functionalized magnetic attapulgite for selective enrichment of nucleosides. *Analytical and Bioanalytical Chemistry* **2015,** *407* (12), 3525-3529.

149. Proença, M.; Borges, J.; Rodrigues, M. S.; Domingues, R.; Dias, J.; Trigueiro, J.; Bundaleski, N.; Teodoro, O.; Vaz, F., Development of Au/CuO nanoplasmonic thin films for sensing applications. *Surface and Coatings Technology* **2018,** *343*, 178-185.

150. Proença, M.; Rodrigues, M. S.; Borges, J.; Vaz, F., Gas sensing with nanoplasmonic thin films composed of nanoparticles (Au, Ag) dispersed in a CuO matrix. *Coatings* **2019,** *9* (5), 337.

151. Rodrigues, M. S.; Borges, J.; Vaz, F., Enhancing the Sensitivity of Nanoplasmonic Thin Films for Ethanol Vapor Detection. *Materials* **2020,** *13* (4), 870.

152. Willets, K. A.; Van Duyne, R. P., Localized surface plasmon resonance spectroscopy and sensing. *Annu. Rev. Phys. Chem.* **2007,** *58*, 267-297.

153. Bhattarai, J. K.; Neupane, D.; Nepal, B.; Alharthi, M. D.; Demchenko, A. V.; Stine, K. J., Adhesion layer-free attachment of gold on silicon wafer and its application in localized surface plasmon resonance-based biosensing. *Sensors and Actuators A: Physical* **2020**, 112155.

154. Riboh, J. C.; Haes, A. J.; McFarland, A. D.; Yonzon, C. R.; Van Duyne, R. P., A nanoscale optical biosensor: Real-time immunoassay in physiological buffer enabled by improved nanoparticle adhesion. *Journal of Physical Chemistry B* **2003,** *107* (8), 1772-1780.
155. Whitney, A. V.; Elam, J. W.; Zou, S.; Zinovev, A. V.; Stair, P. C.; Schatz, G. C.; Van Duyne, R. P., Localized Surface Plasmon Resonance Nanosensor: A High-Resolution Distance-Dependence Study Using Atomic Layer Deposition. *The Journal of Physical Chemistry B* **2005,** *109* (43), 20522-20528.
156. Jackman, J. A.; Rahim Ferhan, A.; Cho, N. J., Nanoplasmonic sensors for biointerfacial science. *Chemical Society Reviews* **2017,** *46* (12), 3615-3660.
157. Chen, H.; Kou, X.; Yang, Z.; Ni, W.; Wang, J., Shape- and size-dependent refractive index sensitivity of gold nanoparticles. *Langmuir* **2008,** *24* (10), 5233-7.
158. Bhattarai, J. K., Electrochemical Synthesis of Nanostructured Noble Metal Films for Biosensing. **2014**.
159. Kim, H.; Kim, Y., Preparation of nanoporous gold using PS bead, Ludox and nanoporous alumina as physical templates. *Current Applied Physics* **2009,** *9* (1, Supplement), S88-S90.
160. Nyce, G. W.; Hayes, J. R.; Hamza, A. V.; Satcher, J. H., Synthesis and Characterization of Hierarchical Porous Gold Materials. *Chemistry of Materials* **2007,** *19* (3), 344-346.
161. Lee, Y., Biochemistry of carbohydrate-protein interaction 1. *The FASEB journal* **1992,** *6* (13), 3193-3200.
162. Zhang, Y.; Luo, S.; Tang, Y.; Yu, L.; Hou, K.-Y.; Cheng, J.-P.; Zeng, X.; Wang, P. G., Carbohydrate−Protein Interactions by "Clicked" Carbohydrate Self-Assembled Monolayers. *Analytical Chemistry* **2006,** *78* (6), 2001-2008.
163. Ahn, K.-S.; Kim, B. K.; Lee, W.-Y., Cyclic voltammetric studies of carbohydrate–protein interactions on gold surface. *Electrochemistry Communications* **2015,** *58*, 69-72.
164. Yu, B.; Tian, C.; Cong, H.; Xu, T., Synthesis of monodisperse poly(styrene-co-divinylbenzene) microspheres with binary porous structures and application in high-performance liquid chromatography. *Journal of Materials Science* **2016,** *51* (11), 5240-5251.
165. Bowers, L. D.; Pedigo, S., Solvent strength studies on polystyrene-divinylbenzene columns. *Journal of Chromatography A* **1986,** *371*, 243-251.
166. Iskandarani, Z.; Pietrzyk, D. J., Liquid chromatographic separation of amino acids, peptides, and derivatives on a porous polystyrene-divinylbenzene copolymer. *Analytical Chemistry* **1981,** *53* (3), 489-495.
167. Lungfiel, K.; Seubert, A., Varying the porous structure of polystyrene/divinylbenzene beads prepared by Ugelstads activated swelling technique and examining its reversed phase HPLC properties. *Journal of Chromatography A* **2014,** *1358*, 117-127.
168. Svec, F.; Fréchet, J. M. J., Molded Rigid Monolithic Porous Polymers: An Inexpensive, Efficient, and Versatile Alternative to Beads for the Design of Materials for Numerous Applications. *Industrial & Engineering Chemistry Research* **1999,** *38* (1), 34-48.
169. Buchmeiser, M. R., Polymeric monolithic materials: Syntheses, properties, functionalization and applications. *Polymer* **2007,** *48* (8), 2187-2198.
170. Inoue, H.; Yamanaka, K.; Yoshida, A.; Aoki, T.; Teraguchi, M.; Kaneko, T., Synthesis and cation exchange properties of a new porous cation exchange resin having an open-celled monolith structure. *Polymer* **2004,** *45* (1), 3-7.
171. Xu, S.; Li, J.; Qiao, G.; Wang, H.; Lu, T., Pore structure control of mesoporous carbon monoliths derived from mixtures of phenolic resin and ethylene glycol. *Carbon* **2009,** *47* (8), 2103-2111.

172. Krajnc, P.; Brown, J. F.; Cameron, N. R., Monolithic Scavenger Resins by Amine Functionalizations of Poly(4-vinylbenzyl chloride-co-divinylbenzene) PolyHIPE Materials. *Organic Letters* **2002,** *4* (15), 2497-2500.
173. Malik, M. A.; Ali, S. W.; Ahmed, I., Sulfonated Styrene−Divinybenzene Resins: Optimizing Synthesis and Estimating Characteristics of the Base Copolymers and the Resins. *Industrial & Engineering Chemistry Research* **2010,** *49* (6), 2608-2612.
174. Panza, M.; Neupane, D.; Stine, K. J.; Demchenko, A. V., The development of a dedicated polymer support for the solid-phase oligosaccharide synthesis. *Chemical Communications* **2020,** *56* (72), 10568-10571.